REPUBLIC OF TÜRKİYE

ALTINBAŞ UNIVERSITY

Institute of Graduate Studies

Mechanical Engineering

THERMAL EFFECT REDUCTION IN ELECTRICAL VEHICLE BATTERY USING LIQUID COOLING TECHNIQUES

Hassnain F. ABASS

Master's Thesis

Supervisor

Asst. Prof. Dr. Yaser ALAIWI

Istanbul, 2023

THERMAL EFFECT REDUCTION IN ELECTRICAL VEHICLE BATTERY USING LIQUID COOLING TECHNIQUES

Hassnaın F. ABASS

Mechanical Engineering

Master’s Thesis

ALTINBAŞ UNIVERSITY
2023

The thesis titled THERMAL EFFECT REDUCTION IN ELECTRICAL VEHICLE BATTERY USING LIQUID COOLING TECHNIQUES prepared by HASSNAIN F.ABASS and submitted on 00/04/2023 has been **accepted unanimously** for the degree of Master of Science in Mechanical Engineering.

Asst. Prof. Dr. Yaser ALAIWI
Supervisor

Thesis Defence Committee Members:

Asst. Prof. Dr. Yaser ALAIWI	Department of Mechanical Engineering, Altınbaş University	________________
Asst. Prof. Dr. Serdar AY	Department of Mechanical Engineering Altınbaş University	________________
Asst. Prof. Dr. Ahmed SADIK	Department of Mechanical Engineering Kırıkkale University	________________

I hereby declare that this thesis meets all format and submission requirements of a Master's thesis.
Submission date of the thesis to Institute of Graduate Studies: ___/___/___

I hereby declare that all information/data presented in this graduation project has been obtained in full accordance with academic rules and ethical conduct. I also declare all unoriginal materials and conclusions have been cited in the text and all references mentioned in the Reference List have been cited in the text, and vice versa as required by the abovementioned rules and conduct.

Hassnian F. ABASS

Signature

PREFACE

I'd like to thank and be grateful to my supervisor, Asst. Prof. Dr. Yaser ALAIWI, and dedicate this study to him for his desire to build the right scientific method through discussions and ideas, especially in battery thermal management system development. and for his careful follow-up during this research project, as well as to all the people close to me who helped me get to this point. I'd also like to extend my gratitude to my illustrious professors and the head of the department for the important responsibilities that they share, as well as to everyone who has contributed in any way to the development and accomplishments of this university as a distinct scientific edifice.

ABSTRACT

THERMAL EFFECT REDUCTION IN ELECTRICAL VEHICLE BATTERY USING LIQUID COOLING TECHNIQUES

ABASS, Hassnain F
M.Sc., Mechanical Engineering, Altınbaş University
Supervisor: Asst. Prof. Dr. Yaser ALAIWI
Date: April / 2023
Pages: 104

The electrical vehicles were used new techniques to improve the boundary condition for work operation of lithium-ion battery which is consider main source for EV's to storage energy and feeding the power to the electrical engine and appliance of it. The lithium-ion battery has operating temperature start from 0 to 35 ℃ degrees, but the ideal range start 16 to25 ℃ degrees.

In the researcher focus on change in perspective of thermal management system that control to the cooling lithium-ion battery packs which is related and effecting on battery performance depending on heat transfer medium such as air, liquid or air-liquid or depending on the techniques of cooling such as liquid jacket, cold plate, micro channel, serpentine channel cooling plates, submerge battery packs in coolant. all these types discussed the cooling system and how maintain the batteries near to operating thermal range.

To make this research go forward, we will discuss the techniques of reducing the different temperature by using cooling liquid medium and these techniques improved to reduction the thermal effect by uniform distribution techniques to achieve the best cooling distribution around the batteries. In present work, the our model results proved that the temperature under controlled at many different discharge load (1C,0.6C,0.667C,0.7C,0.88C) C-rates T_{max} was controlled at 33.82 °C and ΔT_{max} =3.18 °C , ambient temperature (26.5°C).

Keywords: Lithium-Ion Battery, Thermal Management System, Reduction Temperature, Mini Channel, Liquid Cooling Technic.

TABLE OF CONTENTS

LIST OF TABLES

Pages

LIST OF FIGURES

Pages

ABBREVIATIONS

ANSYS	:	Fluent Commercial CFD Package
BTMS	:	Thermal Management System of a Battery Module
CFD	:	Computational Fluid Dynamics
CV	:	Constant Voltage
EV	:	Electric Vehicle
LI-ION	:	Lithium-ION Cell
CP	:	Specific Heat Capacity of the Coolant (J/Kg/K)
C-Rate	:	The Rate at Which a Battery is Charged Or Discharged Re- Lative to Its Nominal Capacity (C)
DOC	:	Depth of Discharge
M	:	Mass Flow Rate (Kg/S)
SOC	:	State of Charge
ΔT	:	Temperature Increase of the Coolant Due to Accepting Qc From the LI-ION Cell (°C)
R	:	Radius of the 18650 Li-ION Cells (M)
HTC	:	Heat Transfer Coefficient (W/M2/K)
TMT	:	Thermal Management Technologies
SOC(T)	:	State of Charge of the Battery at Time (T)
SOC(T-1)	:	State of Charge of the Battery at Time T-1.

1. INTRODUCTION

Three types of commercial and industry lithium-ion battery in market that used to support new HV’s or EV’s engine, it is feeding engine with power energy which storge in LIB’s Pack for working to a long mileage, this reaction accompanied by high temperature in core that can affect to the performance of LIB’s and to lifetime or in worse scenario burning if it exceeds the maximum operation temperature. [1]

Most of companies’ production EV’s made supported chase to protect LIBs from intrusive shocks that cause batteries damaged and protect it from extremely changes of environments especially temperatures, if lithium element reacted at high temperature with oxygen or nitrogen made burns with a strongly red-tinged flame.

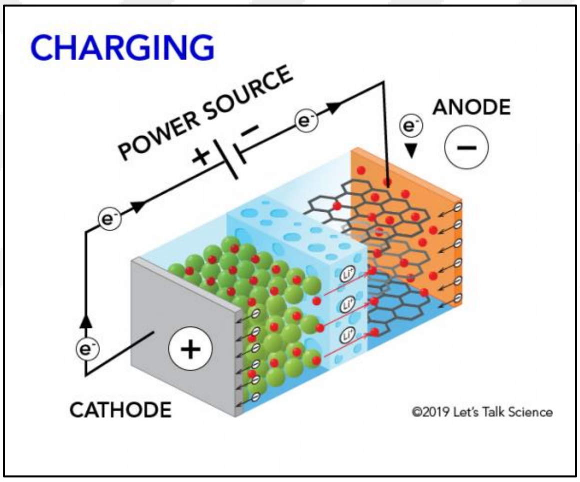

Figure 1.1: LIB’s Layers[1].

Chemical reaction in all LIB’s types (LiFePO4, LiMn2O4 and Li (NiCoMn)O2) are content three layers Anode (+), electrolyte, Cathode (-), positive side represented lithium-ion and carbon is negative side the energy generated between these poles by chemical reaction, where the positive electrons move from side to another to be charging state and the opposite movement in discharge state.

The battery cooling systems are under research and experiments still to improve the techniques for cooling system and the main cooling medium is Air and Liquid cooling system, EV’s used liquid cooling method to cool batteries pack depending on to reduction the thermal effect and increase heat transfer rate between cell and liquid and cell to cell.

Most of the accident happened in LIB's in EV's cause from increase in temperature of core in group or cell after it exposed to short circuit or out damage by accident (Figure 1.2)

Figure 1.2: Lithium-ION Batteries Explosion in EV's [2].

In literature studies in HV's the LIB's operating temperature was recommended between 15- 40 °C degrees and the ΔT equal 5 °C where BTM's controlled and management this operation [3] [4], Higher charging and discharging rates generate more heat due to internal resistance [5].

During discharging, most of the power generated by the cell is supplied to the external circuit at modest discharge rates (2C or less). The internal resistance dissipates more electricity as the discharge rate increases[6] BTMS design considerations were discussed, and four types of BTMS cooling technologies, including air cooling, liquid cooling, PCM, and heat pipe cooling approaches, were detailed[7].

A thermal model of Li-NCA/C battery packs has been constructed and simulated. The TMS cools the pack effectively even at low flow rates and maximum temperature rise within 7 K. It can work effectively under stringent conditions and is a suitable candidate for electric car batteries[8].

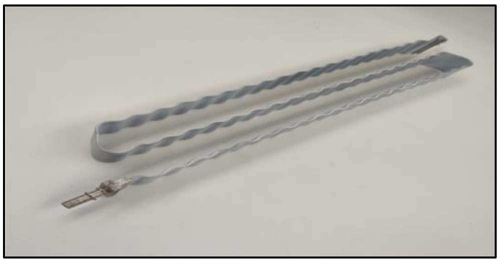

Figure 1.3: Serpentine Channels Cooling Plates.[9]

In addition to providing quantitative study of heat generation for a Li-ion battery under actual load circumstances, examination of the exothermic heat release during cycling also gave guidance for thermally aware design of Li-ion batteries for electric cars[10].

1.1 SAFETY AND THERMAL BEHAVIOR FOR LIB'S

Because several cells are put within EVs and HEVs, battery safety is a critical concern[11] However, The development of Li-ion batteries has been associated with a range of practical challenges, the most critical of which include insufficient safety measures and low cycle performance[12] ,Various chemical and electrochemical processes occur during battery charge and discharge[10] In the initial stages of studying high discharge rates in scaled-up cells, it was found that the increase in temperature posed a significant challenge. High current levels, such as those experienced during rapid acceleration, lead to a substantial amount of heat being produced by batteries during rapid charge and discharge cycles.[13]–[17]. The advancement of battery-powered vehicles necessitates large-scale batteries; yet, as size increases and big packages develop, major thermal stability issues will arise[17], [18] In 2002, Due to a potential overheating danger, the EV Global Motors Corporation has issued a recall of 2000 batteries used in its electric bicycles[19]. Overheating, combustion, and explosion are well-known risks that grow with the quantity of thermal energy contained within the battery or pack. As a result, the state and charge level of the batteries in electric cars (EVs), hybrid electric vehicles (HEVs), and plug-in hybrid electric vehicles (PHEVs) heavily impact their performance[20]. It is critical to understand the mechanism of battery performance loss at high temperatures and discharge currents. Heat may be generated in the solid electrolyte interface (SEI) layer of a Li-ion battery[21]–[23].electrolyte and anode electrical analyses[14]. In general, temperature is a crucial parameter that can significantly impact battery performance. Factors that can be affected by temperature include the electrochemical system, round trip efficiency, charge acceptance, power and energy capability, reliability, cycle life, and cost[24].

1.2 CONCEPT OF BATTERY THERMAL MANAGEMENT SYSTEM (BTMS)

The battery temperature management system (BTMS) can be regarded as the central control unit of a battery pack, which comprises numerous battery cells arranged in diverse series, parallel, and combination configurations. Lithium-ion batteries are widely adopted in commercial applications due to their superior performance over other battery types. Notably, the electrochemical processes underlying battery performance are highly sensitive to temperature variations. According to the Arrhenius equation, the reaction rate in batteries is exponentially proportional to the temperature, and therefore, the proper management of battery temperature is critical for ensuring optimal battery performance and prolonging battery life. In light of this, current research has been conducted to explore and develop effective BTMS technologies[11].

The active area within a battery cell is predominantly concentrated near the electrode due to the extensive surface area of the battery[25]. However, this non-uniform distribution of temperature often leads to thermal non-uniformity[25], which, in turn, undermines the battery cell's performance and longevity. The charging and discharging processes of a battery are known to generate internal heat, contributing to changes in the battery's temperature. This internal heat generation can be attributed to various factors, including ohmic heat, mixing heat, enthalpic heating, and the entropy change that occurs during the electrochemical process.[12]. The electrochemical process is endothermic during charging and exothermic during discharging[26]. One of the problems in using lithium-ion batteries in EVs and HEVs is the internal generation during charge and discharge cycles. As a result, to resolve these discrepancies, BTMS plays a vital role in battery life and overall performance. Many researchers have devoted their efforts to the thermal management of electric vehicle batteries[25].

1.3 BATTERY THERMAL MANAGEMENT DESIGN

Battery thermal management is the process of regulating the temperature of a battery in order to improve its performance and extend its lifespan. This is typically accomplished by using a combination of passive and active cooling methods, such as thermal insulation and cooling fans. The design of a battery thermal management system must take into account the specific characteristics of the battery and its intended use, as well as the operating environment in which it will be used. Proper battery thermal management is important for ensuring the safe and reliable operation of batteries in a wide range of applications, including electric vehicles and renewable energy storage systems.

Battery thermal management systems are not without limitations. Some of the challenges and limitations that can be associated with battery thermal management include the following:

a. Cost: The use of active cooling systems, such as cooling fans or liquid cooling systems, can add to the cost of a battery and its thermal management system.
b. Weight: Cooling systems and other thermal management components can add weight to a battery, which can be a particular concern in applications such as electric vehicles where weight is a critical factor.
c. Complexity: Battery thermal management systems can be complex, requiring careful design and integration with the overall battery system. This can increase the overall complexity of the battery and its associated systems.
d. Inaccurate temperature sensing: Inaccurate temperature sensing can lead to incorrect control of the thermal management system, which can in turn result in inefficient cooling or even overheating of the battery.
e. Limited cooling capacity: In some cases, the cooling capacity of a thermal management system may be inadequate to effectively cool the battery, particularly under high-power or high-temperature operating conditions.

Overall, the challenges and limitations of battery thermal management systems must be carefully considered in the design and implementation of these systems in order to ensure their effectiveness and reliability. [27] , The BTMS design must account for cell surface temperature fluctuations as well as cell-to-cell internal variance, which makes it difficult for the BTMS design to decrease aging and improve battery life [14].

1.4 BATTERY AGING AND THE EFFECT OF OVER

battery aging refers to the gradual decline in a battery's performance and capacity over time. This is a natural process that occurs as a result of repeated charging and discharging of the battery, as well as other factors such as the operating temperature and the depth of discharge. Battery aging can affect the performance and lifespan of the battery, and is an important consideration in the design and use of battery-powered systems.

Overcharging a battery can accelerate the aging process and reduce its lifespan. This occurs because overcharging a battery causes an excess of electrical current to flow through the battery, which can cause chemical reactions within the battery that produce heat and degrade the battery's materials. Overcharging can also cause the battery to become excessively hot, which can further accelerate the aging process and increase the risk of thermal runaway, in which the battery's temperature rapidly increases out of control. In general, it is important to avoid overcharging a battery in order to maintain its performance and extend its lifespan.

aging is the gradual deterioration of a LIB as shown by capacity and power fading, as well as increased internal resistance and impedance [15], [27],[18], Several physical and chemical factors affect the electrodes, electrolyte, separator and current collectors, causing aging [17], [28], shows the levels involved in the cause and effect analysis of aging in LIBs[14], [28].

Table 1.1: Levels Engaged in the Examination of the Cause and Impact of Aging in LIBs.

Level	Description
Generates	Time, temperature, SOC, current load, stoichiometry, and mechanical stress are all stress variables[14].
Methods	SEI development, SEI decomposition, electrolyte decomposition, binder decomposition, graphite exfoliation, structural disordering, lithium plating, loss of electric contact, electrode particle cracking, transition metal dissolution, and current collector corrosion[14][28]

Table 1.1: Levels Engaged in the Examination of the Cause and Impact of Aging in LIBs "Table Continued".

Impacts	In terms of the chemical properties of batteries, two significant factors that can impact their performance and lifespan are the loss of available lithium inventory and the loss of active materials. Lithium inventory loss refers to the gradual reduction of the amount of lithium within the battery over time due to various factors such as cycling, storage conditions, or elevated temperatures. Active material loss, on the other hand, refers to the degradation or depletion of the cathode and anode materials that make up the core of the battery, which can also occur gradually over time and is often linked to factors such as cycling, overcharging, or exposure to corrosive environments.[28]
	Performance: Capacity and decrease in energy, resistance, and impedance increase[28]

Tiny volume changes during cycling, corrosion of the current collector, electrolyte breakdown, and dissolution of the active component in the electrolyte all contribute to the aging of the positive electrode or cathode[29].Aging produces a reduction in porosity in the separator as a result of SEI production and development[20].To maintain adequate ionic conductivity in the electrolyte, the separator must have an acceptable porosity level[21].Because of the intricacy of the aging phenomenon, physics-based models can only include the dominating processes at the cell level, such as SEI creation and development and lithium plating[15], [22]–[24], [28].

1.5 BATTERY THERMAL MANAGEMENT TECHNOLOGIES

There is a lot of options when selecting BTMs for a battery packs. The graphic below depicts an overview of the key TMT that are commercially available or being researched by the scientific community.

The first main categorization of BTMS corresponds to those systems that have fluid in motion and those that do not. It knowns as active BTMs and passive BTMs.

1.5.1 Active BTM System Methods

Active Battery Thermal Management Systems (BTMS) play a crucial role in ensuring the safe and efficient operation of battery systems across various applications, including electric vehicles, stationary energy storage systems, and portable electronics[30]. The function of BTMS is to regulate the temperature of the battery, which is one of the most critical factors that can affect the performance and life of the battery.

Several studies have been conducted to review the recent advancements in BTMS. In a comprehensive review Zhang and Wang [31] discuss the different thermal management methods and their suitability for various applications. Rao and Wang [32] reviewed and discussed the methods of thermal energy management in power batteries.

Another relevant study is by Liu et al. [33]. In this study, the authors discussed various thermal management strategies, including passive and active cooling methods, as well as design considerations for selecting the appropriate thermal management system for a given application.

Jia and Li [34] reviewed, discussing the recent advancements in active BTMS and the use of liquid cooling, phase change materials, and heat pipes. They also discussed the challenges and limitations of these methods.

Kim et al. [35] conducted a review on, discussing the challenges of thermal management in electric vehicles and the various cooling methods used for BTMS. They also discussed the benefits and drawbacks of each method.

The above-mentioned studies highlight the importance of BTMS in ensuring the safe and efficient operation of battery systems. The choice of the method depends on the application requirements, operating conditions, and system constraints. Further research and development of BTMS are necessary to enhance their performance and efficiency.

Active Battery Thermal Management Systems (BTMS) play a crucial role in ensuring the safe and efficient operation of battery systems in various applications, including electric vehicles, stationary energy storage systems, and portable electronics. They are designed to regulate the temperature of the battery, as temperature is one of the most critical factors affecting battery performance and life.

1.5.1.1 Advantages of active BTMS

a. Improved Battery Performance: Active BTMS regulate the temperature of the battery, which helps to improve its performance and increase its life.

b. Enhanced Safety: By regulating the temperature of the battery, active BTMS prevent overheating, which can cause safety concerns such as thermal runaway and fire.

c. Increased Efficiency: Active BTMS help to reduce the heat generated by the battery, which can improve the overall efficiency of the system.

d. Better Control: Active BTMS provide better control over the temperature of the battery, which helps to maintain its performance and life.

1.5.1.2 Disadvantages of active BTMS

a. Complexity: Active BTMS are more complex than passive BTMS, which can lead to higher costs and more maintenance.

b. Additional Power Consumption: Active BTMS consume additional power, which can reduce the overall efficiency of the system.

c. Space Requirements: Active BTMS may require additional space, which can be a constraint in some applications.

d. Limited Compatibility: Active BTMS may not be compatible with all battery systems, which can limit their use.

1.5.2 Passive BTM System Methods

Passive Battery Thermal Management Systems (BTMS) are systems that use natural convection, conduction or phase change materials (PCMs) to regulate the temperature of batteries. Unlike active BTMS, passive BTMS do not use external power sources to cool the battery, making them more energy efficient and cost-effective[30].

One example of a passive BTMS is described in the article [36]. This article discusses the use of water adsorbent materials that can absorb heat and release it at a slower rate, helping to regulate the temperature of lithium-ion batteries in electric vehicles. The authors found that the system was able to significantly reduce the temperature of the battery, leading to improved performance and longer lifespan.

Bandhauer [37] describes a passive BTMS that uses microscale liquid-vapor phase change materials. This system is able to absorb heat generated by the battery and release it slowly, helping to regulate the temperature of the battery. The authors found that this system was able to improve the performance and lifespan of the battery, compared to batteries without thermal management.

El Idi et.al [38] investigates the use of PCM composites for passive BTMS. The authors found that the use of PCM composites was able to effectively regulate the temperature of the Li-ion battery, leading to improved performance and longer lifespan. In conclusion, passive BTMS are an effective way to regulate the temperature of batteries, without the need for external power sources. The use of materials such as water adsorbents, microscale liquid-vapor phase change materials and PCM composites can significantly improve the performance and lifespan of batteries[39].

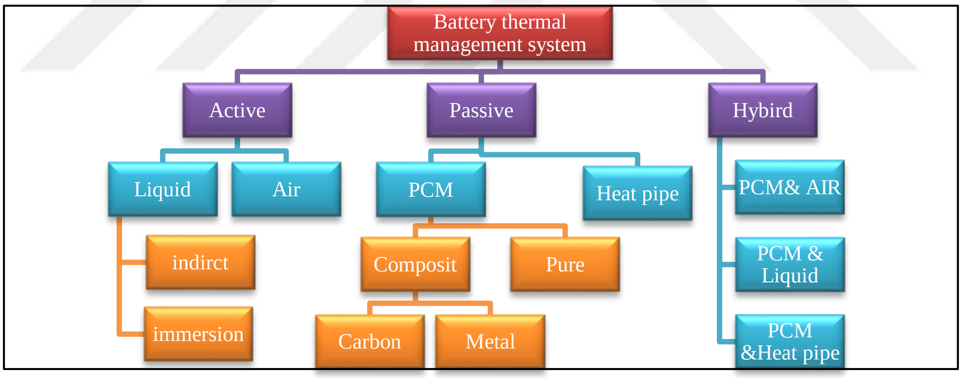

Figure 1.4: Battery Thermal Management System Tree and Main Types Cooling Systems Technology.

1.6 TYPES AND METHODS OF LIQUID COOLING SYSTEMS FOR LIB'S

Liquid cooling method is one of indirect cooling methods depending on the contact the medium to the surface of the LIB's, direct cooling such as the immersion method where the LIB's contact with cooling medium directly. most of studies had waterproofing requirement and noted the problems such as short circuit and chemical reaction. Indirect cooling have five method to cooling the LIB's pack such as (Liquid jacket cooling, Cold plate cooling, Mini/Micro channel cooling, Serpentine channels cooling plates).[40]–[42].

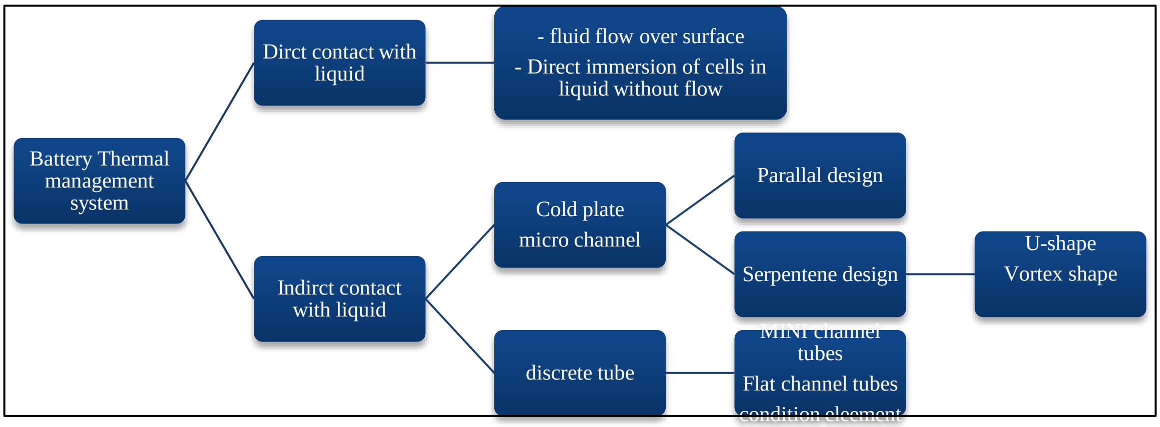

Figure 1.5: Classification of Battery Thermal Management System.

1.7 TYPES OF LIQUID COOLING

The most effectively method to cooling battery is liquid cooling and it different between the types of batteries like rectangular or cylindrical, and the fluid properties should be not conductive that mean it's not conduct between any part of the system or make oxidation in system and low cost. water, oil, glycol, acetone, and other materials are among the usually utilized heat transfer fluids.[43], Liquid cooling mothed provide it high effective way with many different systems and techniques compared to varies techniques like air or air-liquid.

The BTMS cooling system is utilized to preserve the battery from overheating. Due to their inexpensive cost, simple structure, high stability, and strong heat transmission capabilities, air and liquid are extensively utilized coolants. The model is based on three basic equations.

Continuity equation (1.1), Momentum equation (1.2), energy equation(1.3).[44].

$$\nabla . v = F \tag{1.1}$$

$$\frac{\partial \vec{V}}{\partial t} + (V \cdot \nabla)\vec{V} = -\frac{\nabla P}{\rho f} + \frac{\mu}{\rho f} \nabla 2 . \vec{V} + g + F \tag{1.2}$$

$$\rho_f \cdot c_p \cdot \frac{\partial T}{\partial \tau} + u \cdot \frac{\partial T}{\partial x} + v \cdot \frac{\partial T}{\partial y} + w \cdot \frac{\partial T}{\partial z} = \lambda_f \cdot \frac{\partial^2 T}{\partial x^2} + \frac{\partial^2 T}{\partial y^2} + \frac{\partial^2 T}{\partial z^2} + q12 \quad (1.3)$$

This equation takes into account several key factors that contribute to the heat transfer process. These include the coolant's density (ρf), thermal conductivity (λf), and specific heat (cp), as well as the velocity vector of the coolant (V), the dynamic viscosity (μ), the static pressure (P), the gravitational body force (g), external body forces (F), and the rate of heat generation (q) [45].

The BTMS's cooling performance is highly influenced by the flow cycles [46]–[50] and flow rate[51]–[57], both of which may be modified. When efficiency, cost, and battery module area are taken into account, the above BTMS offer distinct benefits [58].

1.8 MINI CHANNEL

Mini channels have become a topic of interest in the field of microfluidics due to their potential in various applications, such as chemical synthesis, biomedical diagnostics, drug delivery, and environmental analysis. However, one significant application of mini-channels is in the development of thermal management systems for high-power lithium-ion batteries.

In recent years, several studies have investigated the use of mini-channel thermal management systems for high-power lithium-ion batteries. Huo et al [59] used a mini-channel cold plate for power battery thermal management and investigated the thermal performance of the system. The authors found that the mini-channel cold plate had high cooling efficiency and low thermal resistance.

Nanofluids have also been studied for their effectiveness in mini-channel thermal management systems for high-power lithium-ion batteries. Liu et al [60] investigated the use of nanofluids and found that they significantly enhanced the heat transfer rate and reduced the thermal resistance of the system.

In addition, Yang et al [61] integrated mini-channel liquid cooling and air cooling in a thermal management system for cylindrical lithium-ion batteries. They found that the combination of the two cooling methods provided better thermal performance than either method alone.

Three-dimensional thermal modelling has also been used to study the thermal performance of mini-channel cooling systems for high-power lithium-ion batteries. Li, Zhou and Wu[62] developed a model to study the cooling of a Li-ion battery cell and a 50 V Li-ion battery pack using a mini-channel cold plate. The authors found that the mini-channel cold plate had excellent cooling performance and could effectively control the temperature of the battery pack.

Recently, Mashayekhi et al [63] investigated the development of a hybrid cooling method using PCM and Al2O3 nanofluid in aluminium mini-channels for the thermal management of Li-ion batteries. The authors found that the combination of PCM and nanofluid resulted in improved thermal performance of the cooling system.

In conclusion, mini-channel thermal management systems have shown great potential for high-power lithium-ion batteries, and the use of nanofluids and hybrid cooling methods can enhance their thermal performance. Further studies are needed to optimize the design of mini-channel cooling systems for different applications.

The development of thermal management systems for high-power lithium-ion batteries is crucial for the efficient and safe operation of these batteries. Mini channels offer a promising solution for thermal management due to their high heat transfer rates and compact size. The studies mentioned above have demonstrated the potential of mini-channel thermal management systems for high-power lithium-ion batteries, and the use of nanofluids and hybrid cooling methods can further enhance their thermal performance[64]. These findings could have significant implications in the development of high-performance batteries for various applications.

Mini channel is one of types cooling system for lithium-ion battery cooling, this part we discussed a lot of paper that deal with mini channel system for cooling lithium-ion battery end cylindrical type.

most of studies deal with rectangular battery with mini channel, The effect of introducing nanoparticles is more noticeable in fluids with reduced heat conductivity, particularly engine oil [60].

There is base several fluids such as water, ethylene glycol (EG), and engine oil (EO) are researched and compared.[60]

$$\text{Using the formula } h_{s=}\dot{Q}.As\,(T_{max} - T_f) \quad (1.4)$$

The heat transfer coefficient between the fluid and the battery is calculated (4) coolant inlet velocity.

$$h_{s=}\frac{\dot{Q}}{A_s\,(T_{\,max} - T_f\,)} \quad (1.5)$$

Where $\dot{Q}$ and T_f calculated by:

$$\dot{Q} = \dot{m}c_p\,(T_{out} - T_{in)} = \rho.V_{in}.A_{in}.c_p(T_{out} - T_{in}) \quad (1.6)$$

$$T_f = \frac{(T_{out} - T_{in})}{2} \quad (1.7)$$

1.9 FLUID USED IN MINI CHANNEL OF BTMS (REVIEW)

The choice of fluid used in a mini-channel thermal management system (BTMS) plays a critical role in determining its thermal performance. Different fluids have different thermal properties, such as thermal conductivity, heat capacity, and viscosity, which can significantly affect the efficiency of heat transfer in a mini- channel. In this regard, the type of fluid used in a mini-channel BTMS should be carefully selected based on the specific application and the desired thermal performance.

Common fluids used in mini-channel BTMS include water, ethylene glycol, and oil-based fluids. Water has a high thermal conductivity and low viscosity, making it an efficient heat transfer fluid in mini- channels. Ethylene glycol is commonly used as a coolant in automotive applications due to its high boiling point and low freezing point. Oil-based fluids, such as mineral oil or synthetic oils, are used in high-temperature applications due to their excellent thermal stability and low flammability.

Nanofluids, which are suspensions of nanoparticles in a base fluid, have also been studied for their potential to enhance the thermal performance of mini-channel BTMS. Liu. H et al[60].investigated the use of nanofluids in mini-channel thermal management systems for high-power lithium-ion batteries and found that they significantly enhanced the heat transfer rate and reduced the thermal resistance of the system.

In conclusion, the choice of fluid used in a mini-channel BTMS should be carefully considered to optimize its thermal performance. Water, ethylene glycol, and oil-based fluids are commonly used in mini-channel cooling systems, and the selection of the appropriate fluid depends on the specific application and the desired thermal performance. Nanofluids also offer a promising solution for enhancing the thermal performance of mini-channel BTMS, and further research is needed to optimize their properties for different application.

Here is a table summarizing the different fluids used in cooling by mini-channel BTMS, along with a brief review of the related articles:

Table 1.2: Summarizing the Different Fluids Used in Cooling by Mini-Channel BTMS.

Fluid	Advantages	Disadvantages	Key findings	Related Articles
Water	High thermal conductivity, low cost, widely available	Corrosive, high freezing point	Water with nanofluids improved heat transfer coefficient [60] . Water cooling had better cooling performance than air cooling for cylindrical lithium-ion batteries [65]	[60][65]
Nanofluids	Enhanced thermal properties, high stability	High cost, potential toxicity	The higher cooling performance of the circulated nanofluid BTMS can be attributed to the higher velocity of the nanofluid flow and the increased heat transfer coefficient.	[66]
Ethylene glycol	High boiling point, good lubrication properties	Lower heat capacity than water, more expensive	The study found that using EG in the BTMS resulted in a higher overall heat transfer coefficient compared to air-cooling. This suggests that the EG-cooled BTMS has a more efficient cooling process due to a higher heat transfer rate	[67]

Table 1.2: Summarizing the Different Fluids Used in Cooling by Mini-Channel BTMS "Table Continued".

Propylene glycol	Non-toxic, good lubrication properties, high boiling point	Lower heat capacity than water, more expensive	use of propylene glycol led to a higher pressure drop in the cooling system, which may need to be considered in the design of BTMS.	[67]
Hydrofluoroether (HFE)	High thermal conductivity, non-flammable, low global warming potential	High cost, potential toxicity	The HFE-7000 system provided better cooling performance under high discharge rates and higher ambient temperatures.	[57]

1.10 T_{MAX}, ΔT_{MAX} FACTORS

The anticipated rate of heat generation has a notable impact on the maximum temperature (T_{max}) and temperature differential (ΔT_{max}) curves [68]. The ΔT_{max} between scenarios employing distinct fluids demonstrated the maximum temperature and temperature decline between the inlet and outlet to BTMS, achieving the desired temperature and enhancing the heat transfer rate between the batteries and cooling mini channels. Therefore, careful consideration must be given to the anticipated rate of heat generation when optimizing the performance and efficiency of battery thermal management systems.[60]

When battery modules are subjected to high discharge rates, a higher level of heat dissipation is necessary. This increased rate of heat dissipation results in elevated power consumption. Therefore, careful consideration must be given to the heat dissipation requirements of battery modules operating at high discharge rates in order to optimize their performance and ensure their safe and reliable operation[69].

N equally spaced Li-ion cells are closely encircled by coolant as they are arranged in a staggered pattern, minimizing the thermal resistance between the coolant channel and the cells. With a mass flow rate of and a temperature of Tw,0 , cold coolant enters the channel at the intake, After absorbing heat from the cells, the coolant exits the channel with a temperature of Tw,N [70].

$$N.Qc = m\ d \times Cp(T_{w,N} - T_{w,0}) \tag{1.8}$$

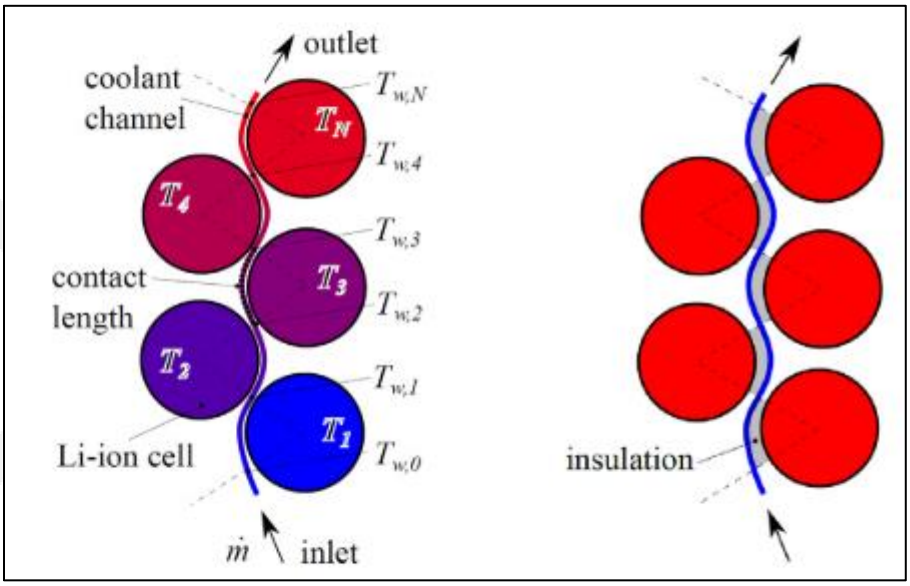

Figure 1.6: The Wave Channels and Analysis the Thermal Performance[70].

1.11 PREVIOUS WORKS

Previous research has focused on utilizing mini-channels in liquid cooling for high power lithium-ion batteries[64]. Several studies have investigated the use of nanofluids to enhance the cooling performance of mini- channels.

One study by Jilte et al. [66] investigated the cooling performance of nanofluid submerged and nanofluid circulated battery thermal management systems. The results showed that the use of nanofluids led to a significant improvement in cooling performance, with a reduction in maximum temperature of up to 10°C compared to pure water.

Another study by Tousi et al. [68] conducted a numerical investigation on a novel liquid-cooled thermal management system for cylindrical Li-ion battery packs under high discharge rate based on AgO nanofluid and copper sheath. The results demonstrated that the proposed cooling system achieved a more uniform temperature distribution and lower maximum temperature compared to traditional air cooling and water-cooling systems.

Chen et al. [71] also conducted a numerical investigation on a unitization-based thermal management system for cylindrical lithium-ion batteries. The results showed that the unitization-based system achieved better cooling performance than the traditional air cooling and liquid cooling systems, with a maximum temperature reduction of up to 7.8°C.

In addition, a study by Yang et al. [72] experimentally studied the liquid immersion cooling for 18650 lithium-ion batteries under different discharging conditions. The results showed that the cooling performance of the immersion cooling system improved with increasing discharge rate, and the maximum temperature of the battery was reduced by up to 11.7°C compared to natural cooling.

Finally, a study by Kim et al.)[54] investigated the effectiveness of nanofluids on the mini-channel thermal management for high power lithium-ion batteries. The results showed that the use of nanofluids led to a significant improvement in heat transfer performance, with a heat transfer enhancement of up to 30%.

2. BATTERY THERMAL ENERGY MANAGEMENT

2.1 METHODS

Two main problems cause heat raising in batteries produced during the charging and discharging and that effecting directly to the performance of the batteries and the threshold of temperature that is designed for it, another possibility is that the battery pack's temperature gradient distributions will cause localized degeneration[43].

Most of the studies used a thermal management system to optimize the performance of the batteries pack/module by:

a. Reduce small temperature differences within cells and modules.

b. Packaging is compact, lightweight, easy to pack, reliable, inexpensive, and easy to maintain.

c. Used thermal sensors to measure highly accurate and instantaneous temperature change measurements and indicate.

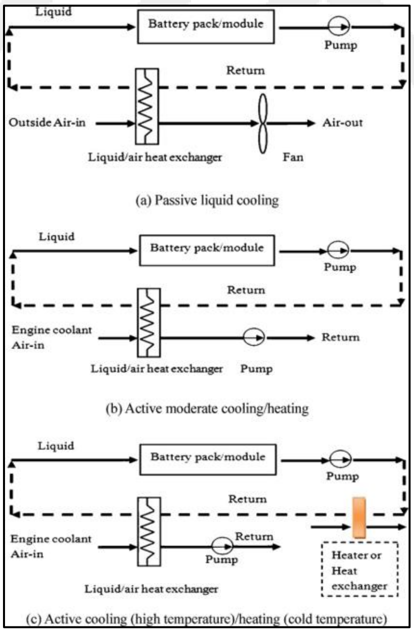

Figure 2.1: Thermal Management System Using (a) Passive Methods/Liquid Cooling. (b)Active Moderate /Heating. (C) Active Cooling [32].

2.2 EFFECT OF HEAT GENERATION ON LIB'S PERFORMANCE

The LIB's cells lost more than 60% of internal energy power at 50◦C after 800 cycles and lost 70% at 55◦C after 500 cycles[73] [74], [75]. also, the LIB's cells are affected to the low temperature in cold environment, and it reduce the chemical reaction between anode and cathode (ionic conductivity) and increase the internal resistance of the battery cause the drainage in the energy of cells[73][76].

2.3 THERMAL EFFECT ON LI- ION BATTERIES

Lithium-ion battery operating and/or storage temperatures have an impact on the functionality, lifespan, and safety of the batteries. An overview of the main thermal problems that need thermal management of lithium-ion batteries is given in this section. These include electrical imbalance between several cells in a battery pack, capacity/power decline, thermal runaway, and low temperature performance. The effect of temperature on each of these occurrences is highlighted. Additionally, the discussion covers the relationship between electrochemical processes and transport phenomena, which in turn impact temperature. Critical research gaps in thermal management strategies may be found by highlighting and discussing studies in each area. [18].

3. THE FACTORS CONTROL TO PERFORMANCE OF LIB'S PACK

3.1 HEAT GENERATION

LIBs, heat is produced by three different processes: joule heating, also known as ohmic heating, which restricts electron motion; electrode reactions, which result from a charge transfer between the electrodes and the electrolyte; and entropic heating[16], [27] Heat generated through intercalation and de-intercalation reactions at the electrode-electrolyte interface are capable of being reversed, whereas heat produced through Joule heating is permanent. The source of heat generation through intercalation and de-intercalation is reversible, but the heating caused by Joule heating is irreversible.[77].

The quantity of heat produced by Joule heating is estimated as follows[27][78]:

$$q^{\circ}=\mu \cdot \Delta \mathring{U}^{2} \tag{3.1}$$

The following presumptions serve as the foundation for the heat transfer equations used in the battery model. Battery temperature up as a result of resistive heating (I2R) and heat production (Qess-gen) occurring in the battery's core, The heat is transferred from the battery to the air or other fluid surrounding it after passing through the material of the casing [79].

There are several elements that effect both reversible and irreversible heating are:

Ambient temperatures: Since polarization losses are greater at lower temperatures, more irreversible heat is generated, heat generation rates rise faster at lower ambient temperatures and higher discharge rates [77].

SOC: According to the entropic coefficient, heat generation rates rise with low SOC (25%) and high DOD (> 75%). Increased overpotential caused by high discharge rates (C-RATE > 2C) leads to a rise in the production of irreversible heat.[77]

Charge and discharge C-rate: As the rate of charging and discharging increases, the heat generation rate also rises. At high charging and discharging rates (above 1C), the predominant source of heat is Ohmic heating. Conversely, at low rates (1C or less), the main contributor to heat generation is the reversible reaction between the electrode and electrolyte[77].

Electrodes microstructure: The microstructure of electrodes can impact the amount of heat generated within the electrodes and the temperature inside the cell. If the electrodes have low porosity, this can result in higher Joule heating rates in the electrolyte and a higher likelihood of hot spots near the electrode-separator interface[77].

3.2 THE IMPACT OF C-RATE ON BATTERY LIFE AND PERFORMANCE

The amount of current used to measure how fast a battery charges and discharges is known as the battery C Rating.

A battery's capacity is typically listed and rated at 1C rate (1C current), which means a fully charged battery with a capacity of 10Ah should be able to deliver 10 Amps for an hour.

The amount of heat produced by Li-ion battery cells is greatly influenced by the discharge rate, temperature of the surrounding environment, and the depth of discharge[80].

the C-rate should be specific in experiments such as (0.5,1,2,3,4,5 C-rate), and this expression for the time of energy consume during load of discharging.

5C most cause rising in the heat of LIB's because the high drainage in energy in short time so most of the experiment depended on DOD method for efficient energies for LIB's.

C-rate	5C	2C	1C	0.5C	0.2C	0.1C	0.05C
Time	12MIN	30MIN	1HOUR	2HOUR	5HOUR	10HOUR	20HOUR

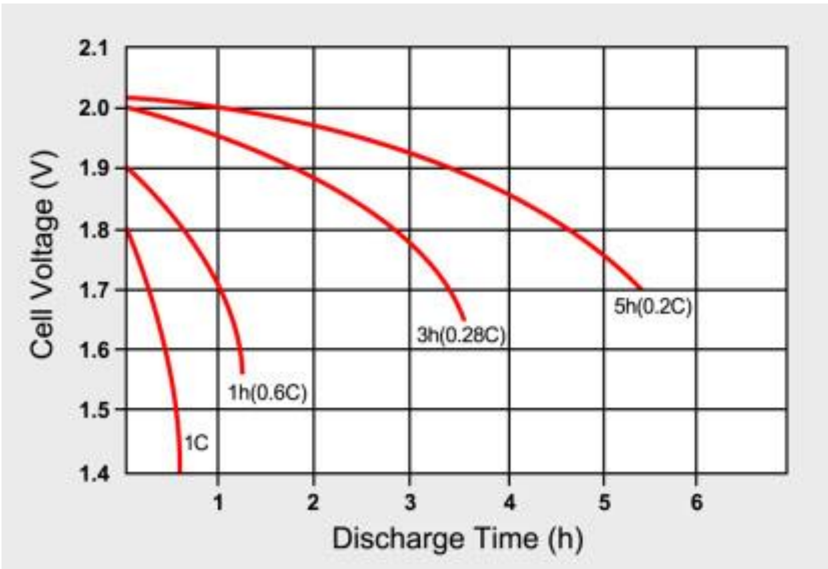

Figure 3.1: C-rate and the Time of Discharge with Voltages.

3.3 FLOWRATE IMPACT FACTORS IN BTMS

The cooling fluid flowrate is one of important factor that can control to reduce the thermal effect to the LIB's pack during load or charging /discharging states, the flowrate most be calculated depending on the number of LIB's[81].

The flowrate can be controlled in EV's by electrical pump that manage the volumetric flow through the system and make the system be highly performance depending on the temperature of the fluid which is already affect to the state of LIB's pack (load/unload, charging /un-charging).

The results of the battery cooling system are impressive, as demonstrated by the highest temperature and temperature difference in the battery pack being 305 K and 1.07 K respectively, with a coolant inflow velocity of 0.28 m/s during discharge. To enhance the performance of the liquid cooling channel system, increasing the coolant flow rate is an effective solution[68].

concluded that a better cooling effect can be achieved in a battery pack by reducing the cell spacing and increasing coolant flow rate.[82]. They come to the conclusion that if the flow rate of the liquid-cooled plate is sufficient, Under short circuit conditions, the temperature and temperature gradient of the battery pack can be effectively kept within an acceptable range[62].To meet a battery pack's cooling needs in some harsher circumstances, the cooling effect can be improved by increasing coolant flow rate.[18], [62]. In additional, Li-ion battery pack's cooling media, mineral oil, has undergone testing. The maximum battery temperature for a single cell was maintained at flow rates of 32.8 °C, 30.8 °C, and 30.6 °C. The temperature of the cell dropped from 0.89 °C to 0.42 °C when the flow rate was increased from 1 L/min to 10 L/min, indicating that lower flow rates are adequate for performance,[83].

4. SIMULATION

4.1 INTRODUCTION

The simulations model is involved in six batteries as a section of the pack batteries and that show the heat distribution of heat a long of the battery and the effect of the BTMS to reduce the heat generated in batteries when it starts to discharge of in load.

Where our BTMS is effective to reduce the risk of overrun and control to prevent the heat generation excessed the limitations temperature (25 ˚C – 40 ˚C), where the batteries were excessed the 37℃ and the low temperature was at 27.39 ˚C, and that be perfect to improve the performance of batteries pack at excessive temperatures and be in the standard of range the batteries design for it.

In this simulation's we set the temperature we get it in experiment and the coil be distributed in 5 rows along the battery two in one side and three in other side ZAGZAG method and the results was balance in the thermal distribution.

4.2 MODELLING

The model of cell simulated is 18650 lithium-ion battery and the specifications of manufacture in where the dimension of battery is:
OD :18mm, length: 65mm, weight :45g, Voltage :3.7V, capacity :2200 mAh.
To model the battery type 18650 cylinder in ANSYS, you would typically start by creating a three-dimensional geometry of the battery cell. The geometry accurately represents the size and shape of the cell, including the cylindrical shape and the dimensions of the positive and negative electrodes the positive electrode shape was neglected and considered the battery as cylinder to avoid To avoid distortions in the shape and change the results of the thermal analysis, the shape and mesh were simplified geometry was design and creating in the SOILDWORKS as first step in producer of simulation, and would need to define material properties for the battery cell, it selected as aluminium alloy for outer cover of battery shield, and including the thermal conductivity (0.144 to 0.165 W/mm.℃), heat capacity constant pressure (8.75 e +05 mJ/kg·°C) , and density (2.77e-06 kg/mm³) . and materials properties of pipes selected copper alloy as the material of pipe which is already used in practical works

and it was isotropic thermal conductivity (0.401W/mm·°C), specific heat constant pressure (3.85e+05 mJ/kg·°C), density (8.3e-06 kg/mm³).

In ANSYS, the mesh is a crucial component in the simulation of an 18650 lithium-ion battery. The mesh should be fine enough to capture the details of the battery's geometry. In the case of an 18650 battery, a cylindrical mesh would be appropriate. And the size of mesh selected to be suitable for short, created time and element size selected (0.9 mm) (see Figure 4.1)it takes about 10minutes for all part of battery and pipes.

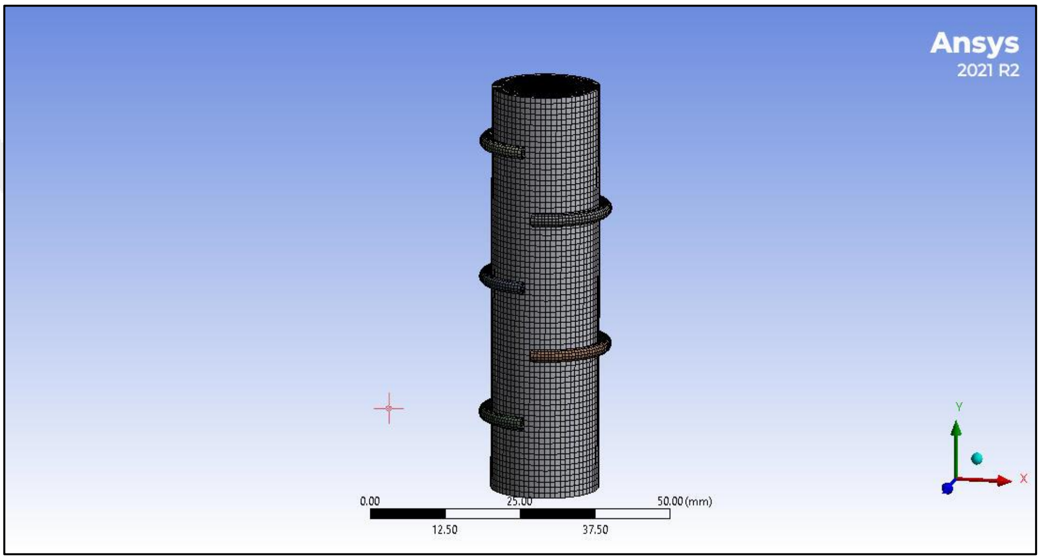

Figure 4.1: Geometry Mesh size 0.9 mm for Battery Type 18650.

Set up the boundary conditions for the simulation involve specifying the initial temperature of the cell at each different test during different Crate and load of discharge, the heat generation rate inside the cell neglected, and the cooling mechanism that is being used to remove the heat from battery to the cooling pipes. In addition, the simulation involved add heat flow from high temperature represented to battery to the lowest temperature represented to the cooling pipes surrounding to the battery as a cooling coil.

Finally, you can run the simulation and analyse the results to determine the temperature distribution and thermal behaviour of the battery cell. This information can be used to optimize the design of the battery cell and the cooling system, to improve its performance and reliability.

4.3 SIMULATION SINGLE CELL BATTERY WITH Z5A COOLING SYSTEM

The simulations model is involved in one battery cell as represented the pack batteries and that show the heat distribution of heat a long of the battery and the effect of the BTMS to reduce the heat generated in battery when it starts to discharge of in load.

The simulation involved five different states for analysis the thermal steady state simulations, it represented the heat flow from the battery to the surrounding area and the effect of cooling system to the battery temperature and how it reducing the heat raising, all geometry and mesh size mention above.

Below is the simulation for (1, 0.6, 0.667, 0.7, 0.88) C-rate all information provided in ANSYS report, The Reports attached in appendixes.

4.3.1 Single Battery Under 1 C-Rate

The simulation involved the temperature of battery which is set as(29.4℃) and the copper pipes temperature set as (25℃) the heat flow set as (6.8 w) and the duration of test in experiment work was at 1 C-rate for discharge ,the Figure 4.2, Figure 4.3 shown thermal distribution along the battery and the effect of pipes to the temperature of battery .(Reported).

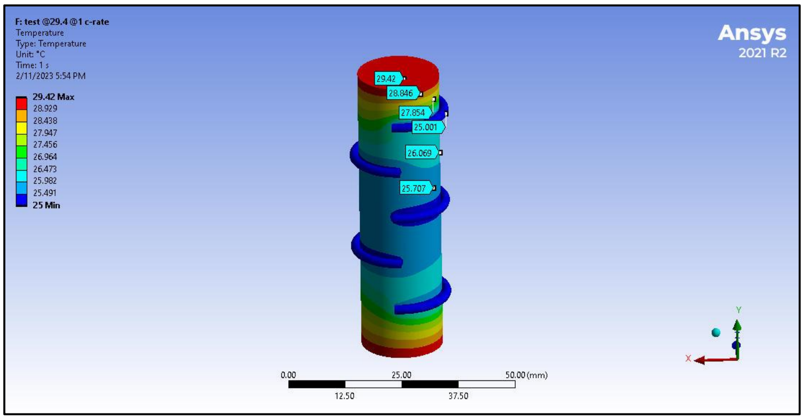

Figure 4.2: Show the Reaction of Lithium Battery at 1 Crate 29.4℃ and the Change in Temperature as Result of Cooling Coil.

Below is the section along of battery and show the effect of pipe to reduction the temperature of battery.

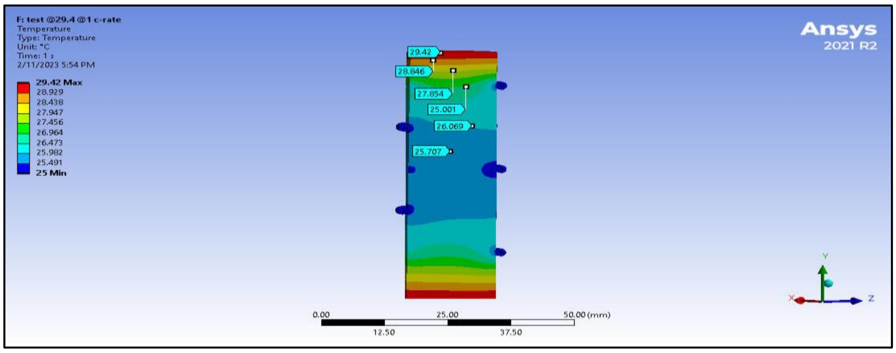

Figure 4.3: Battery Section Show the Heat Distribution Inside the Battery and Maximum, Minimum Temperatures.

(Figure 4.4) Below is the heat flux distribution at area tangent between the battery and the pipe at 29.4°C, 1 C-rate and the result shown the rage between 0.961 w/mm2 and 0.427 w/mm2.

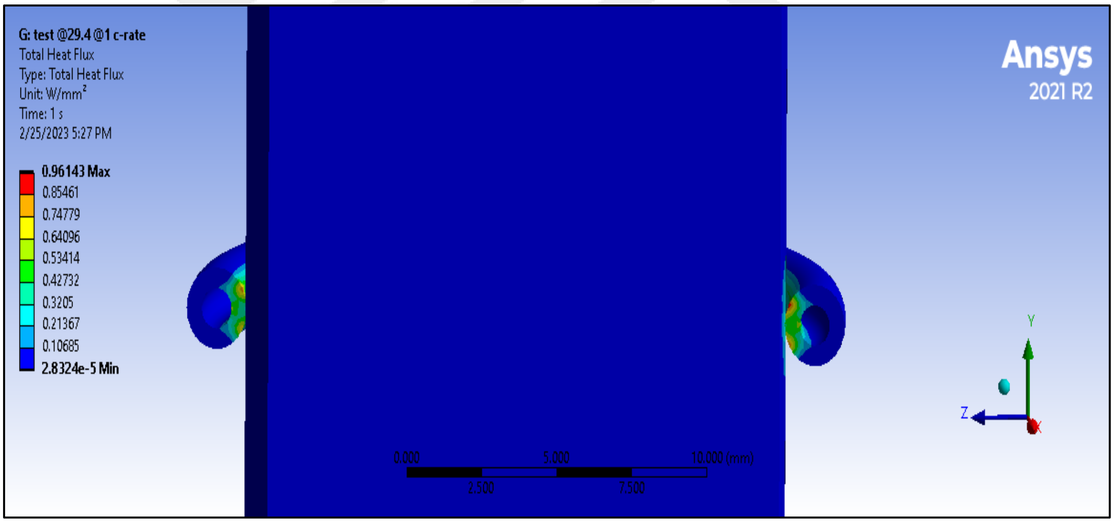

Figure 4.4: Heat Flux for Lithium ION Battery Section at 1 c Rate and 29.4°C.

4.3.2 Single Battery Under 0.6 C-Rate

The simulation involved the temperature of battery which is set as(35°C) and the copper pipes temperature set as (25°C) the heat flow set as (6.8 w) and the duration of test in experiment work was at 0.6 C-rate for discharge , figure (Figure 4.5, Figure 4.6) show thermal distribution along the battery and the effect of pipes to the temperature of battery (Reported).

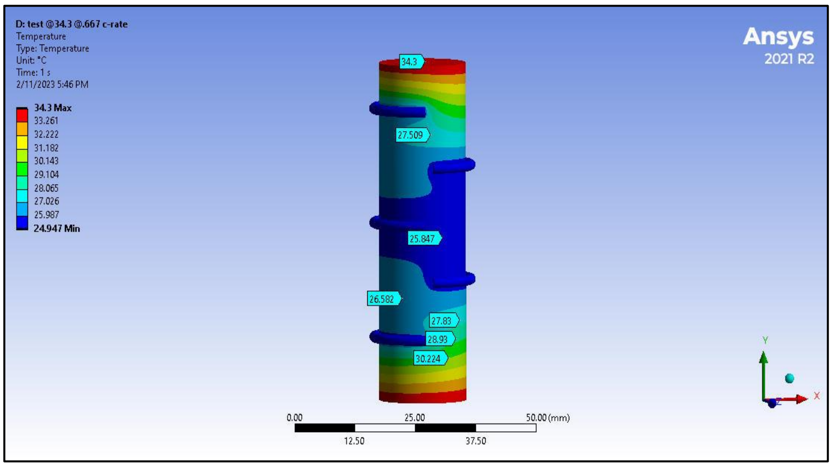

Figure 4.5: Show the Reaction of Lithium Battery at 0.6 Crate 31.14℃ and the Change in Temperature as a Result of Cooling Coil.

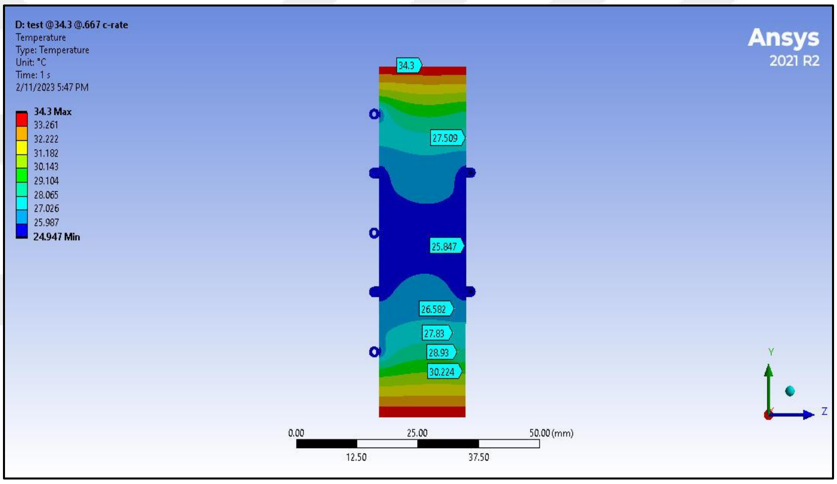

Figure 4.6: Show the Reaction of Lithium Battery-Section-at 0.6 Crate 31.14℃ and the Change in Temperature as a Result of Cooling Coil.

Below (Figure 4.7) is the heat flux distribution at area tangent between the battery and the pipe at 31.14℃, 0.6 Crate and the result shown the rage between 0.23431 w/mm^2 and 0.30864 w/mm^2.

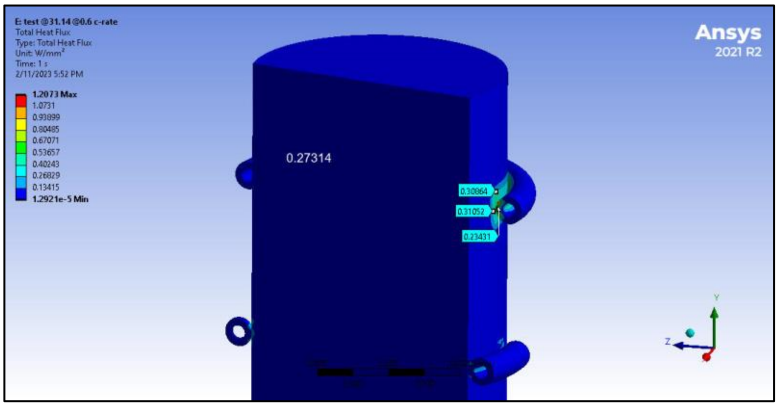

Figure 4.7: Heat Flux Distribution in Area that Tangent Between the Battery and the PIPE at 31.14℃, 0.6 Crate.

4.3.3 Single Battery Under 0.667 C-Rate

The simulation involved the temperature of battery which is set as(34.3℃) and the copper pipes temperature set as (25℃) the heat flow set as (6.8 w) and the duration of test in experiment work was at 0.667 C-rate for discharge , figure (Figure 4.8,Figure 4.9) show thermal distribution along the battery and the effect of pipes to the temperature of battery (Report appendix .3).

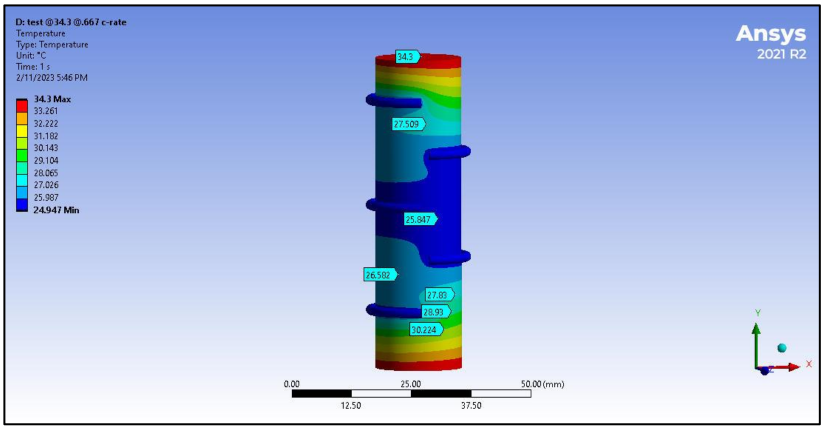

Figure 4.8: Show the Reaction of Lithium Battery at 0.667 Crate 34.3℃ and the Change in Temperature as a Result of Cooling Coil.

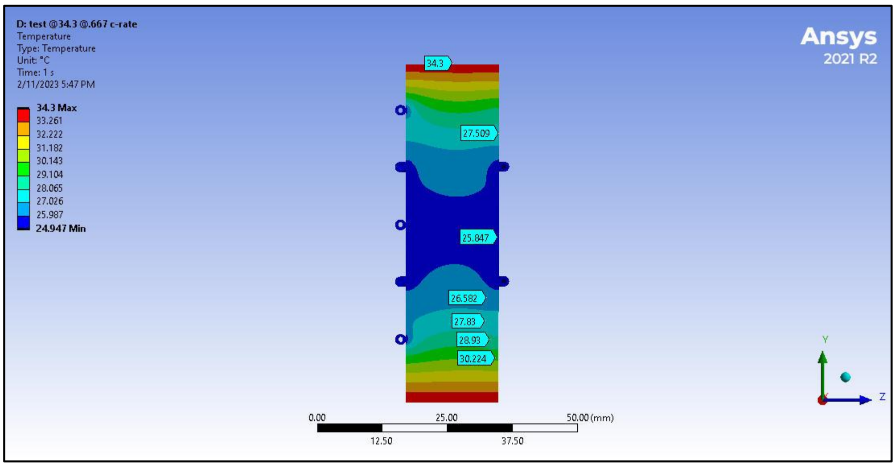

Figure 4.9: Show the Reaction of Lithium Battery-Section- at 0.667 Crate 34.3℃ and the Change in Temperature as a Result of Cooling Coil.

Below (Figure 4.10,Figure 4.11) is the heat flux distribution at area tangent between the battery and the pipe at 34.3℃, 0.667 Crate and the result shown the rage between 0.10737 w/mm^2 and 0.36205 w/mm^2.

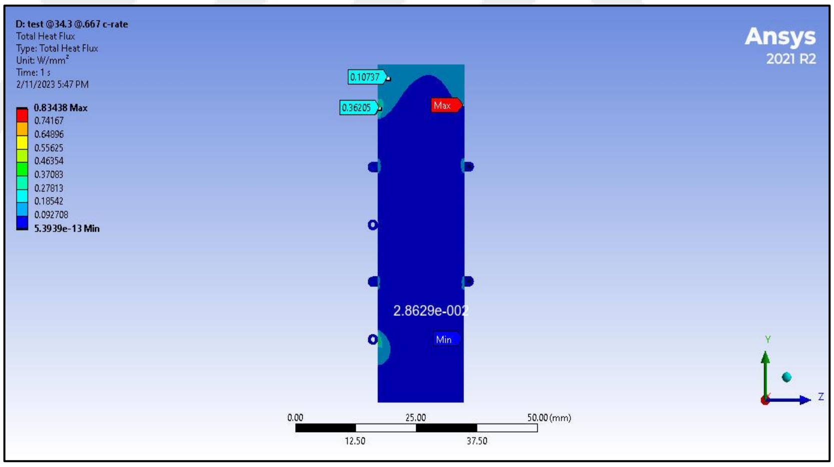

Figure 4.10: Heat Flux Distribution in Area that Tangent Between the Battery and the PIPE at 34.3℃, 0.667 C-Rate.

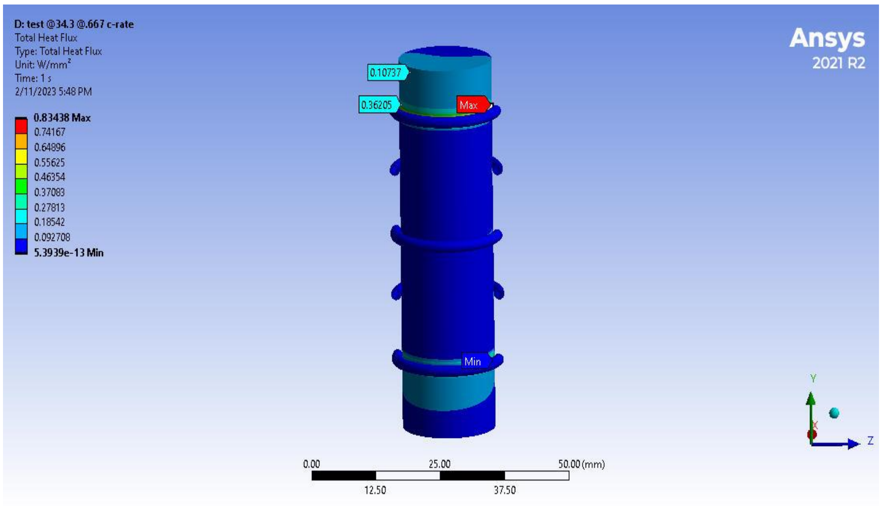

Figure 4.11: Heat Flux Distribution in Area that Tangent Between the Battery and the PIPE at 34.3°C, 0.667 C-Rate.

4.3.4 Single Battery Under 0.7 C-Rate

The simulation involved the temperature of battery which is set as(36.28°C) and the copper pipes temperature set as (25°C) the heat flow set as (6.8 w) and the duration of test in experiment work was at 0.7 C-rate for discharge ,figures (Figure 4.12,Figure 4.15) show thermal distribution along the battery and the effect of pipes to the temperature of battery (Reported).

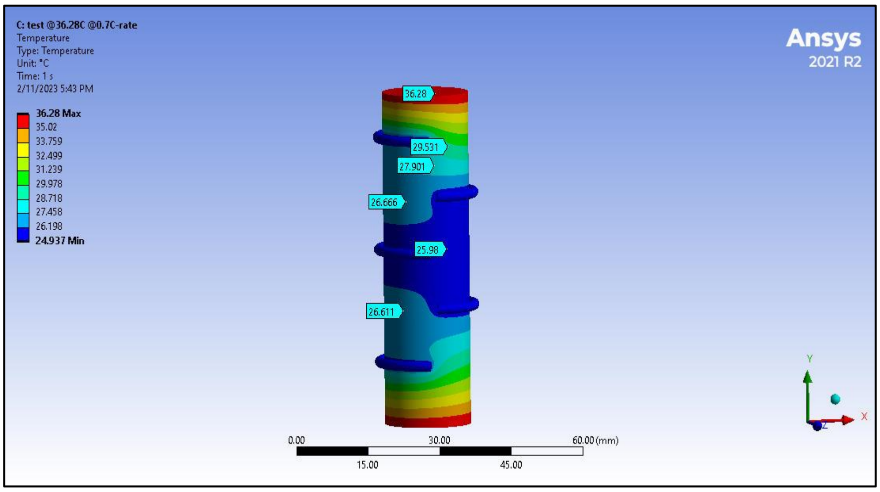

Figure 4.12: Show the Reaction of Lithium Battery at 0.7 Crate 36.28°C and the Change in Temperature as a Result of Cooling Coil.

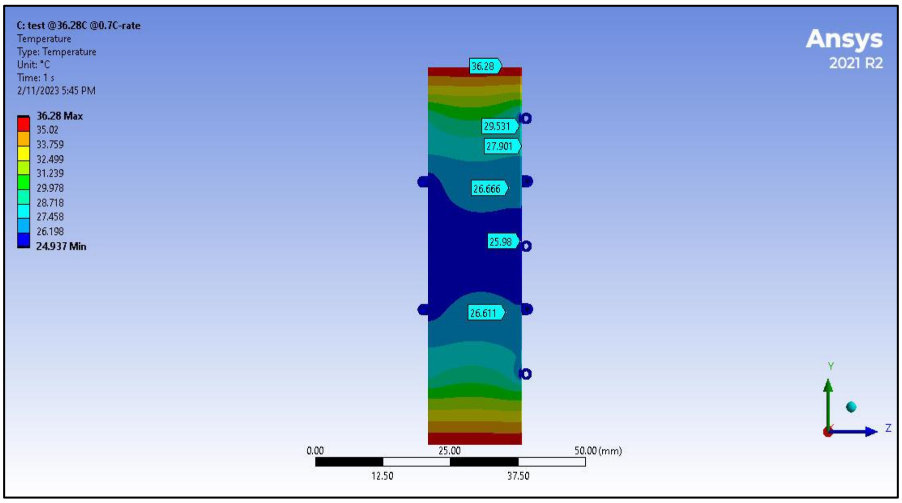

Figure 4.13: Show the Reaction of Lithium Battery-Section at 0.7 Crate 36.28℃ and the Change in Temperature as a Result of Cooling Coil.

Below (Figure 4.15,Figure 4.14) is the heat flux distribution at area tangent between the battery and the pipe at 34.3℃, 0.667 Crate and the results shown the rage between 0.13659 W/mm^2 and 0.89639 W/mm^2.

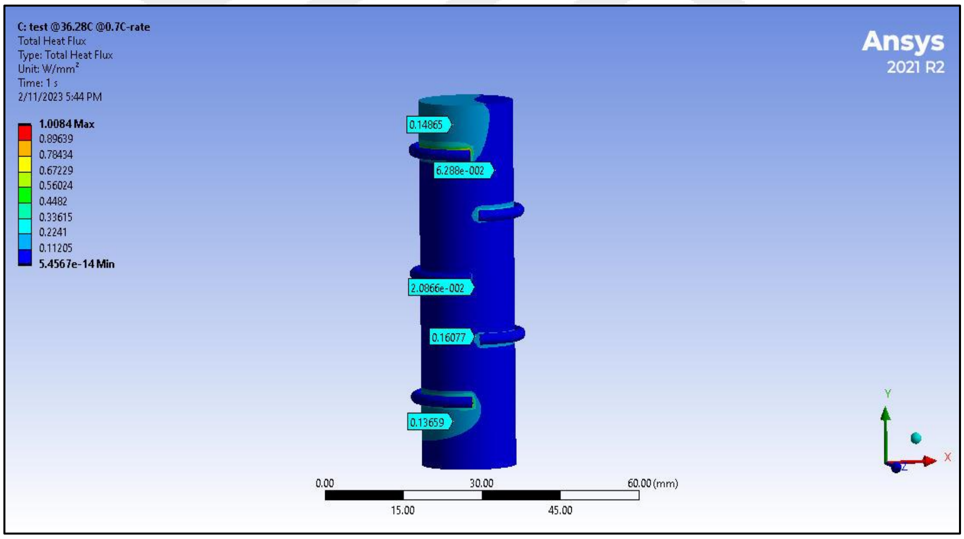

Figure 4.14: Heat Flux Distribution in Area that Tangent Between the Battery and the PIPE at 36.28℃, 0.7 C-Rate.

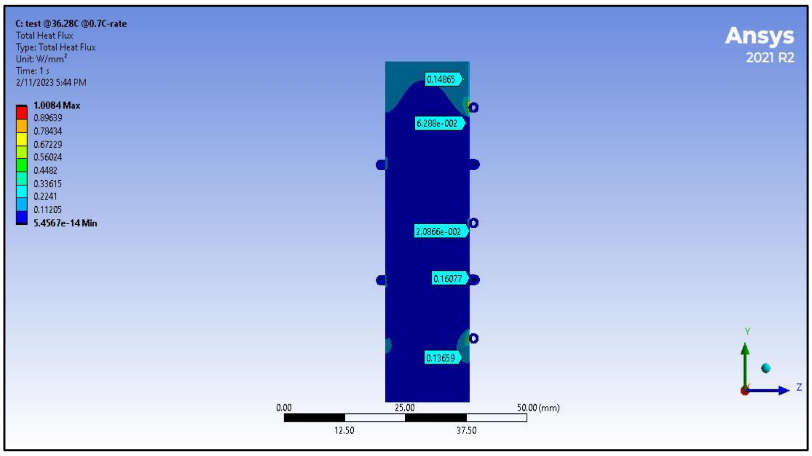

Figure 4.15: Heat Flux Distribution at Section in Area that Tangent Between the Battery and the PIPE at 36.28°C, 0.7 C-Rate.

4.3.5 Single Battery Under 0.88 C-Rate

The simulation involved the temperature of battery which is set as(35°C) and the copper pipes temperature set as (25°C) the heat flow set as (6.8 w) and the duration of test in experiment work was at 0.88 C-rate for discharge , figure (Figure 4.16,Figure 4.17) show thermal distribution along the battery and the effect of pipes to the temperature of battery (Reported).

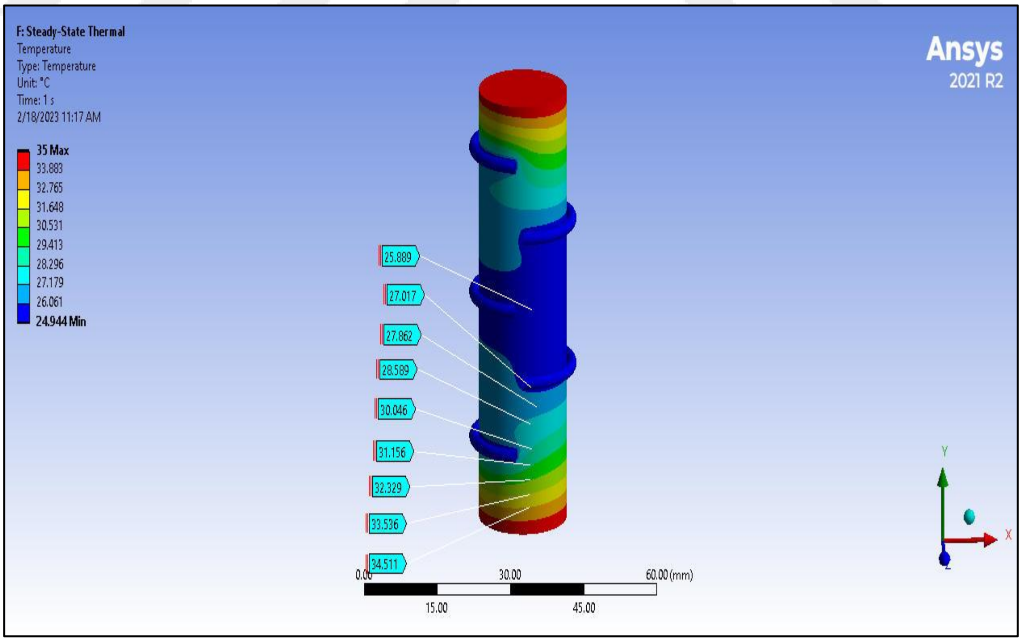

Figure 4.16: Show the Reaction of Lithium Battery at 0.88 Crate 35°C and the Change in Temperature as a Result of Cooling Coil.

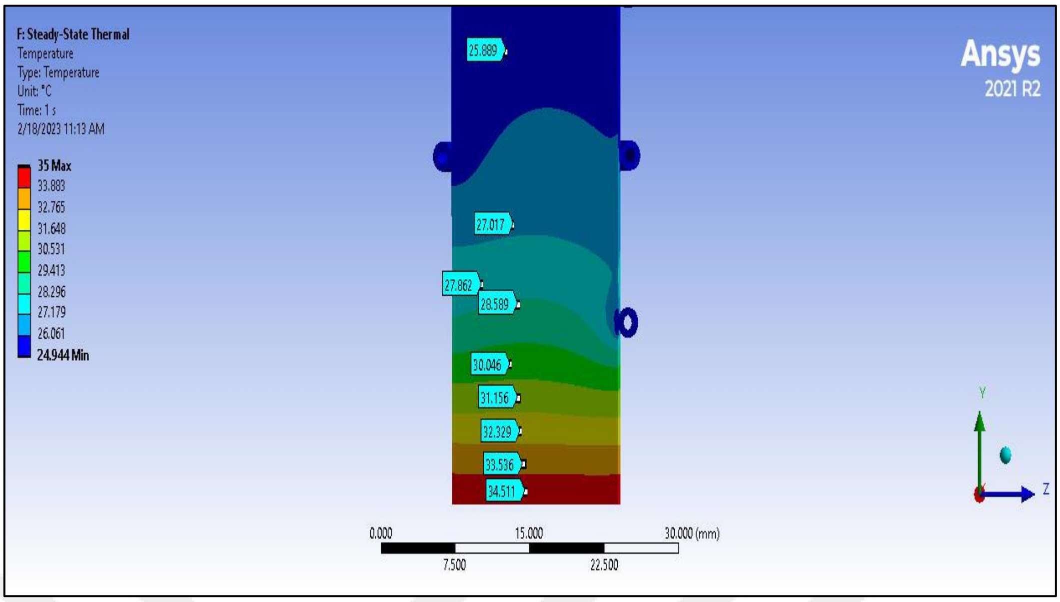

Figure 4.17: Show the Reaction of Lithium Battery Section at 0.88 Crate 35°C and the Change in Temperature as a Result of Cooling Coil.

Below (Figure 4.18,Figure 4.19) is the heat flux distribution at area tangent between the battery and the pipe at 34.3°C, 0.667 Crate and the results shown the rage between 0.0.895 W/mm^2 and 0.0.29862 W/mm^2.

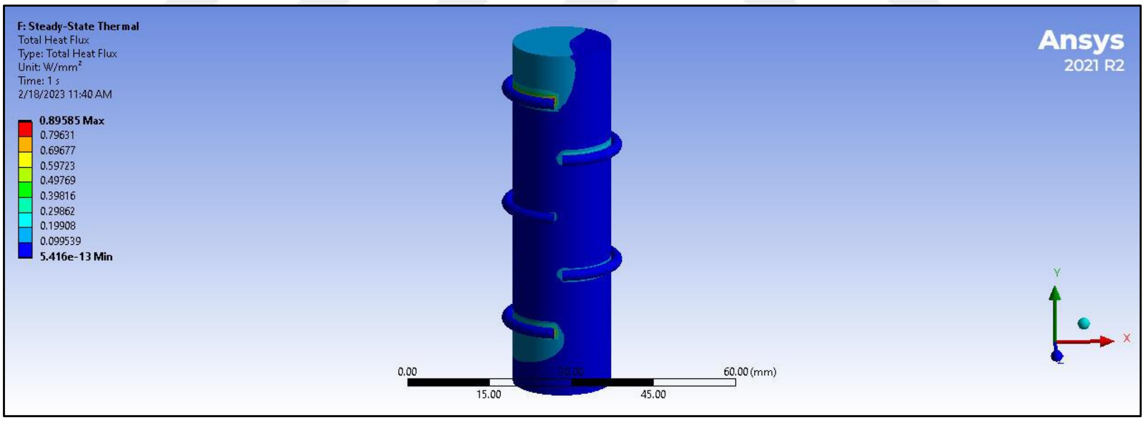

Figure 4.18: Heat Flux Distribution in Area that Tangent Between the Battery and the PIPE at 35°C, 0.88 C-Rate.

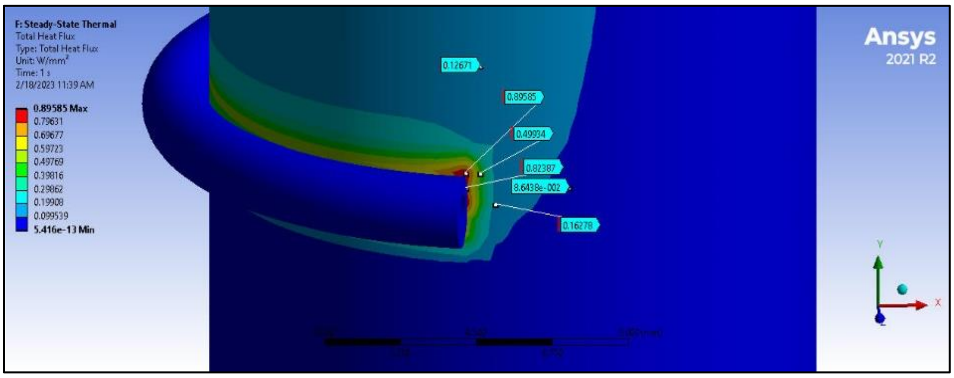

Figure 4.19: Heat Flux Distribution in Area that Tangent Between the Battery and the PIPE at 35℃, 0.88 C-Rate.

4.3.6 Single Battery Under 5C-Rate

The simulation of single battery under high temperature not exceeded 37℃ , the boundary conditions of simulation was considered the flow rate of fluid inside the pipe was limit (1m/s) and the temperature of cell was 37℃ and the pipes of cooling system was 25 ℃ , the heat flow was 0.00005 w/mm^2 , number of cooling coil surrounding the cell considered 5 copper pipe half circle , the pipe tangent the body of cell and effect to temperature of it.

the temperature of pipes effect on individual cell , the responded was started and most be shown at the end of time of test . the studies pointed to that the react of lithium-ion battery and the result of the simulation was the cooling system Z5A reduced the temperature of cell from 37℃ to the 26.4 ℃ and the system still under limit of cooling battery (Figure 4.20).

The temperature behaviour of individual lithium-ion batteries was closely monitored during discharging at rates of 1C and 0.88C. The results showed that the temperature of the battery gradually increases throughout the discharge process, maintaining a relatively steady rate of temperature rise for the majority of the time. However, there is a noticeable spike in temperature at the end of the discharge. This is believed to be due to the presence of a consistent ohmic heat source during constant C-rate discharging. The voltage curve during discharge, depicted in (Figure 6.19), demonstrates a nearly linear pattern due to the electrochemical properties of lithium-ion batteries.

The difference between the voltage of the positive electrode and that of the negative electrode is essentially what constitutes the cell voltage. Although rapid discharge leads to additional kinetic losses, the fundamental form of the voltage during discharge is largely determined by the equilibrium voltage at various states of charge. This explains the sharp drop in voltage at the end of the discharge process. The reversible heat, which is a significant source of heat, closely follows the trend of the Open Circuit Voltage minus the cell voltage. As a result, the temperature of a lithium-ion battery cell will experience a more rapid increase towards the end of the discharge process.

The uppermost temperatures detected within the lithium-ion battery cell were studied, and the maximum temperature curves obtained under four cooling tests at a discharge rate of 1C 0.7C 0.6C 0.8C are shown in the figures below. The data revealed that when depending simply on natural convection, the temperature of the battery exceeds 45°C in the absence of sufficient cooling methods. This can increase the deterioration of the battery's overall performance. When the battery is subjected to alternative cooling techniques, such as forced air cooling, mini-channel liquid cooling, or others, the maximum temperature of the cell remains below 35°C, enabling the battery to work at its ideal operating temperature and extending its lifespan.

However, the pumping power required for natural convection and two-phase immersion cooling cannot be estimated as the liquid domain was not considered in the study. Although the pumping power required to cool the battery's surface is zero, it still requires pumping power to effectively dissipate heat from the system. Further research is needed to determine the pumping power required for constructing a two-phase lithium-ion battery cooling system.

The image below (Figure 4.20) shows the temperature distribution on the surface of a 18650 lithium-ion battery during a thermal analysis simulation in Ansys at discharge is 37℃ and the area surroundings the copper pipes at 25℃ shown the effective of add heat to the surface of battery and reducing the temperature at 5 C-rate of battery from 37℃ to 26.4 ℃ at average temperature and the anode and cathode still at the same temperature of discharge, case that is energy dissipated from battery raise the temperature and the hardships of cooling the two end of the cylinder lithium ion battery .

The cooling system by using mini channel Z5A prove that it can control to the raising of heat during the discharge and keep it at the limit range of operation temperatures.

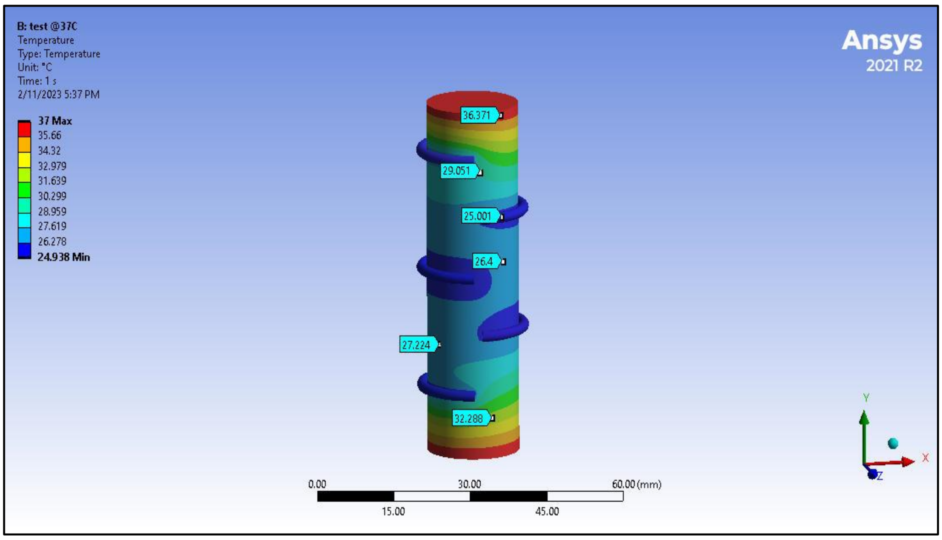

Figure 4.20: Thermal Distribution of Cooling LI-ION Battery Single Cell at 37°C and Effect of Z5A.

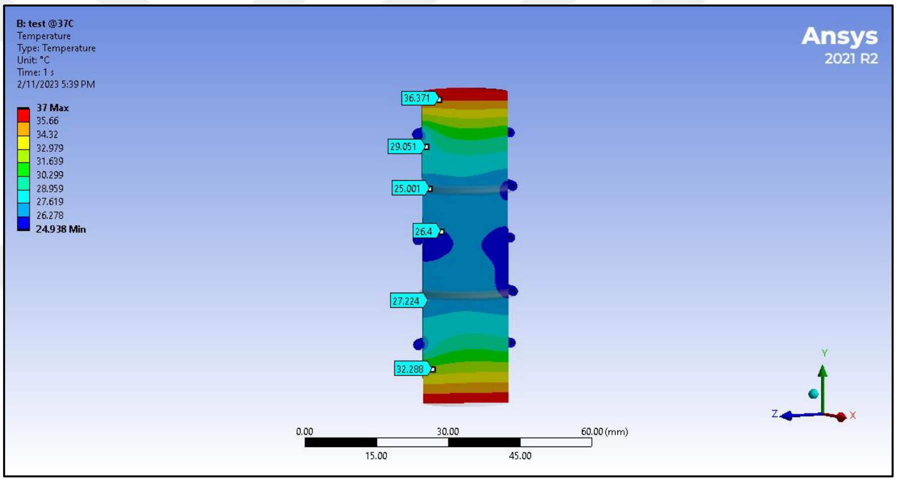

Figure 4.21: Thermal Distribution of Cooling LI-ION Battery Single Cell at 37°C/ Section Figure Shown the Effect of Mini Channel Copper PIPE to Body of Battery.

4.4 SIMULATION OF BATTERY PACK UNDER 5C RATE

The BTM's Z5A is shown that system can be under control and cooling the system when the temperature of batteries exceed the limitations , where the temperature of batteries is normally distributed along the battery, the glycol fluid flows inside the mini channel at 25 °C and the fluid is cooling with radiator content fan to reduce the heat gained due to heat transfer between the pipe and the battery, where the battery is assumed to be at 37 °C at pack load and the heat flow of the single battery is 6.8 w at 80% of efficiency at max load , so the steady state thermal analysis shown below.

The shape of coiling mini channel Z5A is shown in (Figure 4.22) the copper coil diameter and thinks have advantage in practical work were the material have ability to around the batteries without to effect to the battery with condition of spacing between them , and it fixed at 23mm centre to centre and the angle measure to cover the battery is 126 degree(Figure 4.23)and that is the largest angle to coiling the battery with is method.

The channel is distribution in five row and three in one side and the other two in opposite side, Figure 5.5.

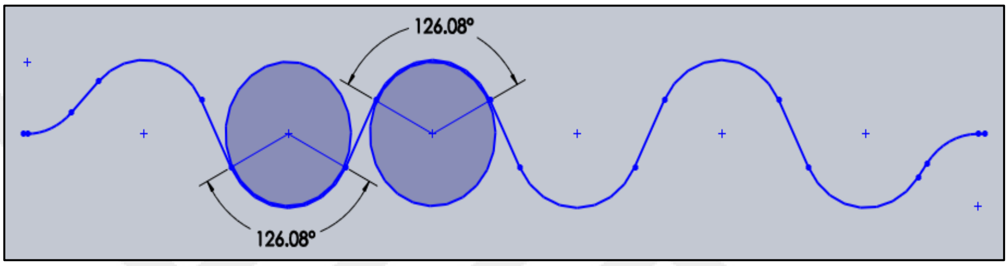

Figure 4.22: Section that Declares the Coil Covered the Cells of Pack with 126◦ Around the Battery and Along of Pack.

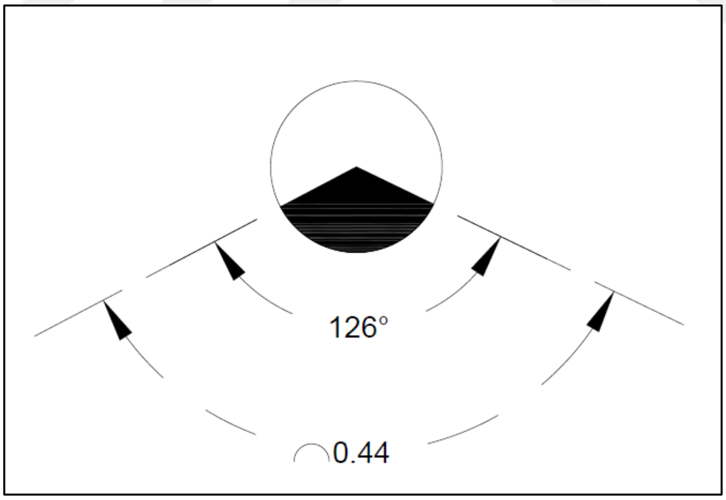

Figure 4.23: Section in Battery that Declare the Area Covered Around the Battery and the Length of Arc Copper PIPE is 0.044 m and the Area is 0.0441 m2.

The area of coiling coil covered the shall of battery and the total area was 39.61mm^2 the (Figure 4.24) show the 3d shape and model in solid works were calculated the area .

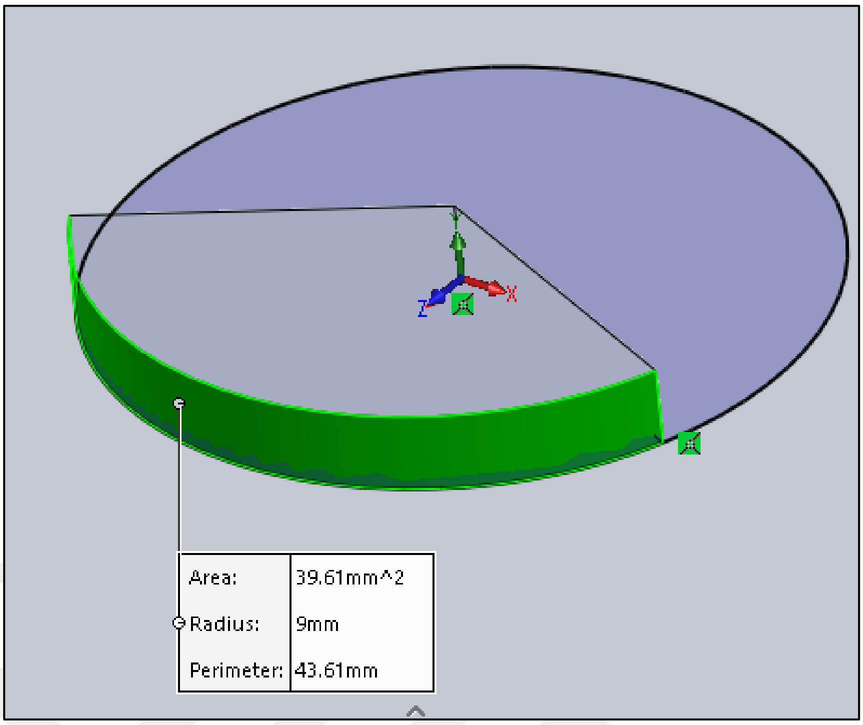

(39.61mm2).

The shown the side view for the 6 batteries as a section from total batteries 18 pcs , reaction of batteries from cooling coil surrounding it shown the thermal distribution and results of thermal reducing was between 5 to 8 ℃ and the maximum temperature is not exceeded the 27 ℃ under full load where the efficiency was at 80%,

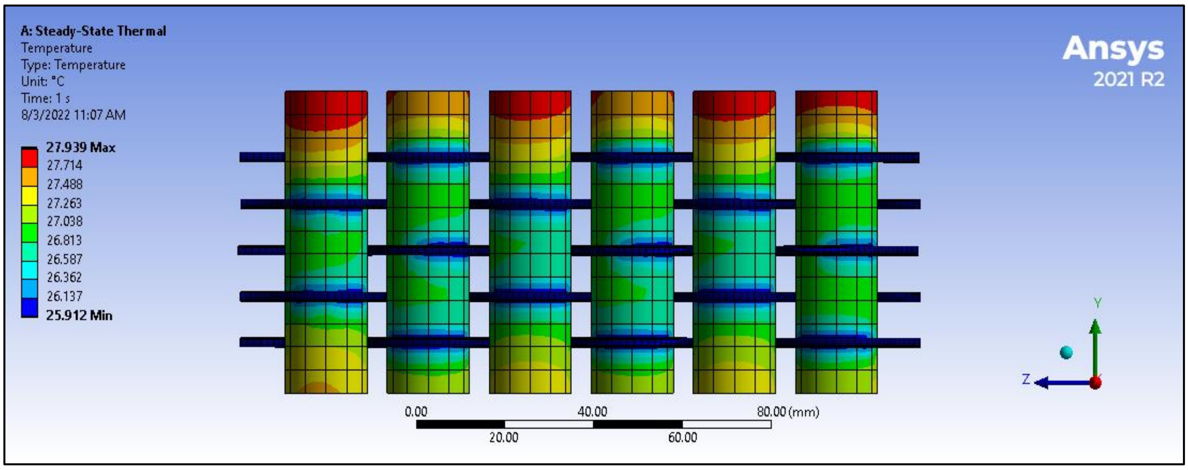

Figure 4.25: The Thermal Distribution Along the Battery Size 2200 Ah , 3.7V with Mini Channel (Z5A) Rounded the Battery Pack with the Effected.

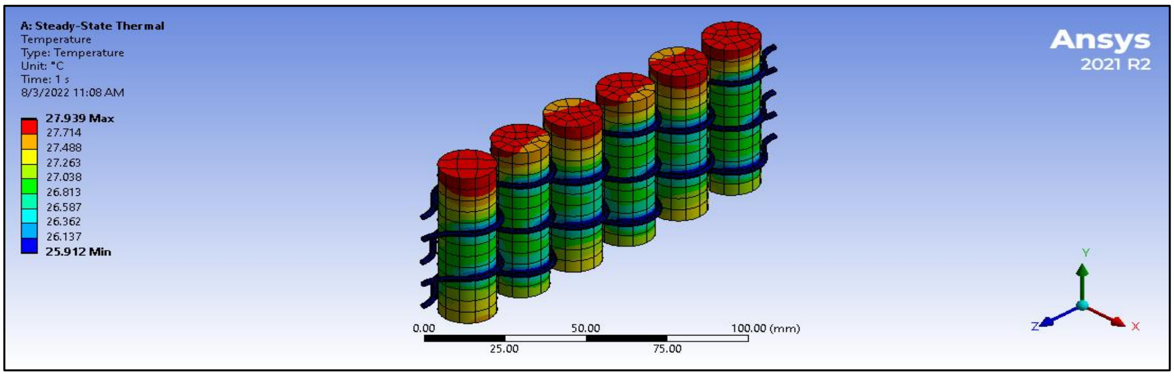

Figure 4.26: Isometric View for Batteries.

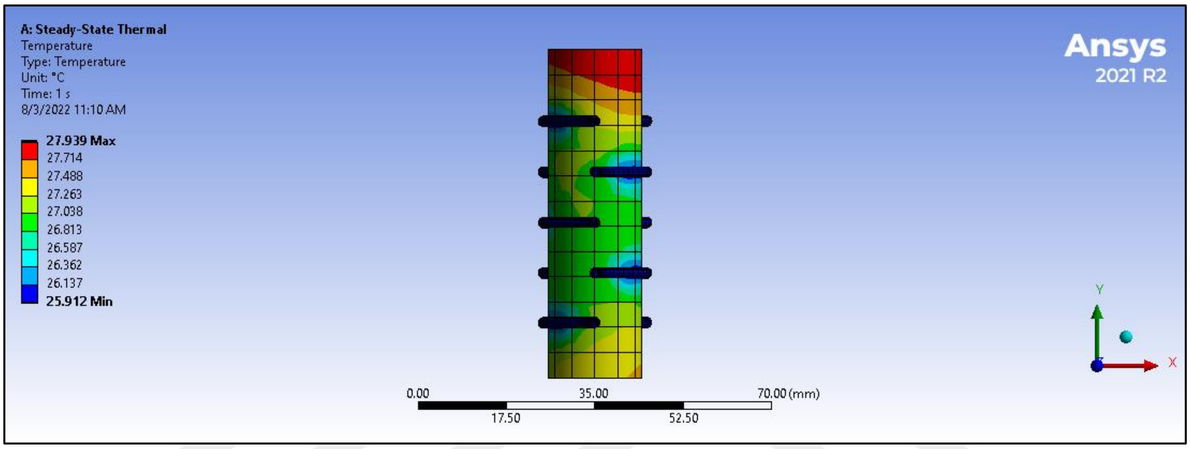

Figure 4.27: Front View for the Battery with Coil.

The heat flux for system was between 0.0356 to 0.0533 W/mm^2 and the battery shown effected area at tangent points to cooling coil.

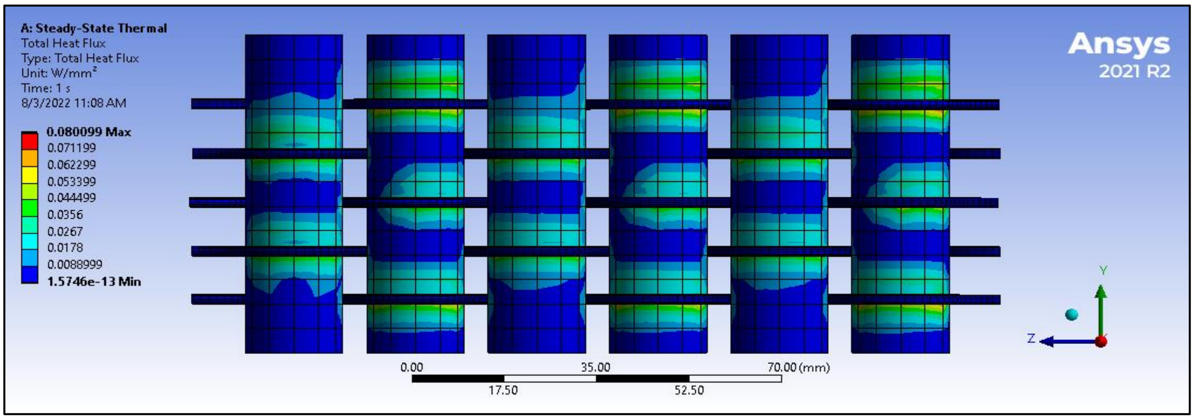

Figure 4.28: Side View for Battery Pack Section Shown the Heat Flux Distribution Along Batteries.

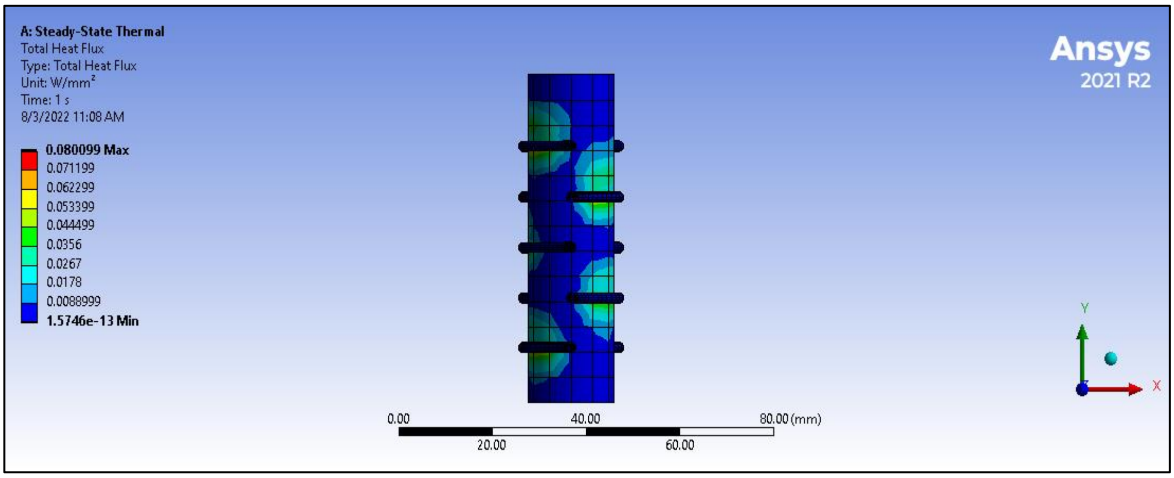

Figure 4.29: Fornt View for Batteries Pack Section.

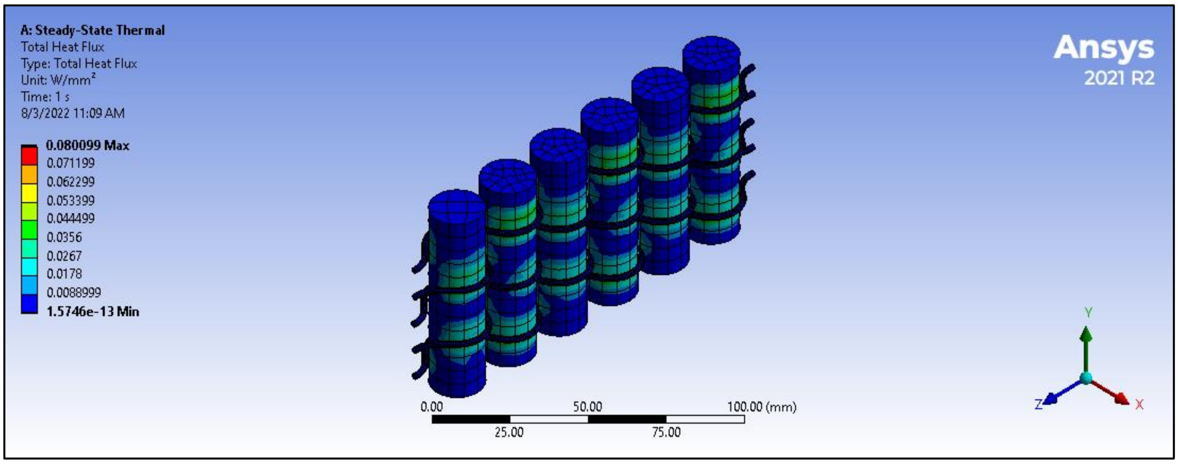

Figure 4.30: 3D View Shown the Batteries as Isometric View.

5. EXPERIMENT WORK AND THE RESULTS

5.1 EXPERIMENT WORK

A 21Ah, cylindrical lithium-ion batteries, basic size was used in this experiment, this research deal with mini channel technique to cooling the cylindrical type of battery type 18650 (Figure 5.3), and the details of package in table (2), this experiment description for the work and the results were analysed , the work consisted the mean parts for build the system and several testes for reacted of batteries under different C-rates where the load was changed every times and recorded the results as shown in result section , the heat exchanger system of BTM's is deals with naturel convection method where the heat exchanger coil is side by side with battery without used any force convection method equipment like fan to make high heat transfer convection between the coil and the batteries that dissipated the heat as react of battery chemical reaction.

5.2 MATHEMATICAL CALCULATION

To calculate the temperature of the lithium battery, it needs to consider the shape of it as cylinder with standard dimensions, if the temperature of the battery is 37°C and the copper pipes are at 25°C with five pipes, we need to consider the heat transfer from the battery to each of the copper pipes. Assuming that the copper pipes are spaced evenly around the circumference of the cylinder, the area of contact between the battery and each copper pipe is:

$$A = \pi \times (18/2) \times 65 \text{ mm} \times 2\pi \times 2 \text{ mm} = 0.0455 \text{ m\^{}2} \quad (5.1)$$

where 2 mm is the diameter of each copper pipe.

Using the same calculations as before, the heat transfer coefficient between the battery and each copper pipe can be calculated as:

$$h = 51.8 \text{ W/m\^{}2}\cdot\text{K} \quad (5.2)$$

Assuming that each copper pipe is at the same temperature of 25°C, the temperature difference between the battery and each copper pipe is:

$$\Delta T = 37 - 25 = 12°C \tag{5.3}$$

The rate of heat transfer from the battery to each copper pipe can be calculated as:

$$q = h \times A \times \Delta T = 51.8\ W/m^2 \cdot K \times 0.0455\ m^2 \times 12°C = 28.5\ W \tag{5.4}$$

The total rate of heat transfer from the battery to all five copper pipes can be calculated as:

$$Q = 5 \times q = 5 \times 28.5\ W = 142.5\ W \tag{5.5}$$

Assuming that the copper pipes are at 25°C and the cylinder generates heat at a rate of 100 W, the total rate of heat transfer from the battery to the copper pipes can be calculated as:

$$Q = 5 \times q = 5 \times 28.5\ W = 142.5\ W \tag{5.6}$$

If we assume that the lithium battery is initially at a temperature of 37°C, we can calculate the temperature of the lithium battery after heat transfer to the copper pipes using the following equation:

$$Q = m \times cp \times (T_{final} - T_{initial}) \tag{5.7}$$

where Q is the heat transferred, m is the mass of the cylinder, cp is the specific heat capacity of the lithium battery material, T_{final} is the final temperature of the lithium battery, and $T_{initial}$ is the initial temperature of the lithium battery.

Assuming that the lithium battery is made of aluminium with a mass of 50 g and a specific heat capacity of 0.9 J/g°C, we can calculate the final temperature of the cylinder as:

$$142.5\ W = 50\ g \times 0.9\ J/g°C \times (T_{final} - 37°C) \tag{5.8}$$

$$T_{final} = 26.2°C \tag{5.9}$$

Therefore, the temperature of the lithium battery would decrease to approximately 26.2°C due to the heat transfer to the copper pipes.

So, if the temperature change typical to the load so need to calculate and consider the new temperature.

The calculation of the final temperature of the lithium battery for different initial temperatures see Figure 5.1

Table 5.1: Initial and Final Temperature for Lithuim ION Battery Tests.

Initial Temperature	Final Temperature
37°C	28.8°C
35°C	28.3°C
36.4°C	23.1°C
31.14°C	21.5°C
29.4°C	26.9°C

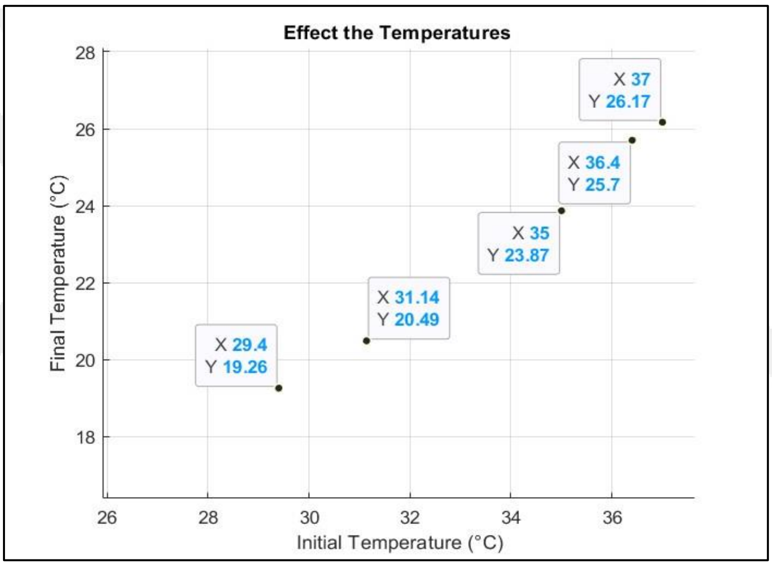

Figure 5.1: Final Temperature of the Lithium Battery for Different Initial Temperatures.

The calculations assume that the copper pipes are at a constant temperature of 25°C and that the cylinder generates heat at a constant rate of 100 W. The heat transfer coefficient between the cylinder and the copper pipes is also assumed to be constant. These assumptions may not hold in practical situations, so the results should be used as a rough estimate only.

If we calculate the heat dissipated [84], by a component can be expressed as:

$$P = I^2 * R \tag{5.10}$$

Where the formula for calculating the internal resistance[84] of a battery is:

$$R = (V1 - V2) / I \tag{5.11}$$

$$\text{Power of battery} = \text{heat dissipated (Q)} = P = I^2 * R \tag{5.12}$$

The load at discharge at peak load is for batteries pack (8.5 A.h) and the pack load for single battery is considered at efficiency is 80% , so the total heat was calculate to be :

$$P(W) = \text{Heat dissipated}(W) = (8.5\ A.h)^2 * (0.09\ \Omega) = 6.5\ W \tag{5.13}$$

That the heat dissipated for single battey will be:

$$\text{Heat dissipated} = (2.2 \times 80\%)^2 * (0.18\ \Omega) = 0.557\ W \tag{5.14}$$

This formula is based on Ohm's Law, which states that the current through a conductor between two points is directly proportional to the voltage across the two points.

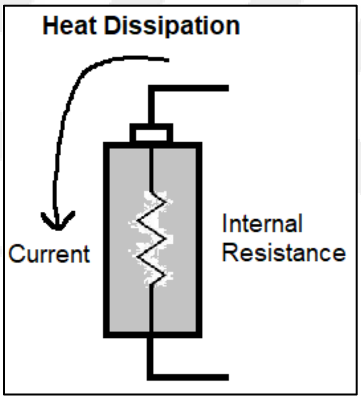

Figure 5.2: Battery Section Shown the Heat Dissipation and Ohmic Law’s.

5.3 BATTERY COULOMB COUNTING ESTIMATION (SOC)

The battery coulomb counting estimation (SOC) [85] is a method used to determine the state of charge (SOC) of a battery. The SOC represents the amount of energy stored in the battery and is often expressed as a percentage of the total capacity of the battery. The SOC can be estimated using the following equation:

$$SOC(t) = SOC(t-1) + i(t) / \mu n \times Vt \times 100 \tag{5.15}$$

This method [32] assumes that the current flowing into or out of the battery is directly proportional to the change in SOC over time.

Our battery pack is :

$$\text{Voltage} = 21 \text{ volt}, \mu_n = 12 \text{ AH}, \text{time } (\Delta t) = 1C \quad (5.16)$$

$$\text{Load current} = (R_T = 1/((1/6.8) + /((1/6.8) + /((1/5.8)), R_T = 2.1435 \text{ ohm} \quad (5.17)$$

$$\text{Load current} = \text{battery capacity} = i(t) = 21V/2.1435 \text{ ohm} = 9.79 \text{ Amper} \quad (5.18)$$

$$Soc(t-1) = 100\% \quad (5.19)$$

$$\text{At} : Vt = 1 \text{ hour} \quad (5.20)$$

$$SOC(t) = SOC(t-1) + i(t)/\mu_n \times V_t \times 100 = 100 + (-9.79/12) \times 1 \times 100 = 100 - 46.65 \approx 53.35\ \% \quad (5.21)$$

$$\text{At} : Vt = 2 \text{ hour} \quad (5.22)$$

$$SOC(t) = SOC(t-1) + i(t)/\mu_n \times V_t \times 100 = 100 + (-9.79/12) \times 2 \times 100 = 100 - 93.31 \approx 7\ \% \quad (5.23)$$

This table was shown the resistance used in practical work where we calculate the resistances and volt of pack considering the changes in time (Vt).

Where the SOC(t) under 2.9 ohm’s resistance shown results at negative and that mean the batteries pack can’t handle the load, In that case battery will dead and will be not able to charging it again.

Table 5.2: SOC Tests Depended on the Resistance.

Resistance	volt	Vt(hour)	SOC(t-1)	i(t)	SOC(t)	
5.8	21	2	100	-3.620689655	66	%
		3	100	-3.620689655	48	%
		4	100	-3.620689655	31	%
		5	100	-3.620689655	14	%
Resistance	volt	Vt(hour)	SOC(t-1)	i(t)	SOC(t)	
6.8	21	2	100	-3.088235294	71	%
		3	100	-3.088235294	56	%
		4	100	-3.088235294	41	%
		5	100	-3.088235294	26	%

Table 5.2: SOC Tests Depended on the Resistance 'Table Continued'.

Resistance	volt	Vt(hour)	SOC(t-1)	i(t)	SOC(t)	
2.9	21	2	100	-7.24137931	31	%
		3	100	-7.24137931	-3	%
		4	100	-7.24137931	-38	%
		5	100	-7.24137931	-72	%
Resistance		Vt(hour)	SOC(t-1)	i(t)	SOC(t)	
3.4	21	2	100	-6.176470588	41	%
		3	100	-6.176470588	12	%
		4	100	-6.176470588	-18	%
		5	100	-6.176470588	-47	%
Resistance	volt	Vt(hour)	SOC(t-1)	i(t)	SOC(t)	
2.143478261	21	2	100	-9.797160243	7	%
	21	3	100	-9.797160243	-40	%
	21	4	100	-9.797160243	-87	%
	21	5	100	-9.797160243	-133	%

It refers to that the battery under this load could not work and cause dead of battery and you should not do test.

5.4 MODELLING PART

The cylindrical lithium-ion battery model 18650 (Figure 5.3)consists of 18 cells, each cell providing 3.7 V and 2200 mAh, with a diameter of 18 mm and a height of 65 mm. These cells are arranged in a matrix of 3x6 to produce an output of 12 mAh and 21.5 V. The technical specifications for the battery model 18650 can be found in Table 2. The battery pack is charged by a DC power supply using a slow charging method with a voltage of 23 V and a current of 2 A, which typically takes between 6 to 8 minutes. The battery pack is discharged through a thermal resistive load.

This cylindrical lithium-ion battery model is a popular choice due to its compact size, high energy density, and long cycle life. It is commonly used in portable electronic devices, electric vehicles, and energy storage systems. The matrix arrangement of the 18 cells allows for a higher voltage output while maintaining a relatively small form factor. The slow charging method used by the DC power supply helps to extend the cycle life of the battery, while the thermal resistive load used for discharging helps to prevent over-discharge and potential damage to the battery.

The cylindrical lithium-ion battery model 18650 is a versatile and reliable choice for a wide range of applications. Its small size, high energy density, and long cycle life make it an ideal choice for portable devices, electric vehicles, and energy storage systems. The use of slow charging and thermal resistive discharging methods helps to prolong the life of the battery and prevent potential damage. (Figure 5.13).

5.5 BATTERIES CELLS

Inserted inside plastic case (polypropylene) thermal conductivity: 0.25 W/mK , it content upper and lower cases (figure 5.18) each one was inserted inside it (18 washer and screw welded to each other) , it put inside the cases and welded to each other for electrical purposes and connection in series and parallel, otherwise , the upper and lower cases fixed to each other's by long screw for more stability and reliability for maintains and arrangements.

Figure 5.3: Power-Xtra PX18650-22E - 3.7V 2200 Mah LI-ION Battery- 5C.

Table 5.3: Technical Information's.

Model: Power-Xtra PX18650-22E - 3.7V 2200 Mah Li-ion Battery- 5C		
Item	Specifications	Conditions
Nominal Voltage	3.7±0.05V	0.2C Discharge
Charging	Method	CC-CV
	Voltage	4.20±0.05V
Typ. Capacity	2.200 mAh	0.2C discharge
Standard Charge Current	1.100 mAh (0.5C)	Constant current at 1100mA charge to 4.20V, then constant voltage at 4.20V charge till current decline to ≤22Ma

Table 5.3: Technical Information's 'Table Continued'.

Standard Discharging Current	440 mAh (0.2C)	440mA to 2.75V
Max. Discharge Current	2.200 mAh (1.0C)	1.0C / 2200 mAh to 2.75V
Maximum Continuous Discharge Current	11.000 mAh	5.0C
Temperature	Charge	0 to +45°C
	Discharge	-20 to +60°C
	Storage	Less than 1 year: -20~25°C
		less than 3 months: -20~40°C
Weight	45 gr	approximately
Cycles Test	During this cycle life test, the ambient temperature should be kept at 23°C ±2°C. The cell shall be charged at CC/CV=0.5C/4.20V, cut off till current decline to 0.05C, stored for 10mins,then discharged at a constant current of 0.5C to a final voltage of 2.75V, after that, stored 10mins prior to next charge/ discharge cycle. The cell shall be continuously charged and discharged for 300 times.	

5.6 COOLING SYSTEM(Z5A)

The cooling system have main parts used to build the system Z5A , See(Figure 5.5) and the main idea that used the most popular materials in market, its copper material as a coil surrounding the batteries, where copper is a popular choice for materials in many industrial and engineering applications due to its high thermal conductivity. Thermal conductivity is a measure of a material's ability to conduct heat, and copper is one of the most thermally conductive metals available. Its thermal conductivity is around 400 W/(m.K) at room temperature, which is significantly higher than most other materials.

Due to its high thermal conductivity, copper is commonly used in applications that require efficient heat transfer. For example, copper is frequently used in heat exchangers, which transfer heat from one fluid to another. It is also used in cooling systems, such as radiators in cars, which transfer heat from the engine to the surrounding air.

In addition to its high thermal conductivity, copper has other properties that make it a useful material for heat transfer applications. It is a good conductor of electricity, which means it can be used in electrical applications that require efficient heat dissipation. Copper is also a durable and corrosion-resistant material, which makes it a good choice for applications in harsh environments.

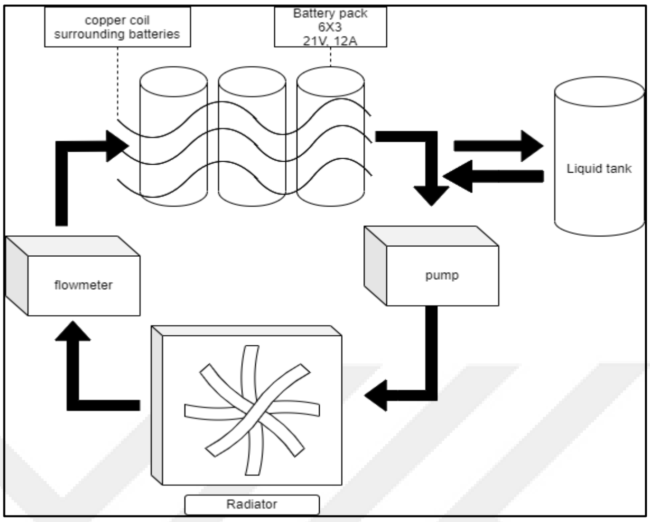

Figure 5.4: Schmatic of Liquid Thermal System (Z5A) Channels.

(Figure 5.5) is content network of copper pipe (OD: 2mm, ID: 1mm) surrounded the batteries, copper channels equipped the LIB’s by wave shape as three main groups in three row, each row content five mini channel(Z5A) along LIB’s , it coated by Varnish materials (thickness is neglected) and it for isolated the system electrically,

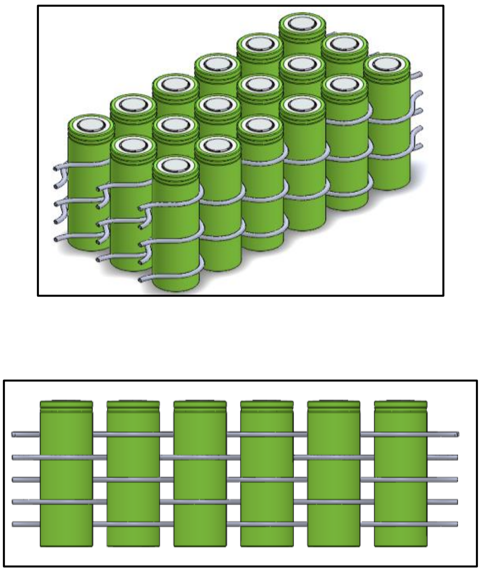

Figure 5.5: 3D Model of Battery Thermal Management System with Z5A Mini Channel.

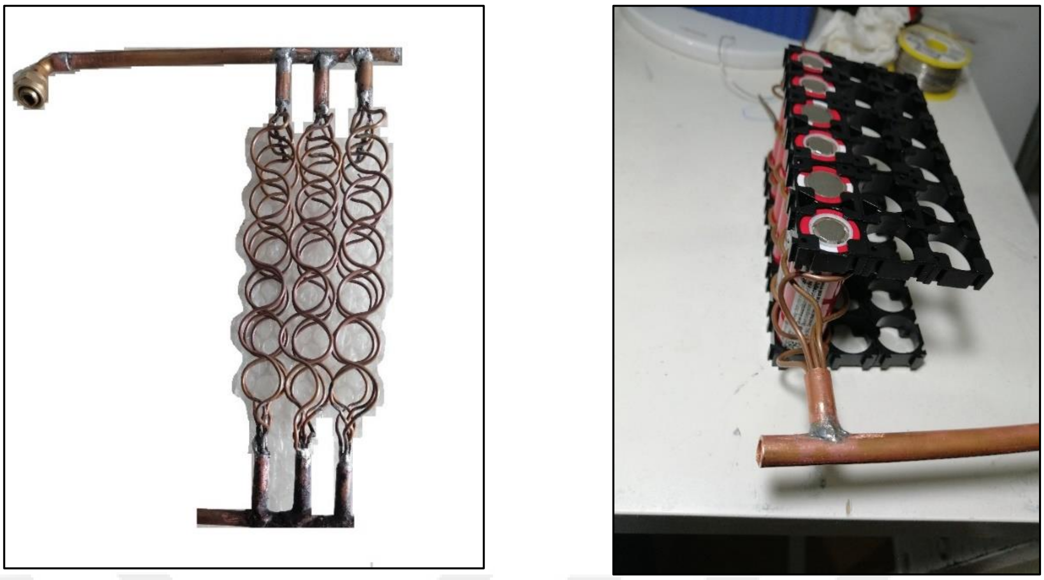

Figure 5.6: Shape of Z5A Mini Channel Model for Cooing Cylinder Lithium-ION Batteries.

Every five mini copper pipes ended collated to main pipe size (12.5 mm) see (Figure 5.6) to connected to main system (pump, radiator, flowmeter).

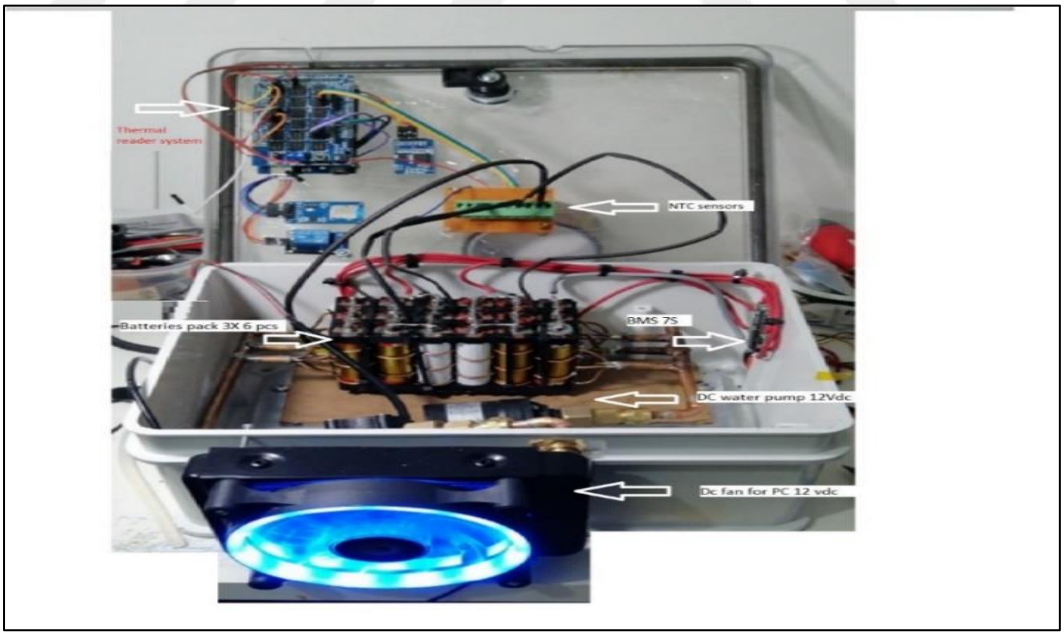

Figure 5.7: Experiment Work for Z5A Cooling System that Implement.

5.6.1 Pump

Experiment used dc motor with submersible case type working with 12 Vdc source and fix flowrate (1 L/min). see (Figure 5.8)

A submersible pump is a device that operates underwater and is designed to move fluids from one location to another. The 12V, 800 L/h submersible pump is a model designed to operate at 12 volts and can pump up to 800 liters of fluid per hour. The pump has a power consumption of 19 watts, which is relatively low for its capacity.

The submersible pump is a compact and durable device, usually made of high-quality plastic or metal material, that can withstand the harsh conditions of being submerged in liquids. It is often used in applications such as aquariums, fountains, and water gardens, as well as in irrigation systems, and other industrial or agricultural applications that require the movement of large volumes of fluids.

The 12V, 800 L/h submersible pump is equipped with a powerful motor that drives an impeller, creating a strong flow of fluid. The pump is designed to be fully submersible in water and can operate at a range of depths, depending on the model. It can also handle different types of fluids, including clean water, saltwater, and even some types of liquids with small particles.

In addition to its high capacity and low power consumption, the 12V, 800 L/h submersible pump is also designed to be easy to install and maintain. It comes with a range of fittings and accessories that make it compatible with different types of plumbing systems. The pump is also designed to be easy to clean and service, which helps to extend its lifespan and reduce the need for repairs.

Overall, the 12V, 800 L/h submersible pump is a versatile and reliable device that can help to move large volumes of fluid in a variety of applications. Its high flow rate and low power consumption make it an efficient option for both residential and commercial use, while its durable design and easy maintenance help to ensure long-lasting performance.

Below is the manufacturing specifications:

a. Specification

b. Voltage: DC12V

c. Maximum-circulating water temperature:100°C

d. Maximum-Water lifter: 5 meters

e. Working environment temperature:1-60 ℃

f. Material: ABS

g. Maxi Rated Current: 1000MA

h. Flow-Rate:800L/h (m^3/h)

i. Power:19W

j. Cable line:50cm

k. Type: Fountain & Water Feature Pump

Figure 5.8: Pump 12 v 1 L/min.

5.6.2 Liquid Tank

Plastic tank connected to the system by plastic tubes, used for equipped the fluid used in system.

5.6.3 Radiator

Radiator made from aluminium and normally used in computers Figure 5.9for cooling the system, it two halves for inflow and outflow, the size for 120mm and fixed fan from same size for cooling the liquid. see (Figure 5.9,Figure 5.10).

This radiator type can handle up to 300w for cooling but depend on speed of fan that can extracted the heat from it and the recommended speed to cooling it 4000 rpm.

Figure 5.9: Radiator 120 mm.

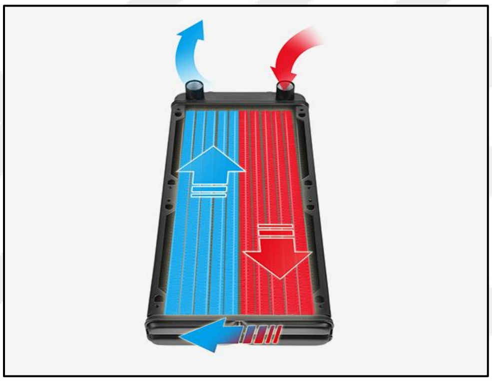

Figure 5.10: Radiator Flow Type and the Image Clear the Flow Direction.

5.6.4 Flowrate Sensor

The YF-S201 Water Flow Sensor is a G1/2" flow rate sensor[86] that can be easily integrated with Arduino and other microcontroller boards to measure the flow rate of liquids like water. This sensor is widely used in various water flow monitoring applications, such as irrigation systems, industrial process control, and household water usage monitoring. See (Figure 5.11)

Figure 5.11: YF-S201 Water Flow Sensor.

The YF-S201 sensor operates based on the Hall effect principle, which measures the electromagnetic field created by the flow of liquid through the sensor. The sensor has a measuring range of 1-30 litters per minute and a maximum operating pressure of 1.75 MPa. The accuracy of the sensor is rated at ± 3% and the output of the sensor is a digital square wave signal that can be easily read and processed by Arduino and other microcontrollers[86].

The sensor is made of high-quality food-grade plastic and has a water-resistant rating of IP68, making it suitable for submersion in water. The sensor has a compact and lightweight design, making it easy to install and integrate into water flow systems. It also has a low power consumption of 15mA, making it ideal for battery-powered systems.

The YF-S201 sensor has two wires that need to be connected to a power source and a microcontroller board for signal processing. It is important to note that the sensor requires a minimum operating voltage of 4.5V and a maximum voltage of 24V DC. The sensor is compatible with a wide range of microcontroller boards, including Arduino, Raspberry Pi, and ESP8266.

In summary, the YF-S201 Water Flow Sensor is a reliable and accurate G1/2" flow rate sensor that can be easily integrated with Arduino and other microcontroller boards to measure the flow rate of liquids like water. Its compact design, low power consumption, and high accuracy make it an ideal choice for various water flow monitoring applications. the flowrate adjusted as 1 L/min and fixed the flow to cooling the system, in future need to experiment other model to study the effect of flowrate to cooling system.

5.6.5 Resistance Load

This load content three resistance and it represented the peak load that suitable to discharge and in limited of batteries voltage (2.75 V), this labour load normally dissipated high temperature exceeded 150 ◦C so we fixed Dc fan over it to increase high heat dissipated from it and preventing the load to crushing or out of control. See (Figure 5.12),
Thermal resistance is a type of device used in laboratories to measure or control the temperature of various substances. The thermal resistance 100W is a particular type of thermal resistance that is designed to handle power loads of up to 100 watts. It is an essential tool for many types of laboratory experiments that involve heat transfer, including but not

limited to temperature control of chemical reactions, heat flux measurement, and temperature mapping of various surfaces.

The thermal resistance 100W is typically used in conjunction with a temperature control system, which can regulate the temperature of the resistance to maintain a specific temperature in the experimental setup. The device is usually constructed from a high-temperature ceramic material and features a small size to allow for ease of integration into experimental setups.

One of the most common applications of thermal resistance 100W is in experiments that involve heat transfer through a solid medium. In such experiments, the device is placed in contact with the medium, and the heat transfer through the medium is measured by monitoring the temperature change across the resistance. The resistance can also be used to measure the heat transfer coefficient between the solid medium and a fluid medium such as air or water.

In addition to laboratory applications, thermal resistance 100W is also used in various industrial applications, including the thermal management of electronic components, control of fluid temperature, and control of process temperature in chemical and pharmaceutical industries.

To ensure accurate temperature measurements and control, it is important to use high-quality thermal resistance 100W devices from reputable manufacturers. Many such devices are available from various suppliers and can be sourced from online marketplaces or laboratory equipment suppliers.

In conclusion, thermal resistance 100W is a valuable tool in laboratory experiments that involve heat transfer and temperature control. Its applications range from heat flux measurement to temperature control of chemical reactions, and it is also widely used in industrial applications for thermal management and process temperature control.

Figure 5.12: Thermal Resistance Load 100W.

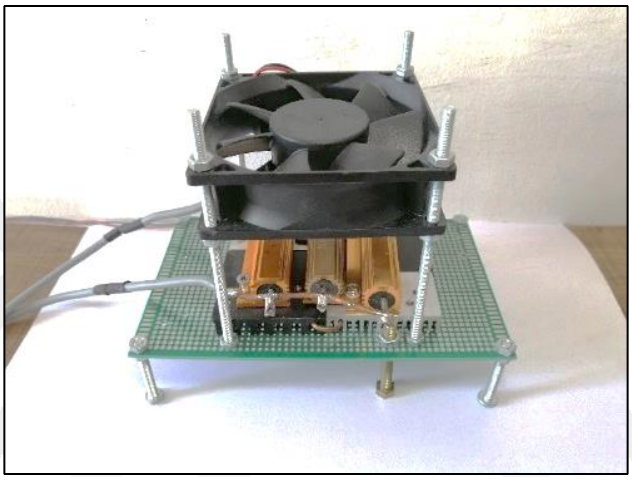

Figure 5.13: Thermal Resistances Load for Discharge the Battery Pack System with Fan for Cooling Them.

5.6.6 Coil of Cooling System

The coil used in this experiment from the copper tube ID is 1.5mm and the OD is 2mm, the copper tubes was collected and welded together to one input/output that connected to system. The distance between the cells was experimented to be suitable for passing the copper tubes between it , and the space centre to centre is 0.023mm .(Figure 5.14,Figure 5.16).

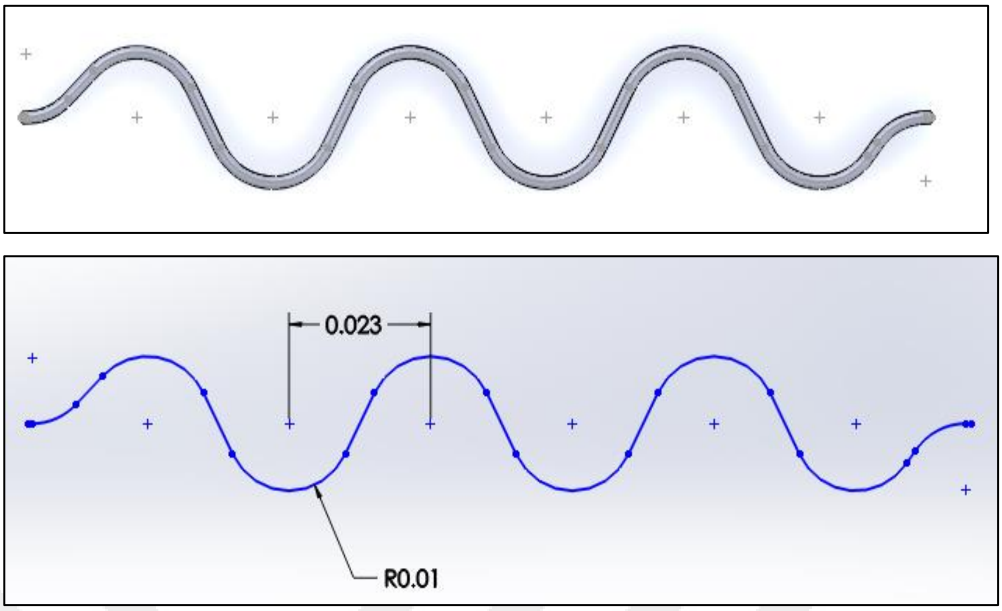

Figure 5.14: Z5A Mini Channel Cooling System.

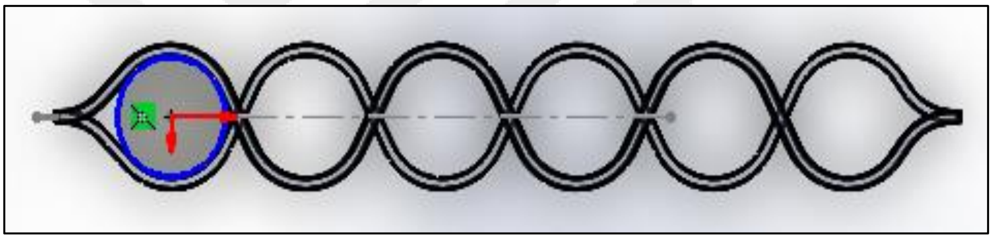

Figure 5.15: Schematic for the Mini Channel Z5A.

The Figure 5.16 show the cooling coil Z5A in step of build it and the cover between the coils for hold the batteries , prepared to the connected to the mean pipe sizes (12.5mm) and the this is one part from total 3 groups for batteries pack.

The shall of copper coil was isolated by using varnish material to prevent connected the battery to copper and be electric conducted between them, the thickness not exceed 0.001 mm, it tested as electrical insulation, this method so effected in electric coils in commercial manufacturing for electric motors.

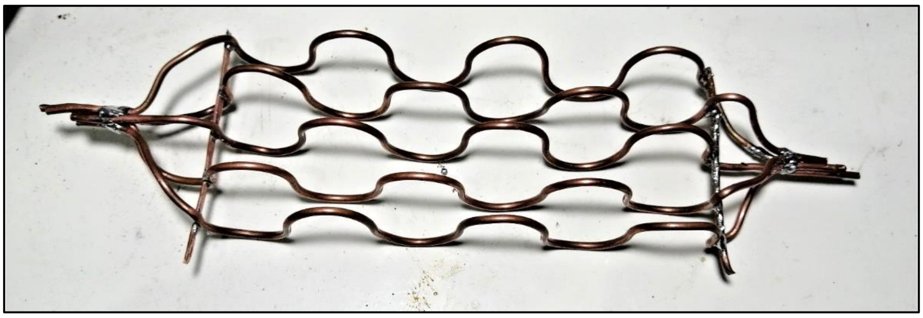

Figure 5.16: Z5A Mini Channel Practical Work (Copper PIPE ID:2mm).

5.6.7 Plastic Holder

Normal holder in market had specific spacer between the batteries side by side and it limited by 20.5 mm form center to center of two batteries see(Figure 5.17), it normally prevented the copper pipe of heat exchanger coil passed between them , where the space required most be 23 mm, see (figure 5.18), we design new holder bracket had with more spacer sizes that allowed coppers pipe surroundings it, the new holder printed in 3d printer from PLA materials with upper and lower case the can fixed to each other by screws the case can hold the 18 cells and in future we can modify that to hold more than experiment cells .

Definition: Polylactic Acid (PLA) is a bio-based and biodegradable thermoplastic polymer derived from renewable resources such as corn starch or sugarcane. PLA is widely used in various applications, including packaging, 3D printing, and biomedical implants, due to its desirable properties such as biocompatibility, easy processing, and low toxicity.

Furthermore, PLA is a popular material in 3D printing due to its ease of use and biodegradability. In the study by Rodríguez et al. [87], the authors investigated the effect of printing parameters on the mechanical properties of PLA printed parts. They found that adjusting the printing speed and temperature can significantly improve the mechanical properties of the final product.

Another application of PLA is in biomedical implants. provides an overview of the use of PLA composites in biomedical applications such as bone tissue engineering and drug delivery systems. The authors discussed the importance of tailoring the mechanical and biological properties of PLA composites for specific biomedical applications.

PLA is a versatile material with a range of applications in various industries such as packaging, 3D printing, and biomedical engineering. Its biodegradability and easy processing make it an attractive alternative to traditional plastics.

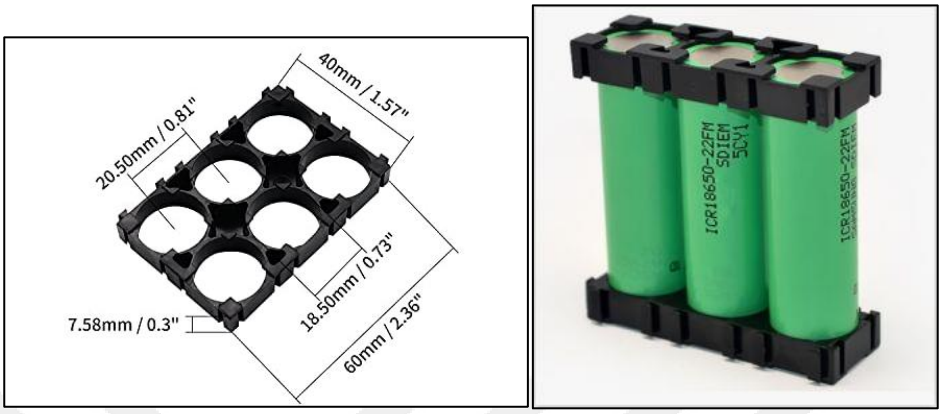

Figure 5.17: Standard Bracket Holder the Commonly used in Market, the Space Between Two Batteries is 20.5 mm.

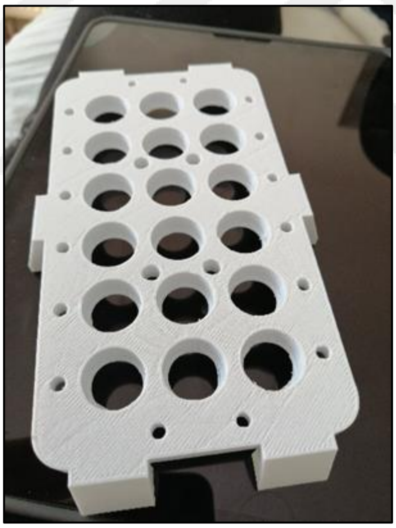

Figure 5.18: Plastic Holder.

Top Bottom

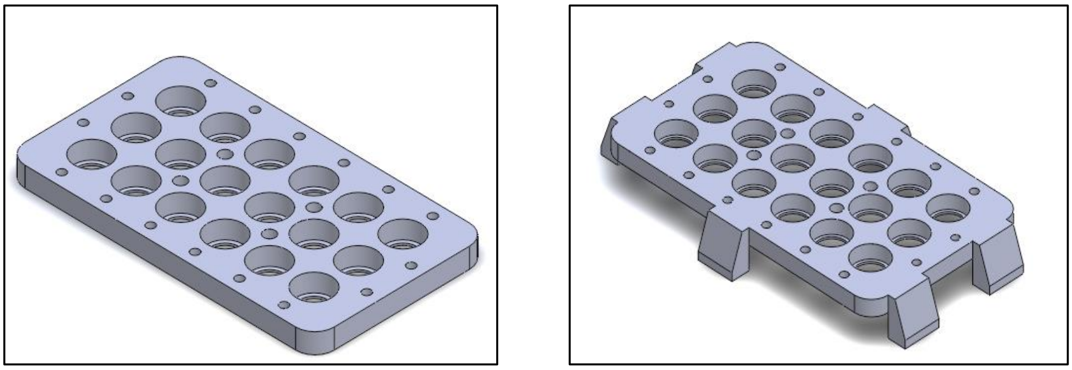

Figure 5.19: New Bracket Holder of Batteries with New Mechanism for Easy Disassembly Top& Bottom, Where the Space Between Them is 23mm from Center to Center.

5.7 FLUID OF BTM SYSTEM Z5A

5.7.1 Propylene and Glycol Varieties

Propylene glycol and ethylene glycol are the two forms of glycol used in hydronics, There are two major considerations. First, ethylene glycol is a more poisonous chemical than propylene glycol and can be dangerous if consumed. We avoid using glycol in heating systems where there is a risk of exposure to the system fluid or where there is a risk of the glycol polluting potable water. In today's world, ethylene glycol is only found in carefully controlled i Propylene have lower freezing point for glycol given us gain and privileges and come out to a cost, where it makes low ability to heat transfers. most glycol fluid had mix with water at certainly percentages (40%, 50% as example) and the total heat transfer at specific flowrate flows with difference of temperature across the heat exchanger coil expressed as:

$$BTUH = GPM * dT * 500 \tag{5.24}$$

And as the consideration that were differences in specific heat of water and the glycol at mix fluid where the water should be pure, Propylene glycol at a 40% concentrated mix with water have a specific heat transfer it(0.895)w/k-1 /m2, That decrease eventually limits the overall amount of heat transfer we can achieve with equal flow rates and temperature deltas when compared to 100% water.

Because ethylene glycol solutions have a lower specific heat than propylene glycol solutions, they enable greater heat transmission at the same mixing percent (glycol concentration).

Below is the formula after modifying and the total heat transfer considerate that the fluid is not made from pure water,

$$BTUH = GPM * dT * 500 * Specific\ Heat * Specific\ Gravity \tag{5.25}$$

However, ethylene glycol solutions do not impact specific heat as much as propylene glycol solutions, and therefore provide better heat transfer at the same mixture percentage (glycol concentration).

Propylene glycol, on the other hand, has been authorized by the FDA as safe. It is extensively utilized in packaged foods, pharmaceuticals, and cosmetic items due to its minimal oral toxicity. chemical solution wide used as (application) Polymers, Food and drug and Antifreeze.

5.7.2 Properties Mono Propylene Glycol

The most advanced properties to used Mono propylene glycol as cooling fluid for BTM's was:

a.Initial: cost is low and availably to the markets.

b.Inflammable: and that's one of advantages in EV that make the working with this fluid more safely.

c.Efficient: the maximum and the average temperature was good results as shown in this research and control to Batteries heat under different load applied to the system.

d.Oxidation: the most important considerations in BTM's the keep system to long period for used without impact to the reaction from fluid properties, like water oxidations on the copper pipe, the glycol not shown any impact to the copper tubes.

Below Table 5.4 are chemical properties for Mono propylene glycol [88]:

Table 5.4: Properties Mono Propylene Glycol.

Chemical formula	C3H8O2
Molar mass	76.095 g·mol−1
Appearance	colorless liquid
Odor	Odorless
Density	1.036 g/cm3
Melting point	−59 °C (−74 °F; 214 K)
Boiling point	188.2 °C (370.8 °F; 461.3 K)
Solubility in water	Miscible
Solubility in ethanol	Miscible
Solubility in diethyl ether	Miscible
Solubility in acetone	Miscible
Solubility in chloroform	Miscible
log P	-1.34[2]
Thermal conductivity	0.34 W/m-K (50% H2O @ 90 °C (194 °F))
Viscosity	0.042 Pa·s

5.7.3 Fluid Percentage

The glycol percentage mostly used were (50% glycol – 50% water) , in this research we used 70% mono propylene glycol type(99.9 %) and 30% water as mixed fluid and we experimented the effect of the fluid on the BTM's.

5.8 RECORD SYSTEM AND THERMAL SENSOR

It builds from open-source microcontroller called Arduino card, it used for development student project, this system deal with C++ and C# program languages, code wrote to measure the temperature and recorded results to SD card to used it in analysis step, this system content.

5.8.1 Arduino Mega Card

Using the ATmega2560 as its foundation, the Arduino Mega 2560 is a microcontroller board. It contains 16 analogue inputs, 4 hardware serial ports, a 16 MHz crystal oscillator, 54 digital input/output pins, 15 of which may be used as PWM outputs, a USB port, a power connector, an ICSP header, and a reset button. It also has a 16 MHz crystal oscillator. It comes with everything required to support the microcontroller; to get started, just plug in an AC-to-DC converter or battery, or use it to power a computer through USB. Most shields made for the Uno and older boards like the Duemilanove and Diecimila are compatible with the Mega 2560 board.

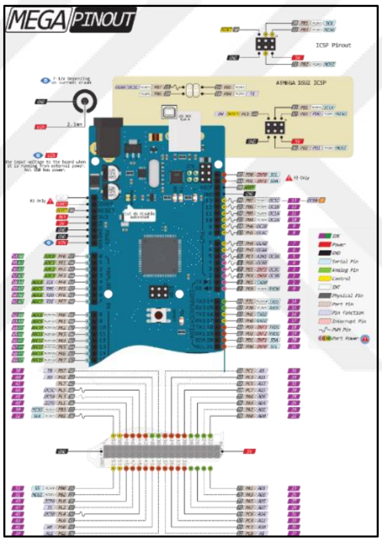

Figure 5.20: Arduino Mega Card and the Image Shown of Inputs and Outputs Pins.

5.8.2 Thermal Sensors

5.8.3 Sensor (NTC) Type

An NTC (Negative Temperature Coefficient) 10 kΩ thermal sensor is a type of thermistor used to measure temperature. It is called a "negative temperature coefficient" sensor because its resistance decreases as the temperature increases. The resistance of the NTC 10 kΩ thermal sensor is typically 10 kΩ at room temperature and changes based on temperature variations. Figure 5.21.

Figure 5.21: NTC 10KΩ Thermistor.

The NTC 10 kΩ thermal sensor is a passive device, meaning it requires no external power source to function. When it is exposed to a temperature change, its resistance changes accordingly, and this change can be used to determine the temperature.

The NTC 10 kΩ thermal sensor is typically used in a variety of applications, including temperature control and monitoring in industrial processes, HVAC systems, and automotive systems[89]. In these applications, the sensor is often used in conjunction with an analog-to-digital converter or other electronic device to measure and display the temperature.

One of the key advantages of NTC thermistors is their non-linear response to temperature changes, which makes them useful for temperature compensation in electronic circuits. By using an NTC thermistor in a circuit, the temperature of the circuit can be monitored and compensated for, allowing the circuit to operate reliably over a wide range of temperatures[90].

Some general details of NTC 10 kΩ thermal sensors include:

a. Operating temperature range: The operating temperature range of the NTC 10 kΩ thermal sensor typically varies from -40°C to 125°C, but it may vary depending on the manufacturer and specific model.

b. Precision: The precision of the NTC 10 kΩ thermal sensor is typically specified in terms of its tolerance, which is the maximum error between the actual temperature and the temperature indicated by the sensor. A typical tolerance for NTC 10 kΩ thermal sensors is ±1°C to ±2°C.

c. Response time: The response time of the NTC 10 kΩ therma l sensor refers to the time it takes for the sensor to reach approximately 63.2% of its final temperature after being exposed to a sudden temperature change. This time can vary depending on the thermal mass of the sensor and the thermal conductivity of its surroundings. A typical response time for NTC 10 kΩ thermal sensors is a few milliseconds.

d.Power dissipation: The NTC 10 kΩ thermal sensor is a passive device and therefore requires no external power source. However, the power dissipation of the sensor refers to the amount of power it consumes when it is used in an electronic circuit. This power consumption can vary depending on the resistance and other specifications of the sensor.

The NTC 10 kΩ thermal sensor is a widely used temperature sensing device that is commonly used in a variety of applications. Its ability to change resistance in response to temperature changes makes it an attractive choice for temperature measurement and control.

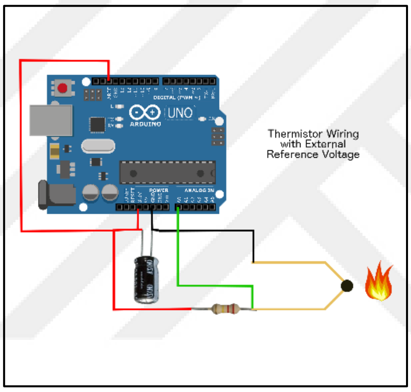

Figure 5.22: NTC 10KΩ Temperature Sensor with Circuit to Measure Temperature for the System.

5.8.4 Calibrate Steinhart-Hart Coefficients for Thermistors

The Steinhart-Hart equation[91] is a mathematical expression used to describe the relationship between the resistance of a thermistor and its temperature(aşağıda). It is widely used in temperature sensing applications where a thermistor is used to measure temperature. Calibrating Steinhart-Hart coefficients involves determining the values of the three coefficients (A, B, and C) in the equation, which are unique to a specific thermistor and its operating conditions.

To calibrate Steinhart-Hart coefficients, multiple temperature-resistance measurements are taken over the thermistor's operating range, typically at multiple temperatures between 0°C and 100°C. These measurements are then used to calculate the coefficients through a regression analysis, which fits a mathematical model to the data.

Once the coefficients are known, the thermistor's resistance can be used to determine its temperature at any point in its operating range. This calibration ensures that the thermistor's temperature readings are accurate and consistent, making it possible to use the thermistor in a variety of temperature sensing applications.

In summary, calibrating Steinhart-Hart coefficients for thermistors is a necessary step to ensure the accuracy and reliability of temperature measurements taken using these devices. It involves determining the values of the three coefficients in the Steinhart-Hart equation, which describe the relationship between the thermistor's resistance and its temperature, by analysing multiple temperature-resistance measurements.

According to [91], the resistance-temperature characteristic of an NTC thermistor can be described by the Steinhart-Hart equation:

$$1/T = A + B * \ln(R) + C * \ln^3(R) \tag{5.26}$$

Where T is the temperature in Kelvin, R is the resistance of the thermistor at temperature T, and A, B, and C are coefficients that are specific to the thermistor. These coefficients can be determined experimentally by measuring the resistance of the thermistor at a number of known temperatures and using a curve fitting algorithm to find the values of A, B, and C that best fit the data.

The calibrate the Steinhart-Hart coefficients for a thermistor depend on Measure the resistance of the thermistor at a number of known temperatures, for example, 0°C, 25°C, 50°C, and 100°C, and Convert the temperatures to Kelvin by adding 273.15 to each temperature in degrees Celsius and Calculate the natural logarithm of the resistance at each temperature.

Use a curve fitting algorithm to find the values of A, B, and C that best fit the data. The algorithm will minimize the sum of the squared differences between the calculated and measured temperatures.

Once you have the coefficients, you can use the Steinhart-Hart equation to calculate the temperature based on the measured resistance.

consider that the accuracy of the calculation depends on the accuracy of the coefficients and the measurement of resistance, as well as the temperature range over which the coefficients were calibrated. It is also important to use a thermistor that is suitable for the temperature range you want to measure.

The calculation needed to calibrate the thermistor is : see Figure 5.25

T_1 = 0°C when the resistance of a 10kΩ thermistor R_1 is 32650 Ω

T_2 = 50°C when the resistance of a 10 kΩ thermistor R_2 is 3603 Ω

T_3 = 100°C when the resistance of a 10 kΩ thermistor R_3 is 678.3 o Ω

$1/T = A + B(\ln R_1) + C(\ln R_1)^3$

$1/T = A + B(\ln R_2) + C(\ln R_2)^3$

$1/T = A + B(\ln R_3) + C(\ln R_3)^3$

For a 10 kΩ thermistor, the value of constants A, B and C are:

A = 0.001125308852122

B = 0.000234711863267

C = 0.000000085663516

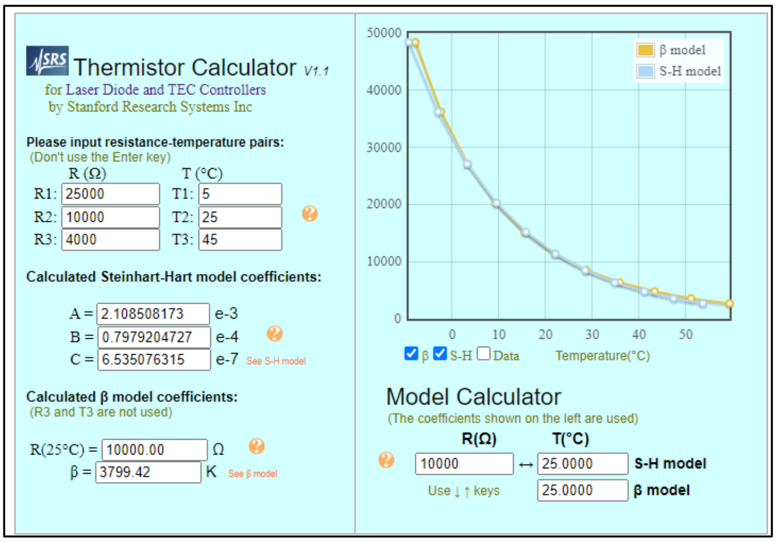

Figure 5.23: SRS Web-Based Thermistor Calculator.

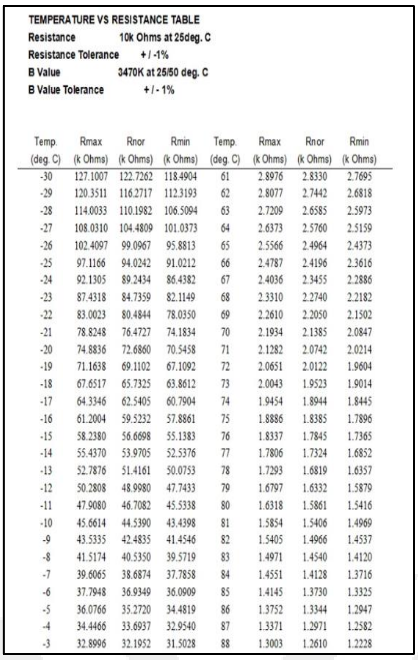

TEMPERATURE VS RESISTANCE TABLE
Resistance 10k Ohms at 25deg. C
Resistance Tolerance + / -1%
B Value 3470K at 25/50 deg. C
B Value Tolerance + / - 1%

Temp. (deg. C)	Rmax (k Ohms)	Rnor (k Ohms)	Rmin (k Ohms)	Temp. (deg. C)	Rmax (k Ohms)	Rnor (k Ohms)	Rmin (k Ohms)
-30	127.1007	122.7262	118.4904	61	2.8976	2.8330	2.7695
-29	120.3511	116.2717	112.3193	62	2.8077	2.7442	2.6818
-28	114.0033	110.1982	106.5094	63	2.7209	2.6585	2.5973
-27	108.0310	104.4809	101.0373	64	2.6373	2.5760	2.5159
-26	102.4097	99.0967	95.8813	65	2.5566	2.4964	2.4373
-25	97.1166	94.0242	91.0212	66	2.4787	2.4196	2.3616
-24	92.1305	89.2434	86.4382	67	2.4036	2.3455	2.2886
-23	87.4318	84.7359	82.1149	68	2.3310	2.2740	2.2182
-22	83.0023	80.4844	78.0350	69	2.2610	2.2050	2.1502
-21	78.8248	76.4727	74.1834	70	2.1934	2.1385	2.0847
-20	74.8836	72.6860	70.5458	71	2.1282	2.0742	2.0214
-19	71.1638	69.1102	67.1092	72	2.0651	2.0122	1.9604
-18	67.6517	65.7325	63.8612	73	2.0043	1.9523	1.9014
-17	64.3346	62.5405	60.7904	74	1.9454	1.8944	1.8445
-16	61.2004	59.5232	57.8861	75	1.8886	1.8385	1.7896
-15	58.2380	56.6698	55.1383	76	1.8337	1.7845	1.7365
-14	55.4370	53.9705	52.5376	77	1.7806	1.7324	1.6852
-13	52.7876	51.4161	50.0753	78	1.7293	1.6819	1.6357
-12	50.2808	48.9980	47.7433	79	1.6797	1.6332	1.5879
-11	47.9080	46.7082	45.5338	80	1.6318	1.5861	1.5416
-10	45.6614	44.5390	43.4398	81	1.5854	1.5406	1.4969
-9	43.5335	42.4835	41.4546	82	1.5405	1.4966	1.4537
-8	41.5174	40.5350	39.5719	83	1.4971	1.4540	1.4120
-7	39.6065	38.6874	37.7858	84	1.4551	1.4128	1.3716
-6	37.7948	36.9349	36.0909	85	1.4145	1.3730	1.3325
-5	36.0766	35.2720	34.4819	86	1.3752	1.3344	1.2947
-4	34.4466	33.6937	32.9540	87	1.3371	1.2971	1.2582
-3	32.8996	32.1952	31.5028	88	1.3003	1.2610	1.2228

Figure 5.24: Table Show the Temperature Equivalent to the Resistance Applied on Steinhart Equations.

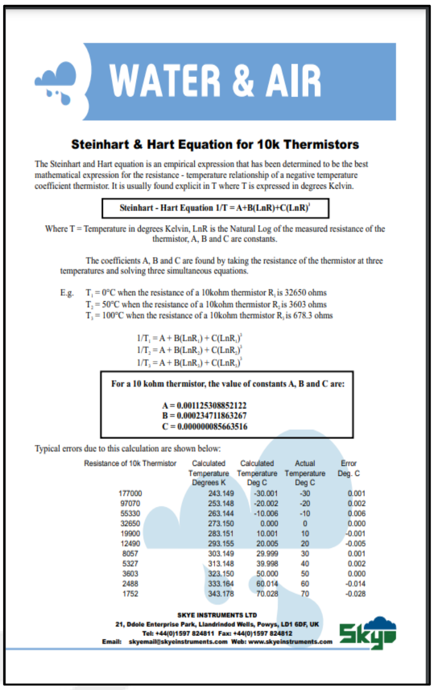

WATER & AIR

Steinhart & Hart Equation for 10k Thermistors

The Steinhart and Hart equation is an empirical expression that has been determined to be the best mathematical expression for the resistance - temperature relationship of a negative temperature coefficient thermistor. It is usually found explicit in T where T is expressed in degrees Kelvin.

Steinhart - Hart Equation $1/T = A+B(LnR)+C(LnR)^3$

Where T = Temperature in degrees Kelvin, LnR is the Natural Log of the measured resistance of the thermistor, A, B and C are constants.

The coefficients A, B and C are found by taking the resistance of the thermistor at three temperatures and solving three simultaneous equations.

E.g. T_1 = 0°C when the resistance of a 10kohm thermistor R_1 is 32650 ohms
T_2 = 50°C when the resistance of a 10kohm thermistor R_2 is 3603 ohms
T_3 = 100°C when the resistance of a 10kohm thermistor R_3 is 678.3 ohms

$$1/T_1 = A + B(LnR_1) + C(LnR_1)^3$$
$$1/T_2 = A + B(LnR_2) + C(LnR_2)^3$$
$$1/T_3 = A + B(LnR_3) + C(LnR_3)^3$$

For a 10 kohm thermistor, the value of constants A, B and C are:

A = 0.001125308852122
B = 0.000234711863267
C = 0.000000085663516

Typical errors due to this calculation are shown below:

Resistance of 10k Thermistor	Calculated Temperature Degrees K	Calculated Temperature Deg C	Actual Temperature Deg C	Error Deg. C
177000	243.149	-30.001	-30	0.001
97070	253.148	-20.002	-20	0.002
55330	263.144	-10.006	-10	0.006
32650	273.150	0.000	0	0.000
19900	283.151	10.001	10	-0.001
12490	293.155	20.005	20	-0.005
8057	303.149	29.999	30	0.001
5327	313.148	39.998	40	0.002
3603	323.150	50.000	50	0.000
2488	333.164	60.014	60	-0.014
1752	343.178	70.028	70	-0.028

SKYE INSTRUMENTS LTD
21, Ddole Enterprise Park, Llandrindod Wells, Powys, LD1 6DF, UK
Tel: +44(0)1597 824811 Fax: +44(0)1597 824812
Email: skyemail@skyeinstruments.com Web: www.skyeinstruments.com

Figure 5.25: Steinhart Equations and Applied the Calibration.

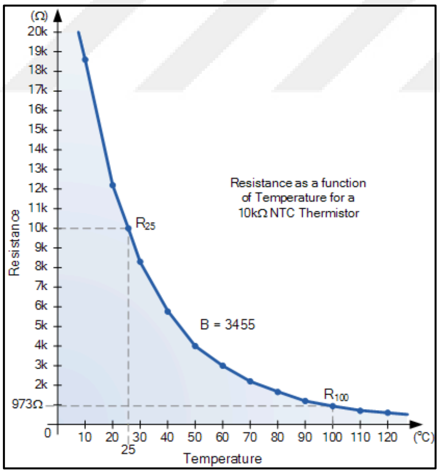

Figure 5.26: 10KΩ Ntc Thermistor Calibration (R&T) Chart.

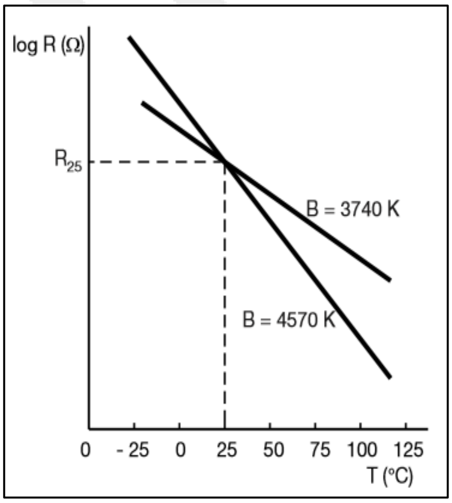

Figure 5.27: NTC Thermistor 10k Features Specifications Parameters Datasheet.

$$B_{(25/100)} = \frac{(100+273.15)\times(25+273.15)}{(100+273.15)-(25+273.15)} \times \ln\left(\frac{10000}{R_X}\right)$$

$$3455 = \frac{111254.6725}{75} \times \ln\left(\frac{10000}{R_X}\right)$$

$$3455 = 1483.4 \times \ln\left(\frac{10000}{R_X}\right)$$

$$e^{\left[\frac{3455}{1483.4}\right]} = \frac{10000}{R_X}$$

$$\therefore R_X = \frac{10000}{e^{2.33}} = 973\Omega$$

Figure 5.28: Example for Applied the Steinhart Equation and the Value of the Resistance that a Pointed to Temperature that Read from Body.

5.8.5 Flowrate Sensor Work

If the output valve of the pipe is opened. The water flows through the sensor, which in turn rotates the wheel inside the sensor (Figure 5.29). In this condition, we can observe pulses, which are generated from the sensor. These pulses will act as an interrupt signal to the Arduino UNO. For every interrupt signal (rising edge), the count of the flow frequency variable will be increased by one. The current time and clop Time variable ensure that for every one second the value of the flow frequency is taken for calculation of flow rate and volume. After the calculation is finished, the flow frequency variable is set to zero and the whole procedure is started from the beginning. (**Figure 5.29**).

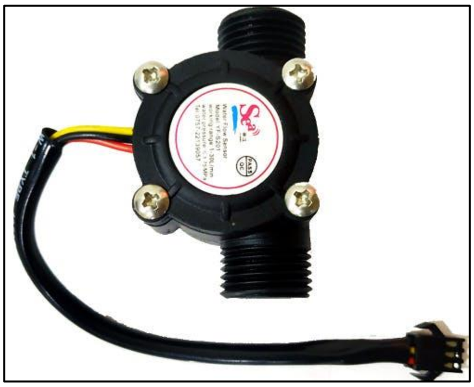

Figure 5.29: Flowrate Sensor.

If the pipe's output valve is opened. The wheel inside the sensor turns as a result of the water flowing through it. We can see the sensor-generated pulses under these circumstances. The Arduino UNO will use these pulses as an interrupt signal. The count of the flow frequency variable will rise one for each interrupt signal (rising edge). The flow frequency value is taken into account for the calculation of flow rate and volume once per second thanks to the current time and clop Time variable. The flow frequency variable is set to zero when the computation is complete, and the process is then repeated from the beginning.

Applications of Flow Sensors:

In addition to industrial sectors, other applications of flow sensors include agriculture, food processing, water management, mining, water recycling, coffee makers, etc.

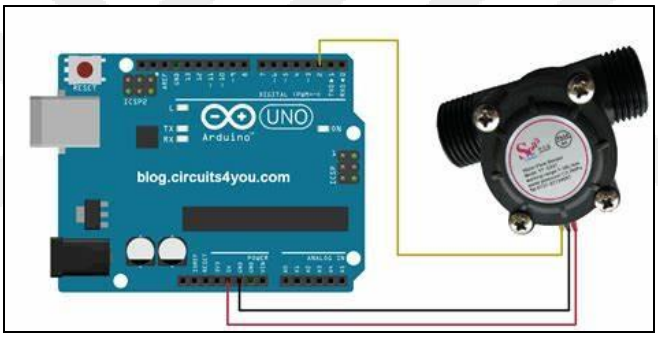

Figure 5.30: Fluid flowrate with Arduino Card System to Measure the Flow.

5.8.6 DC Voltage Sensor

Definition: A potential divider is used by the Voltage Sensor Module, a straightforward but extremely practical module, to lower an input voltage by a factor of 5. The 0-25V Voltage Sensor Module enables you to monitor voltages far greater than what a microcontroller can sense using the analog input of the device.

In this thesis it used three voltage sensors to read the voltage in battery pack and set limit of drop voltage that should stop the experiment and protect the batteries from dead under manufacturing limit for lithium ion cylindrical battery type 18650 where the limit was 2.7 volt, below is the voltage sensor specifications and (Figure 5.32) the show the physical shape

The voltage sensor used specifications is see (Figure 5.31):

a. Output Type: Analog.

b. Input Voltage (V): 0 to 25.

c. Voltage Detection Range (V): 0.02445 to 25.

d. Analog Voltage Resolution (V): 0.00489.

e. Dimensions: 4 × 3 × 2 cm.

The voltage sensor module has 5 pins, 2 on the front side and 3 on the backside Pinout:

a. VCC: Positive terminal of the External voltage source (0-25V).

b. GND: Negative terminal of the External voltage source.

c. S: Analog pin connected to Analog pin of the microcontroller.

d. (+): Not Connected.

e. (-): Ground Pin connected to GND of microcontroller.

5.8.7 Voltage Sensor Module Design & Construction

The Voltage Sensor is essentially a Voltage Divider composed of two resistors with resistances of 30K and 7.5K, resulting in a voltage divider with a 5 to 1 ratio. As a result, for each input voltage, the output voltage is lowered by a factor of 5. The Voltage Sensor Module's internal circuit schematic is shown below.

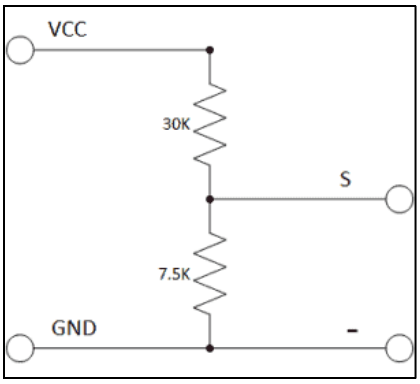

Figure 5.31: Voltage Divider Schematic that Used in Voltage Sensor.

The Arduino analog input pin has a maximum voltage input of 5V, which makes it compatible with this module. However, if the controller operates on a 3.3V system, the input voltage must not exceed 16.5V (3.3V x 5). The Arduino AVR chips have a 10-bit AD, allowing this module to achieve a resolution of 0.00489V (5V/1023). Therefore, the minimum detectable input voltage for this module is 0.02445V (0.00489V x 5). To interface the 0-25V DC Voltage Sensor Module with an Arduino, connect the Signal (S) and Negative (-) pins of the Voltage Sensor to Arduino's A0 and GND pins, respectively. The circuit diagram is provided below.

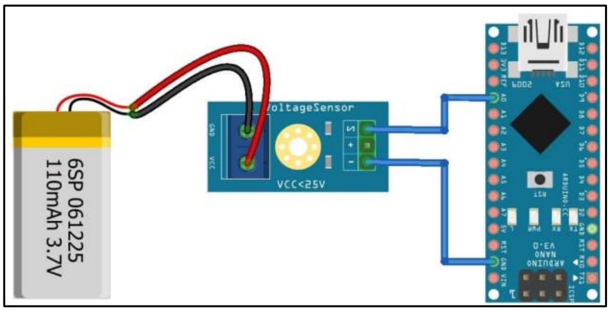

Figure 5.32: Connection of Voltage Sensor with Arduino Board.

5.8.8 Dc Current Sensor (Acs712/Ac-Dc Sensor)

5.8.8.1 Definition

The ACS712 is a fully integrated, hall effect-based linear current sensor with 2.1kVRMS voltage isolation and a integrated low-resistance current conductor. Technical terms aside, it’s simply put forth as a current sensor that uses its conductor to calculate and measure the amount of current applied [Copyright 2022, Allegro Microsystems].

Arduino is a popular microcontroller platform that allows you to create a variety of electronic projects. One of the key features of Arduino is its ability to interface with a variety of sensors and modules, including current sensors like the ACS712/AC-DC.

The ACS712/AC-DC current sensor is a small, inexpensive module that can be used to measure the current flowing through a circuit. It is a Hall effect-based sensor, which means that it measures the magnetic field generated by the current flowing through a conductor. The sensor has a built-in amplifier, so it can output an analog voltage that is proportional to the measured current.

5.8.8.2 Key features of the ACS712/AC-DC current sensor include

a. High Accuracy: The ACS712/AC-DC sensor has a high accuracy of around ±1.5% when measuring currents ranging from 0 to 5A. This makes it suitable for a wide range of applications.
b.Wide Operating Voltage Range: The sensor can operate over a wide voltage range of 5V to 30V DC, which makes it compatible with a variety of Arduino boards and other microcontroller platforms.
c. Low Noise: The ACS712/AC-DC sensor has low noise, which means that it can provide stable and accurate readings even in noisy environments.
d. Easy to Use: The sensor is easy to use, as it only requires a few connections to the Arduino board. The output voltage can be read using one of the analog input pins on the Arduino board.
e. Bidirectional Current Measurement: The ACS712/AC-DC sensor can measure current in both directions, which makes it suitable for applications where the current can change direction.

5.8.8.3 Applications of the ACS712/AC-DC current sensor include

a. Measuring Battery Charge/Discharge Currents: The sensor can be used to measure the current flowing into or out of a battery, which can be useful for monitoring battery health and performance.
b. Monitoring Power Consumption: The sensor can be used to monitor the power consumption of devices or appliances, which can help to identify energy-saving opportunities.
c. Motor Control: The sensor can be used in motor control applications to monitor the current flowing through the motor, which can help to prevent damage due to overcurrent.
d. Robotics: The sensor can be used in robotics applications to monitor the current flowing through motors and other components, which can help to improve performance and prevent damage. Real Time clock card (RTC) module (DS3231).
e. The module's ability to operate at 3.3 or 5 V makes it compatible with a wide range of development platforms and microcontrollers. A standard CR2032 3V battery can run the module and preserve the information for more than a year. The battery input is 3V. (Figure 5.33).

f. The module connects to the Arduino Board extremely easily since it uses the (I2C) Communication Protocol.

5.8.9 Arduino SD card

Arduino is an open-source platform for building electronic projects, and it is widely used by hobbyists and professionals alike. One of the most popular features of Arduino is its ability to interface with SD cards, allowing you to store and retrieve data easily.

An SD card is a small, portable storage device that uses flash memory to store data. They are commonly used in digital cameras, smartphones, and other portable devices. The Arduino SD library allows you to communicate with SD cards using the SPI interface.

To use an SD card with your Arduino, you'll need to connect it to the Arduino's SPI pins. The SPI pins vary depending on the specific model of Arduino you are using, but they are typically labelled MOSI, MISO, SCK, and CS. You'll also need to connect the SD card's power and ground pins to the appropriate pins on the Arduino.

Once you have the SD card connected to the Arduino, you can use the SD library to read and write data to the card. The library provides functions for initializing the card, opening files, reading and writing data, and closing files.

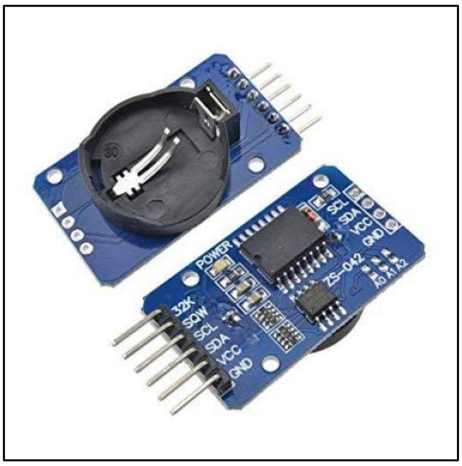

Figure 5.33: Real Time Clock Card.

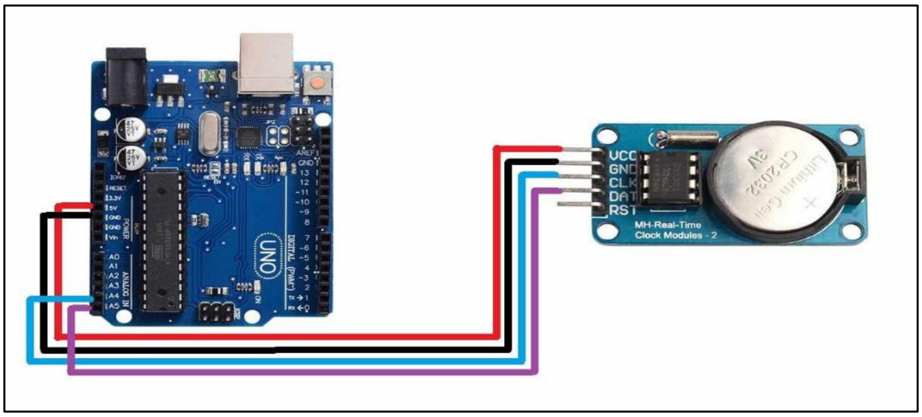

Figure 5.34: RTC Connection with Arduino Uno Card.

6. RESULTS AND DISCUSSION

In this research we recorded temperatures at vary loaded (1C, 0.7C,0.66C,0.6C,0.88C) and the graph shown the changes in temperatures, at peak load we recorded 37 ℃ without using BTMS. And noted that battery pack did not exceed the 35℃ by using our system Z5A and that will be keep system at range of operation temperature.

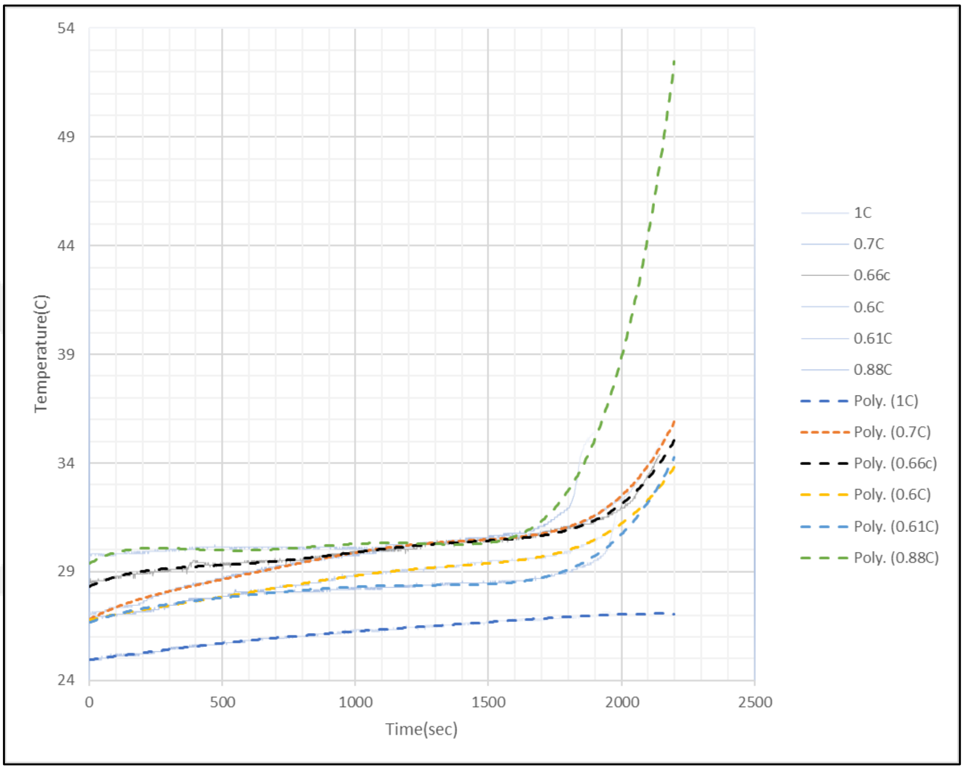

Figure 6.1: Experiment Results for Crate at Different Loads, the Figure Modified to Show Soft Curves and Cancel Noises.

6.1 EXPERIMENT .1 AT (0.7 C-RATE)

At this test we recorded the temperature at 0.7C-rate and the temperature of system not exceeded 36.8℃ by using the BTMS Z5A and it be under control during the time of test and figures down shown all the varying in current drop and the voltages at batteries pack cells.

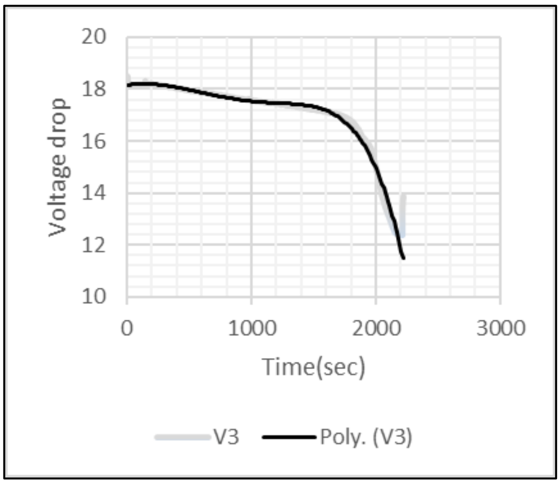

Figure 6.2: Voltage(V3) Measured During Discharge (7,2V) (0.7C).

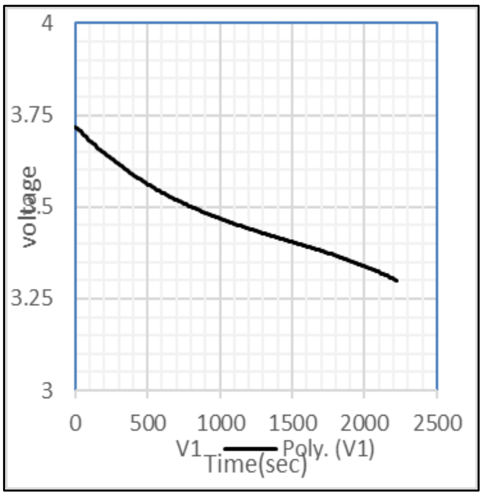

Figure 6.3: Voltage(V1) Measured During Discharge (7,2V) (0.7C).

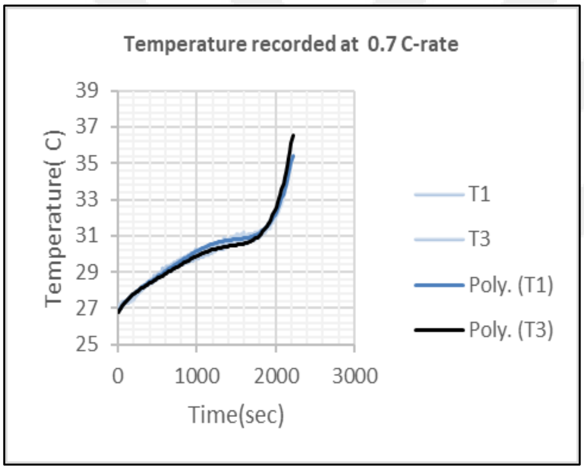

Figure 6.4: Temperatures Recorded by Sensor (0.7C).

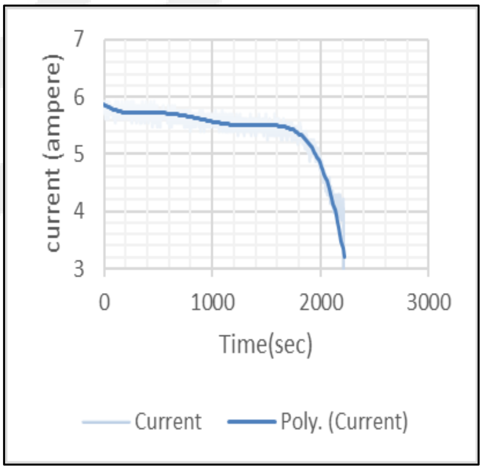

Figure 6.5: Current Drop Recorded Dthe Discharge (0.7C).

6.2 EXPERIMENT.2 AT (0.66 C-RATE)

At this test we recorded the temperature at 0.66C-rate and the temperature of system not exceeded 34.3°C by using the BTMS Z5A and it be under control during the time of test and figures down shown all the varying in current drop and the voltages at batteries pack cells. At the test we noted some improving in cooling battery and performance.

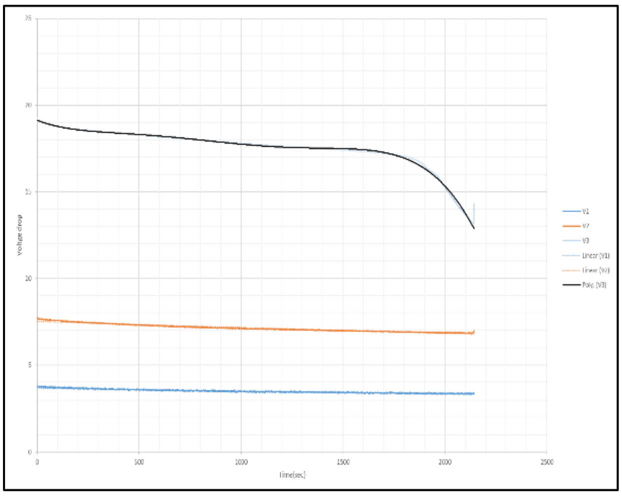

Figure 6.6: Voltage Measured During Discharge (V1, V2&V3 (0.66 C).

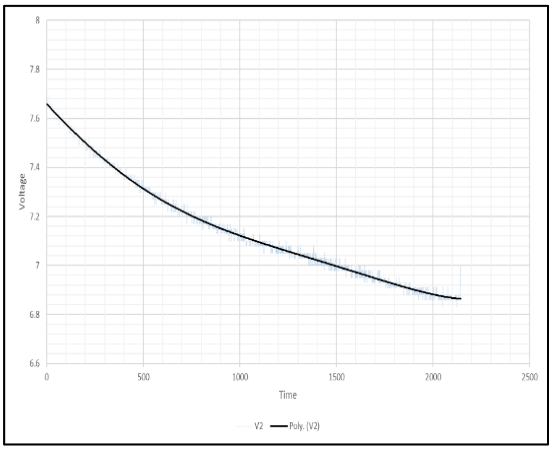

Figure 6.7: Voltage Measured During Discharge (7.2V) (0.66C).

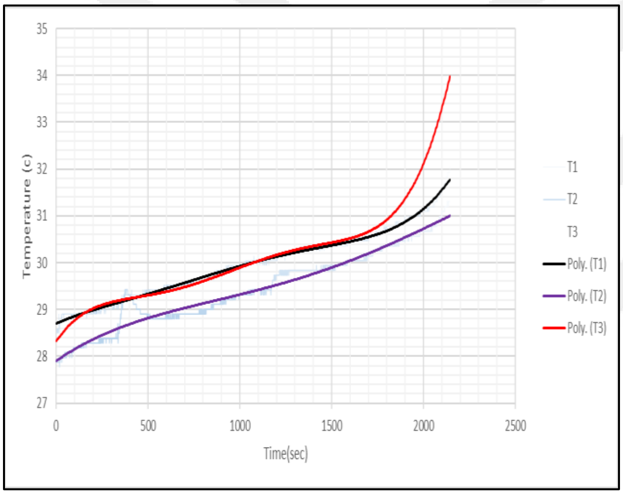

Figure 6.8: Temperatures Measured During Discharge (0.66C).

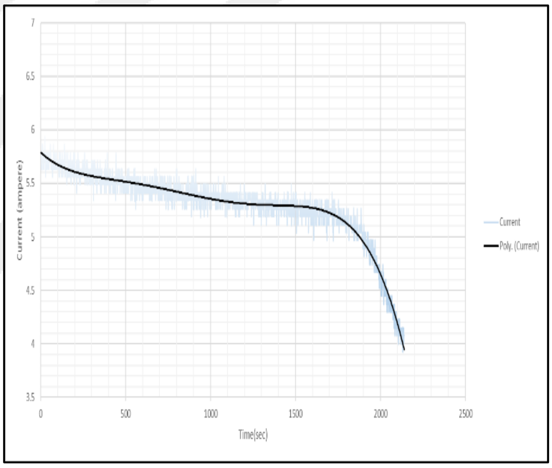

Figure 6.9: Current Drop Recorded During the Discharge (0.66C).

6.3 EXPERIMENT.3 AT (0.6 C-RATE)

At this test we recorded the temperature at 0.66C-rate and the temperature of system not exceeded 31.14°C by using the BTMS Z5A and it be under control during the time of test and figures down shown all the varying in current drop and the voltages at batteries pack cells. At the test we noted some improving in cooling battery and performance.

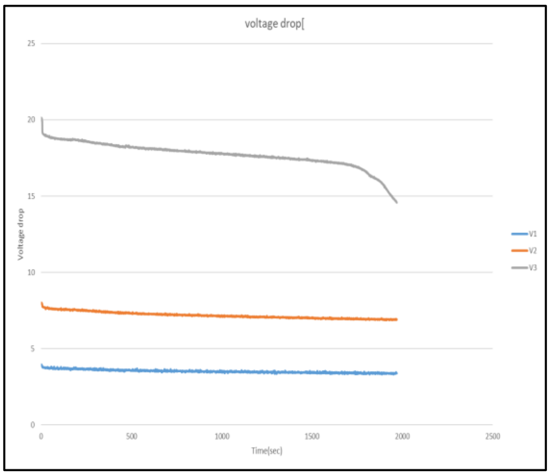

Figure 6.10: Voltage Measured During Discharge (7,2V) (0.6C).

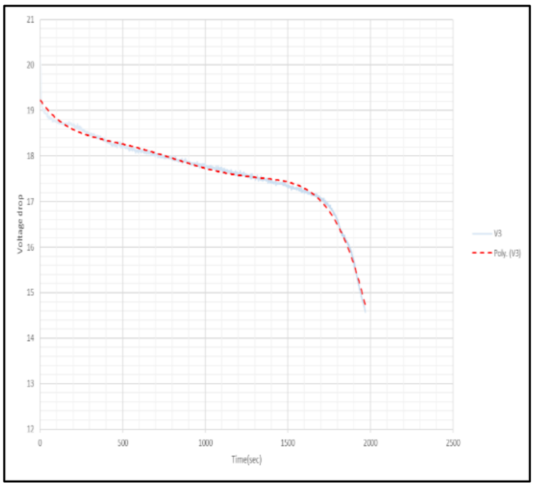

Figure 6.11: Voltage Measured During Discharge (7,2V) (0.6C).

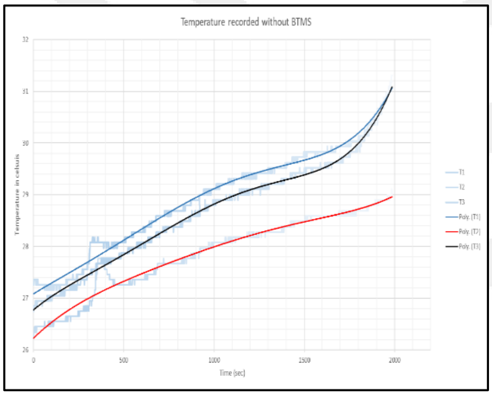

Figure 6.12: Temperatures Recorded by Sensor at (0.6C).

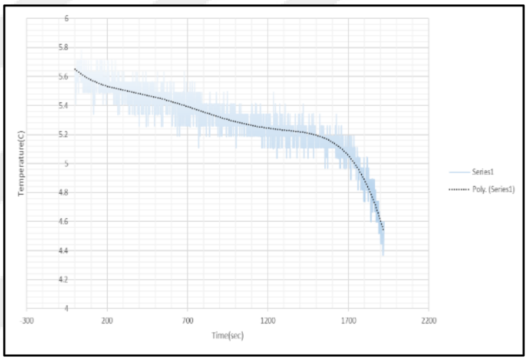

Figure 6.13: Current Drop Recorded During the Discharge (0.6C).

6.4 EXPERIMENT.4 AT (1 C-RATE)

At this test we recorded the temperature at 1C-rate and the temperature of system not exceeded 29.42 ℃ by using the BTMS Z5A and it be under control during the time of test and figures down shown all the varying in current drop and the voltages at batteries pack cells. At the test we noted some improving in cooling battery and performance, and that will be the perfect test at nominal boundary conditions, in load, environment of test and discharge, temperatures of system.

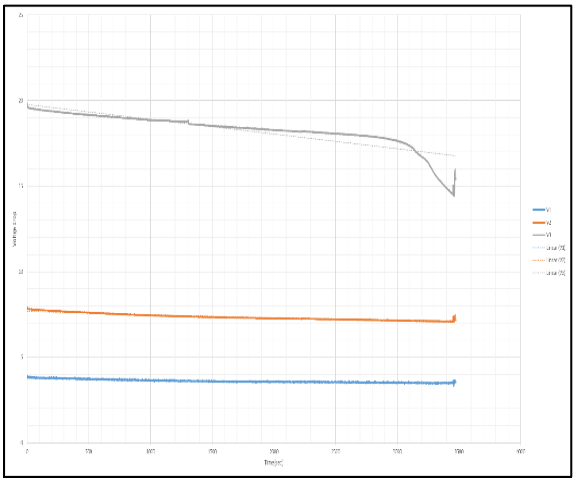

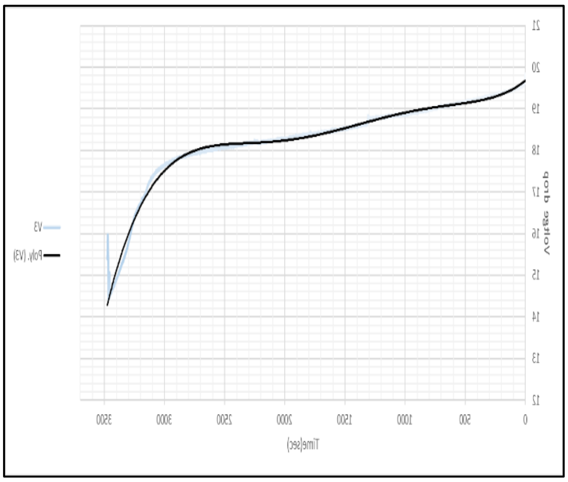

Figure 6.14: Voltage Measured During Discharge (7,2V) (1C).

Figure 6.15: Voltage (V3)Measured During Discharge (7,2V) (1C).

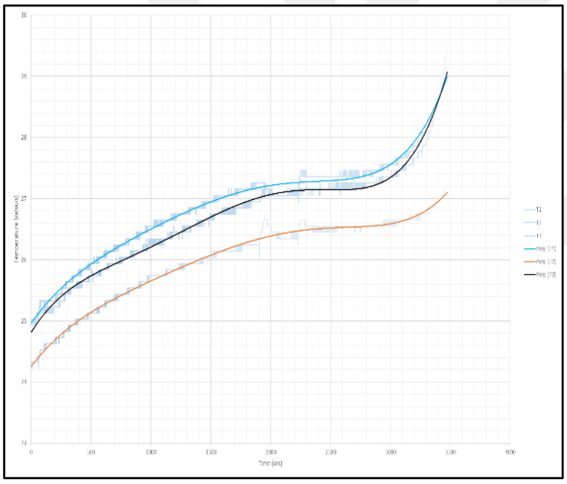

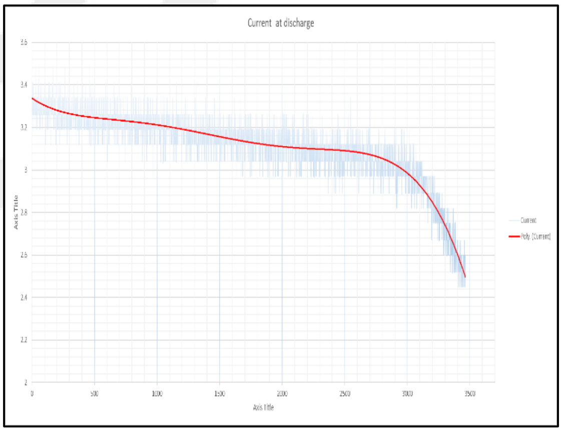

Figure 6.16: Temperatures Recorded by Sensor at (1C).

Figure 6.17: Current Drop Recorded During the Discharge (1C).

6.5 EXPERIMENT.5 AT (0.88 C-RATE)

At this test we recorded the temperature at 1C-rate and the temperature of system not exceeded 35 °C by using the BTMS Z5A and it be under control during the time of test and figures down shown all the varying in current drop and the voltages at batteries pack cells. At the test we noted some improving in cooling battery and performance, and that will be the perfect test at nominal boundary conditions, in load, environment of test and discharge, temperatures of system.

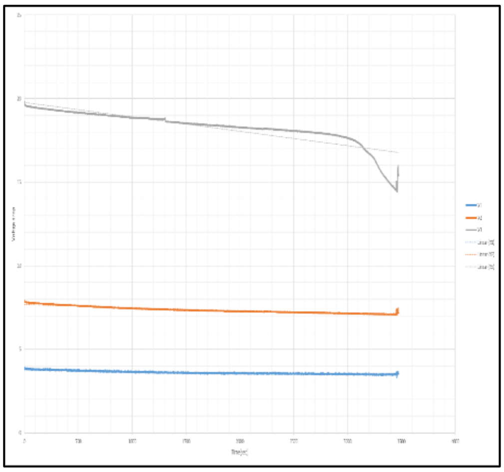

Figure 6.18: Voltage Measured During Discharge (7,2V) (0.88C).

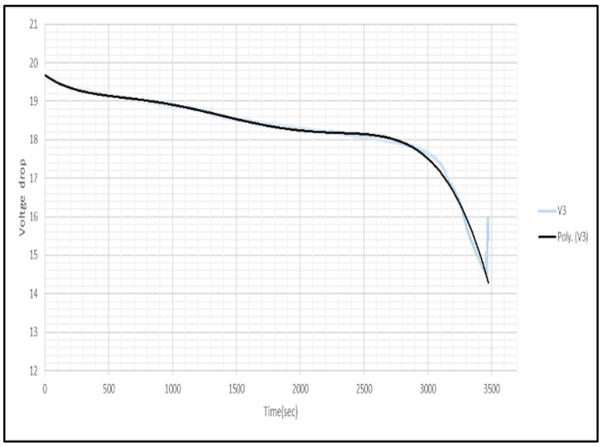

Figure 6.19: Voltage (V3)Measured During Discharge (7,2V) (0.88C).

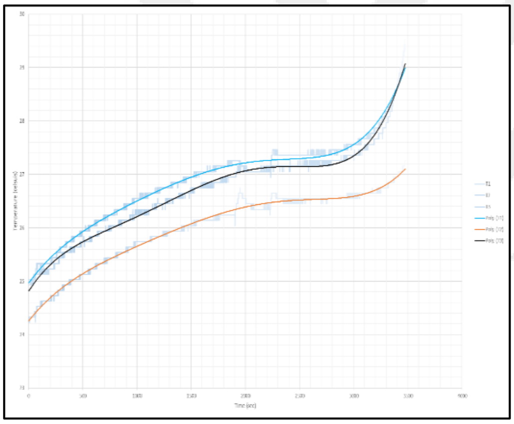

Figure 6.20: Temperatures Recorded by Sensor at (0.88C).

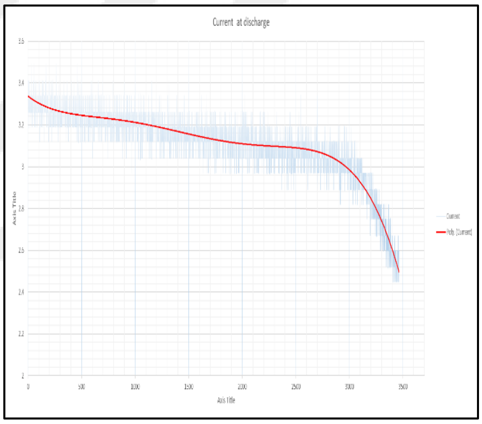

Figure 6.21: Current Drop Recorded During the Discharge (0.88C).

7. CONCLUSION

The cooling mini channel of battery thermal management system (Z5A) was design and implement in practical works and simulation it in ANSYS program thermal steady state to show the thermal behaviour for battery lithium ion type 18650 3.7V and 2200 mAh cylindrical shape and distribution, the Z5A cooling system was design to cover the shell of battery and isolated electrically to avoid the connection between system and batteries , the design prove that we can used to different types of cylindrical batteries sizes that because the material used which is copper with 2mm diameter , the system reduced the thermal effect of battery and the results shown good performance for battery under many discharges load tests, where the heat flow as expression of heat generation inside battery , the temperature of fluid was 25℃ and where it was cooling the fluid by using small size of computer radiator it was perfect solutions to safe the temperature of the fluid under high discharge load, the reader sensors system was implement and calibration to read all temperatures and measure the thermal behavior under discharge load , the system used Arduino and ntc10k sensors, voltage ,current sensors . this system was so effective and need to development to read a lot of sensors.

The cooling system is effective with lithium-ion cylindrical shape battery type 18650 it reduced the temperature ± 5 degree and under small discharge load it exceeds 10 degrees.

Future works: this system needs to experiment with different high-power batteries and different speed of fluid to studying the efficiency of system to reducing temperature under high load.

REFERENCES

[1] X. Zhang, Z. Li, L. Luo, Y. Fan, and Z. Du, “A review on thermal management of lithium-ion batteries for electric vehicles,” *Energy*, vol. 238, p. 121652, 2022, doi: 10.1016/j.energy.2021.121652.

[2] “Dean C. Smith via Twitter.” https://twitter.com/DeanCSmith/status/977286282991755264.

[3] Y. Saito, K. Kanari, and K. Takano, “Thermal studies of a lithium-ion battery,” *J Power Sources*, vol. 68, no. 2, pp. 451–454, Oct. 1997, doi: 10.1016/S0378-7753(96)02583-9.

[4] Y. M. Alkhulaifi, N. A. A. Qasem, and S. M. Zubair, “Improving the performance of thermal management system for electric and hybrid electric vehicles by adding an ejector,” *Energy Convers Manag*, vol. 201, p. 112133, Dec. 2019, doi: 10.1016/J.ENCONMAN.2019.112133.

[5] Q. Norman, “Industry developments in thermal management of electric vehicle batteries.” [Online]. Available: https://www.qats.com/cms/category/ battery-cooling/

[6] J. Gate, “Rechargeable Batteries Applications Handbook,” *Newnes*, 1998.

[7] Z. An, L. Jia, Y. Ding, C. Dang, and X. Li, “A review on lithium-ion power battery thermal management technologies and thermal safety,” *Journal of Thermal Science*, vol. 26, no. 5, pp. 391–412, 2017, doi: 10.1007/s11630-017-0955-2.

[8] S. Basu, K. S. Hariharan, S. M. Kolake, T. Song, D. K. Sohn, and T. Yeo, “Coupled electrochemical thermal modelling of a novel Li-ion battery pack thermal management system,” *Appl Energy*, vol. 181, pp. 1–13, Nov. 2016, doi: 10.1016/j.apenergy.2016.08.049.

[9] Brand: TRUMONY, “Serpentine channels cooling plates,” *https://www.trumony.com/*.

[10] S. al Hallaj and J. R. Selman, “A Novel Thermal Management System for Electric Vehicle Batteries Using Phase-Change Material,” *J Electrochem Soc*, vol. 147, no. 9, p. 3231, 2000, doi: 10.1149/1.1393888.

[11] YalianAU - Hu Yang XiaosongAU - Qing DatongAU - Chen, “Arrhenius Equation-Based Cell-Health Assessment: Application to Thermal Energy Management Design

of a HEV NiMH Battery Pack," *Energies*, vol. 6, no. 5. pp. 2709–2725, 2013. doi: 10.3390/en6052709.

[12] J. Esmaeili and H. Jannesari, "Developing heat source term including heat generation at rest condition for Lithium-ion battery pack by up scaling information from cell scale," *Energy Convers Manag*, vol. 139, pp. 194–205, 2017, doi: 10.1016/j.enconman.2017.02.052.

[13] S. Basu, K. S. Hariharan, S. M. Kolake, T. Song, D. K. Sohn, and T. Yeo, "Coupled electrochemical thermal modelling of a novel Li-ion battery pack thermal management system," *Appl Energy*, vol. 181, pp. 1–13, Nov. 2016, doi: 10.1016/j.apenergy.2016.08.049.

[14] Y. Saito, "Thermal behaviors of lithium-ion batteries during high-rate pulse cycling," *J Power Sources*, vol. 146, no. 1–2, pp. 770–774, 2005, doi: 10.1016/j.jpowsour.2005.03.089.

[15] X. G. Yang, Y. Leng, G. Zhang, S. Ge, and C. Y. Wang, "Modeling of lithium plating induced aging of lithium-ion batteries: Transition from linear to nonlinear aging," *J Power Sources*, vol. 360, pp. 28–40, 2017, doi: 10.1016/j.jpowsour.2017.05.110.

[16] T. M. Bandhauer, S. Garimella, and T. F. Fuller, "A Critical Review of Thermal Issues in Lithium-Ion Batteries," *J Electrochem Soc*, vol. 158, no. 3, p. R1, 2011, doi: 10.1149/1.3515880.

[17] M. R. Palacín, "Understanding ageing in Li-ion batteries: A chemical issue," *Chem Soc Rev*, vol. 47, no. 13, pp. 4924–4933, 2018, doi: 10.1039/c7cs00889a.

[18] T. M. Bandhauer, S. Garimella, and T. F. Fuller, "A Critical Review of Thermal Issues in Lithium-Ion Batteries," *J Electrochem Soc*, vol. 158, no. 3, p. R1, 2011, doi: 10.1149/1.3515880.

[19] Z. Rao and S. Wang, "A review of power battery thermal energy management," *Renewable and Sustainable Energy Reviews*, vol. 15, no. 9, pp. 4554–4571, Dec. 2011, doi: 10.1016/J.RSER.2011.07.096.

[20] F. M. Kindermann, J. Keil, A. Frank, and A. Jossen, "A SEI Modeling Approach Distinguishing between Capacity and Power Fade," *J Electrochem Soc*, vol. 164, no. 12, pp. E287–E294, 2017, doi: 10.1149/2.0321712jes.

[21] D. R. Rajagopalan Kannan, P. K. Terala, P. L. Moss, and M. H. Weatherspoon, "Analysis of the Separator Thickness and Porosity on the Performance of Lithium-

Ion Batteries," *International Journal of Electrochemistry*, vol. 2018, pp. 1–7, 2018, doi: 10.1155/2018/1925708.

[22] B. Balagopal, C. S. Huang, and M. Y. Chow, "Effect of calendar ageing on SEI growth and its impact on electrical circuit model parameters in Lithium ion batteries," *Proceedings - 2018 IEEE International Conference on Industrial Electronics for Sustainable Energy Systems, IESES 2018*, vol. 2018-Janua, pp. 32–37, 2018, doi: 10.1109/IESES.2018.8349846.

[23] M. B. Pinson and M. Z. Bazant, "Theory of SEI Formation in Rechargeable Batteries: Capacity Fade, Accelerated Aging and Lifetime Prediction," *J Electrochem Soc*, vol. 160, no. 2, pp. A243–A250, 2013, doi: 10.1149/2.044302jes.

[24] A. A. Tahmasbi, T. Kadyk, and M. H. Eikerling, "Statistical Physics-Based Model of Solid Electrolyte Interphase Growth in Lithium Ion Batteries," *J Electrochem Soc*, vol. 164, no. 6, pp. A1307–A1313, 2017, doi: 10.1149/2.1581706jes.

[25] P. R. Tete, M. M. Gupta, and S. S. Joshi, "Developments in battery thermal management systems for electric vehicles: A technical review," *Journal of Energy Storage*, vol. 35. Elsevier Ltd, Mar. 01, 2021. doi: 10.1016/j.est.2021.102255.

[26] S. Neupane, M. Alipanah, D. Barnes, and X. Li, "Heat generation characteristics of LiFePO4 pouch cells with passive thermal management," *Energies (Basel)*, vol. 11, no. 5, 2018, doi: 10.3390/en11051243.

[27] C. Zhang, S. Santhanagopalan, M. A. Sprague, and A. A. Pesaran, "Coupled mechanical-electrical-thermal modeling for short-circuit prediction in a lithium-ion cell under mechanical abuse," *J Power Sources*, vol. 290, pp. 102–113, 2015, doi: 10.1016/j.jpowsour.2015.04.162.

[28] C. R. Birkl, M. R. Roberts, E. McTurk, P. G. Bruce, and D. A. Howey, "Degradation diagnostics for lithium ion cells," *J Power Sources*, vol. 341, pp. 373–386, 2017, doi: 10.1016/j.jpowsour.2016.12.011.

[29] R. Hausbrand *et al.*, "Fundamental degradation mechanisms of layered oxide Li-ion battery cathode materials: Methodology, insights and novel approaches," *Mater Sci Eng B Solid State Mater Adv Technol*, vol. 192, no. C, pp. 3–25, 2015, doi: 10.1016/j.mseb.2014.11.014.

[30] Iñigo Ortega, "The Battery Thermal Management System (BTMS) is the device responsible for managing/dissipating the heat generated during the electrochemical

processes occurring in cells, allowing the battery to operate safely and efficiently.," *Thermal Energy Solutions Area.*, 2021. https://cicenergigune.com/en/blog/battery-thermal-management-system-btms-electric-vehicle

[31] Z. Zhang and Y. Wang, "Thermal management of lithium-ion batteries in electric vehicles: A review," *J Power Sources*, vol. 369, pp. 511–527, 2021.

[32] Z. Rao and S. Wang, "A review of power battery thermal energy management," *Renewable and Sustainable Energy Reviews*, vol. 15, no. 9, pp. 4554–4571, Dec. 2011, doi: 10.1016/j.rser.2011.07.096.

[33] X. F. Q. S. and X. Z. Y. Liu, "Thermal management strategies for lithium-ion batteries in electric vehicles," *Energy Convers Manag*, vol. 186, pp. 699–717, 2019.

[34] S. Jia and H. Li, "The development of active battery thermal management systems for electric vehicles," *Journal of Energy Storage*, vol. 25, pp. 143–157, 2019.

[35] G. Karimi and X. Li, "Thermal management of lithium-ion batteries for electric vehicles," *Int J Energy Res*, vol. 37, no. 1, pp. 13–24, Jan. 2013, doi: 10.1002/er.1956.

[36] Q. L. Yue, C. X. He, J. Sun, J. B. Xu, and T. S. Zhao, "A passive thermal management system with thermally enhanced water adsorbents for lithium-ion batteries powering electric vehicles," *Appl Therm Eng*, vol. 207, May 2022, doi: 10.1016/j.applthermaleng.2022.118156.

[37] T. M. Bandhauer and S. Garimella, "Passive, internal thermal management system for batteries using microscale liquid-vapor phase change," *Appl Therm Eng*, vol. 61, no. 2, pp. 756–769, 2013, doi: 10.1016/j.applthermaleng.2013.08.004.

[38] M. M. El Idi, M. Karkri, and M. Abdou Tankari, "A passive thermal management system of Li-ion batteries using PCM composites: Experimental and numerical investigations," *Int J Heat Mass Transf*, vol. 169, Apr. 2021, doi: 10.1016/j.ijheatmasstransfer.2020.120894.

[39] A. K. Thakur *et al.*, "A state of art review and future viewpoint on advance cooling techniques for Lithium–ion battery system of electric vehicles," *Journal of Energy Storage*, vol. 32. Elsevier Ltd, Dec. 01, 2020. doi: 10.1016/j.est.2020.101771.

[40] S. Yang, C. Ling, Y. Fan, Y. Yang, X. Tan, and H. Dong, "A review of lithium-ion battery thermal management system strategies and the evaluate criteria,"

International Journal of Electrochemical Science, vol. 14, no. 7. Electrochemical Science Group, pp. 6077–6107, 2019. doi: 10.20964/2019.07.06.

[41] S. Basu, K. S. Hariharan, S. M. Kolake, T. Song, D. K. Sohn, and T. Yeo, "Coupled electrochemical thermal modelling of a novel Li-ion battery pack thermal management system," *Appl Energy*, vol. 181, pp. 1–13, Nov. 2016, doi: 10.1016/j.apenergy.2016.08.049.

[42] W. Wu, S. Wang, W. Wu, K. Chen, S. Hong, and Y. Lai, "A critical review of battery thermal performance and liquid based battery thermal management," *Energy Conversion and Management*, vol. 182. Elsevier Ltd, pp. 262–281, Jan. 01, 2019. doi: 10.1016/j.enconman.2018.12.051.

[43] Z. Rao and S. Wang, "A review of power battery thermal energy management," *Renewable and Sustainable Energy Reviews*, vol. 15, no. 9. pp. 4554–4571, Dec. 2011. doi: 10.1016/j.rser.2011.07.096.

[44] M. A. Bamdezh and G. R. Molaeimanesh, "Impact of system structure on the performance of a hybrid thermal management system for a Li-ion battery module," *J Power Sources*, vol. 457, no. March, p. 227993, 2020, doi: 10.1016/j.jpowsour.2020.227993.

[45] J. Lin, X. Liu, S. Li, C. Zhang, and S. Yang, "A review on recent progress, challenges and perspective of battery thermal management system," *International Journal of Heat and Mass Transfer*, vol. 167. Elsevier Ltd, Mar. 01, 2021. doi: 10.1016/j.ijheatmasstransfer.2020.120834.

[46] S. Wang *et al.*, "A forced gas cooling circle packaging with liquid cooling plate for the thermal management of Li-ion batteries under space environment," *Appl Therm Eng*, vol. 123, pp. 929–939, 2017, doi: 10.1016/j.applthermaleng.2017.05.159.

[47] M. S. Patil, J. H. Seo, S. Panchal, S. W. Jee, and M. Y. Lee, "Investigation on thermal performance of water-cooled Li-ion pouch cell and pack at high discharge rate with U-turn type microchannel cold plate," *Int J Heat Mass Transf*, vol. 155, p. 119728, 2020, doi: 10.1016/j.ijheatmasstransfer.2020.119728.

[48] M. S. Patil, J. H. Seo, S. Panchal, and M. Y. Lee, "Numerical study on sensitivity analysis of factors influencing liquid cooling with double cold-plate for lithium-ion pouch cell," *Int J Energy Res*, vol. 45, no. 2, pp. 2533–2559, 2021, doi: 10.1002/er.5946.

[49] H. Zhang, C. Li, R. Zhang, Y. Lin, and H. Fang, "Thermal analysis of a 6s4p Lithium-ion battery pack cooled by cold plates based on a multi-domain modeling framework," *Appl Therm Eng*, vol. 173, no. March, p. 115216, 2020, doi: 10.1016/j.applthermaleng.2020.115216.

[50] C. Menale, F. D'Annibale, B. Mazzarotta, and R. Bubbico, "Thermal management of lithium-ion batteries: An experimental investigation," *Energy*, vol. 182, pp. 57–71, 2019, doi: 10.1016/j.energy.2019.06.017.

[51] M. Al-Zareer, I. Dincer, and M. A. Rosen, "A novel approach for performance improvement of liquid to vapor based battery cooling systems," *Energy Convers Manag*, vol. 187, no. March, pp. 191–204, 2019, doi: 10.1016/j.enconman.2019.02.063.

[52] W. Zhang, J. Qiu, X. Yin, and D. Wang, "A novel heat pipe assisted separation type battery thermal management system based on phase change material," *Appl Therm Eng*, vol. 165, no. May 2019, p. 114571, 2020, doi: 10.1016/j.applthermaleng.2019.114571.

[53] M. Al-Zareer, I. Dincer, and M. A. Rosen, "A novel approach for performance improvement of liquid to vapor based battery cooling systems," *Energy Convers Manag*, vol. 187, no. March, pp. 191–204, 2019, doi: 10.1016/j.enconman.2019.02.063.

[54] J. Jaguemont and J. van Mierlo, "A comprehensive review of future thermal management systems for battery-electrified vehicles," *J Energy Storage*, vol. 31, no. January, p. 101551, 2020, doi: 10.1016/j.est.2020.101551.

[55] Y. Wang, Q. Gao, G. Wang, P. Lu, M. Zhao, and W. Bao, "A review on research status and key technologies of battery thermal management and its enhanced safety," *Int J Energy Res*, vol. 42, no. 13, pp. 4008–4033, 2018, doi: 10.1002/er.4158.

[56] M. Shen and Q. Gao, "System simulation on refrigerant-based battery thermal management technology for electric vehicles," *Energy Convers Manag*, vol. 203, no. November 2019, p. 112176, 2020, doi: 10.1016/j.enconman.2019.112176.

[57] Y. F. Wang and J. T. Wu, "Thermal performance predictions for an HFE-7000 direct flow boiling cooled battery thermal management system for electric vehicles," *Energy Convers Manag*, vol. 207, no. January, p. 112569, 2020, doi: 10.1016/j.enconman.2020.112569.

[58] R. Zhao, S. Zhang, J. Liu, and J. Gu, “A review of thermal performance improving methods of lithium ion battery: Electrode modification and thermal management system,” *J Power Sources*, vol. 299, pp. 557–577, 2015, doi: 10.1016/j.jpowsour.2015.09.001.

[59] Y. Huo, Z. Rao, X. Liu, and J. Zhao, “Investigation of power battery thermal management by using mini-channel cold plate,” *Energy Convers Manag*, vol. 89, pp. 387–395, Jan. 2015, doi: 10.1016/j.enconman.2014.10.015.

[60] H. Liu, E. Chika, and J. Zhao, “Investigation into the effectiveness of nanofluids on the mini-channel thermal management for high power lithium ion battery,” *Appl Therm Eng*, vol. 142, pp. 511–523, Sep. 2018, doi: 10.1016/j.applthermaleng.2018.07.037.

[61] W. Yang, F. Zhou, H. Zhou, Q. Wang, and J. Kong, “Thermal performance of cylindrical lithium-ion battery thermal management system integrated with mini-channel liquid cooling and air cooling,” *Appl Therm Eng*, vol. 175, no. April, p. 115331, 2020, doi: 10.1016/j.applthermaleng.2020.115331.

[62] Y. Li, Z. Zhou, and W. T. Wu, “Three-dimensional thermal modeling of Li-ion battery cell and 50 V Li-ion battery pack cooled by mini-channel cold plate,” *Appl Therm Eng*, vol. 147, pp. 829–840, 2019, doi: 10.1016/j.applthermaleng.2018.11.009.

[63] M. Mashayekhi, E. Houshfar, and M. Ashjaee, “Development of hybrid cooling method with PCM and Al2O3 nanofluid in aluminium minichannels using heat source model of Li-ion batteries,” *Appl Therm Eng*, vol. 178, Sep. 2020, doi: 10.1016/j.applthermaleng.2020.115543.

[64] M. Subramanian *et al.*, “A technical review on composite phase change material based secondary assisted battery thermal management system for electric vehicles,” *Journal of Cleaner Production*, vol. 322. Elsevier Ltd, Nov. 01, 2021. doi: 10.1016/j.jclepro.2021.129079.

[65] W. Yang, F. Zhou, H. Zhou, Q. Wang, and J. Kong, “Thermal performance of cylindrical lithium-ion battery thermal management system integrated with mini-channel liquid cooling and air cooling,” *Appl Therm Eng*, vol. 175, no. January, p. 115331, 2020, doi: 10.1016/j.applthermaleng.2020.115331.

[66] R. D. Jilte, R. Kumar, and M. H. Ahmadi, “Cooling performance of nanofluid submerged vs. nanofluid circulated battery thermal management systems,” *J Clean Prod*, vol. 240, Dec. 2019, doi: 10.1016/j.jclepro.2019.118131.

[67] S. Vikram, S. Vashisht, and D. Rakshit, “Performance analysis of liquid-based battery thermal management system for Electric Vehicles during discharge under drive cycles,” *J Energy Storage*, vol. 55, Nov. 2022, doi: 10.1016/j.est.2022.105737.

[68] M. Tousi, A. Sarchami, M. Kiani, M. Najafi, and E. Houshfar, “Numerical study of novel liquid-cooled thermal management system for cylindrical Li-ion battery packs under high discharge rate based on AgO nanofluid and copper sheath,” *J Energy Storage*, vol. 41, Sep. 2021, doi: 10.1016/j.est.2021.102910.

[69] H. Zhou, F. Zhou, L. Xu, J. Kong, and QingxinYang, “Thermal performance of cylindrical Lithium-ion battery thermal management system based on air distribution pipe,” *Int J Heat Mass Transf*, vol. 131, pp. 984–998, 2019, doi: 10.1016/j.ijheatmasstransfer.2018.11.116.

[70] J. Bohacek, M. Raudensky, and E. Karimi-Sibaki, “Polymeric hollow fibers: Uniform temperature of Li-ion cells in battery modules,” *Appl Therm Eng*, vol. 159, Aug. 2019, doi: 10.1016/j.applthermaleng.2019.113940.

[71] G. Liang, J. Li, J. He, J. Tian, X. Chen, and L. Chen, “Numerical investigation on a unitization-based thermal management for cylindrical lithium-ion batteries,” *Energy Reports*, vol. 8, pp. 4608–4621, Nov. 2022, doi: 10.1016/j.egyr.2022.03.081.

[72] Y. Li *et al.*, “Experimental studies of liquid immersion cooling for 18650 lithium-ion battery under different discharging conditions,” *Case Studies in Thermal Engineering*, vol. 34, Jun. 2022, doi: 10.1016/j.csite.2022.102034.

[73] P. R. Tete, M. M. Gupta, and S. S. Joshi, “Developments in battery thermal management systems for electric vehicles: A technical review,” *J Energy Storage*, vol. 35, no. September 2020, p. 102255, Mar. 2021, doi: 10.1016/j.est.2021.102255.

[74] P. Ramadass, B. Haran, R. White, and B. N. Popov, “Capacity fade of Sony 18650 cells cycled at elevated temperatures Part I. Cycling performance.”

[75] P. Ramadass, B. Haran, R. White, and B. N. Popov, “Capacity fade of Sony 18650 cells cycled at elevated temperatures Part II. Capacity fade analysis.”

[76] D. Ouyang, Y. He, J. Weng, J. Liu, M. Chen, and J. Wang, “Influence of low temperature conditions on lithium-ion batteries and the application of an insulation material,” *RSC Adv*, vol. 9, no. 16, pp. 9053–9066, 2019, doi: 10.1039/c9ra00490d.

[77] R. Kantharaj and A. M. Marconnet, “Heat Generation and Thermal Transport in Lithium-Ion Batteries: A Scale-Bridging Perspective,” *Nanoscale and Microscale Thermophysical Engineering*, vol. 23, no. 2, pp. 128–156, 2019, doi: 10.1080/15567265.2019.1572679.

[78] David J. Griffiths, *Introduction to Electrodynamics*, 4th ed., vol. 7. 1999.

[79] A. D. Kloos, “Battery thermal models for hybrid vehicle simulations,” *Neurology Report*, vol. 16, no. 1, pp. 9–13, 1992, doi: 10.1097/01253086-199216010-00008.

[80] S. Arora and A. Kapoor, “Experimental study of heat generation rate during discharge of lifePO4 pouch cells of different nominal capacities and thickness,” *Batteries*, vol. 5, no. 4, Dec. 2019, doi: 10.3390/batteries5040070.

[81] W. Cao, C. Zhao, Y. Wang, T. Dong, and F. Jiang, “rd,” *Int J Heat Mass Transf*, vol. 138, pp. 1178–1187, Aug. 2019, doi: 10.1016/j.ijheatmasstransfer.2019.04.137.

[82] M. Costa *et al.*, “Numerical Simulations for Indirect and Direct Cooling of 54 V LiFePO 4 Battery Pack,” 2022, doi: 10.3390/en15134581.

[83] M. S. Patil *et al.*, “A Novel Design for Lithium ion Battery Cooling using Mineral Oil,” no. December, pp. 164–168, 2016, doi: 10.14257/astl.2016.141.34.

[84] R. L. , and L. N. Boylestad, *Electronic Devices and Circuit Theory 11th ed*. Pearson Education Inc., 2018.

[85] B. Zine, K. Marouani, M. Becherif, and S. Yahmedi, “Estimation of Battery Soc for Hybrid Electric Vehicle using Coulomb Counting Method,” *International Journal of Emerging Electric Power Systems*, vol. 19, no. 2, Apr. 2018, doi: 10.1515/ijeeps-2017-0181.

[86] Y. -C. Tsao, “Implementation and Design of Water Flow Meter of Smart Home Integrated with Environment Monitor System,” *2022 IEEE 4th Eurasia Conference on Biomedical Engineering, Healthcare and Sustainability (ECBIOS)*, pp. 126–131, 2022.

[87] Kovan V, Tezel T, Camurlu HE, and Topal ES, “EFFECT OF PRINTING PARAMETERS ON MECHANICAL PROPERTIES OF 3D PRINTED PLA/CARBON FIBRE COMPOSITES.”

[88] S. Hanessian, “Mono propylene glycol properties,” *Total Synthesis of Natural Products: The “Chiron” Approach. Pergamon press*, 1983.

[89] George K. Morris, *Introduction to Electronics.* . John Wiley & Sons., 2012.

[90] H. Schade, “Temperature Measurement with Thermistors,” *EDN Magazine, 18(15),* pp. 109–112, 1973.

[91] J. S. Steinhart and S. R. Hart, “INSTRUMENTS AND METHODS Calibration curves for thermistors,” 1968.